THE CRYOSPHERE AND NORTH ATLANTIC TROPICAL CYCLONE ACTIVITY: STATISTICAL FORECASTING AND PHYSICAL MECHANISMS

By

Johannes Mack

B.S., Southern Illinois University, 2011

A Thesis
Submitted in Partial Fulfillment of the Requirements for the
Master of Science.

Department of Geography & Environmental Resources
in the Graduate School
Southern Illinois University Carbondale
May 2013

THESIS APPROVAL

THE CRYOSPHERE AND NORTH ATLANTIC TROPICAL CYCLONE ACTIVITY: STATISTICAL FORECASTING AND PHYSICAL MECHANISMS

By

Johannes Mack

A Thesis Submitted in Partial

Fulfillment of the Requirements

for the Degree of

Master of Science

in the field of

Geography & Environmental Resources

Approved by:

Dr. Justin T. Schoof, Chair

Dr. Matthew Therrell

Dr. Jonathan Remo

Graduate School
Southern Illinois University Carbondale
May 7, 2013

AN ABSTRACT OF THE THESIS OF

Johannes Mack, for the Master's of Science degree in GEOGRAPHY & ENVIRONMENTAL RESOURCES, presented on 2 May, 2013, at Southern Illinois University Carbondale.

TITLE: THE CRYOSPHERE AND NORTH ATLANTIC TROPICAL CYCLONE ACTIVITY: STATISTICAL FORECASTING AND PHYSICAL MECHANISMS

MAJOR PROFESSOR: Dr. Justin Schoof

The components of the northern hemisphere cryosphere and their relationship to Atlantic tropical cyclone activity are investigated in this study. Multiple ordinary least-squares regression with a stepwise selection procedure is used to develop a new statistical forecasting scheme for 13 seasonal tropical cyclone parameters at four lead times for the period 1980-2010. Sea ice area and sea ice extent in 10 geographic regions, snow cover extent in three geographic regions and five indices reflecting major modes of climate variability were analyzed as possible predictors. Three model groups, based on predictors, were constructed and evaluated: 1) only climate mode predictors, 2) only cryosphere predictors, and 3) both cryosphere and climate mode predictors. Models using only climate mode predictors showed poor predictability of the tropical cyclone parameters across all four lead times while the models using only cryosphere predictors and those using both sets of predictors showed improved predictability. Baffin Bay and Hudson Bay sea ice area were found to be the most significant predictors, exhibiting an inverse relationship with overall tropical cyclone activity. The developed models were also compared to current operational statistical models of tropical cyclone activity. While the operational models were generally more skillful, June hindcasts of major hurricanes outperformed the operational models by as much as 20%.

DEDICATION

I would like to dedicate this thesis to my mother and sister, Inge and Lena. They have been so encouraging and supportive throughout my entire graduate studies, and I thank them dearly for that.

ACKNOWLEDGEMENTS

This research project would never have been possible without the guidance and invaluable expertise from Dr. Justin Schoof. Discussions with Dr. Matthew Therrell and Dr. Jonathan Remo were also very helpful in guiding this research project.

TABLE OF CONTENTS

APPENDICES

LIST OF TABLES

LIST OF FIGURES

FIGURE PAGE

DEFINITONS AND ACRONYMS

Accumulated Cyclone Energy – ACE

Antarctic Oscillation – AAO

Arctic Oscillation – AO

Atlantic Meridional Mode – AMM

Atlantic Multidecadal Oscillation – AMO

Atlantic Warm Pool – AWP

Climate Mode – CM

Colorado State University – CSU

Coupled Forecast System – CFS

Cuban Meteorological Institute – INSMET

Earliest tropical cyclogenesis – MID

Earth Systems Research Laboratory – ESRL

El Niño-Southern Oscillation – ENSO

Florida State University – FSU

Global Snow Lab – GSL

Hurricane – H

Hurricane Days – HD

Intense Hurricane (IH): Term is synonymous with major hurricanes

Intense Hurricane Days – IHD

Inter-Tropical Convergence Zone – ITCZ

Land falling tropical cyclone – LF

Latest tropical cyclogenesis – MAD

Lifetime mean duration of a tropical cyclone – LMD

Main Development Region (MDR) – Defined as the area within the tropical Atlantic where a majority of tropical cyclones form, typically 10-20°N, 20-70°W.

Major Hurricane – MajH

Mean annual peak wind of a season's tropical cyclones – PW

Mean Square Error Skill Score – MSSS

Minor Hurricane – MinH

Named Storm (NS): Term is synonymous with tropical cyclone

Named Storm Days – NSD

National Center for Atmospheric Research – NCAR

National Centers of Environmental Prediction – NCEP

National Hurricane Center – NHC

National Oceanic and Atmospheric Administration – NOAA

National Snow and Ice Data Center – NSIDC

Near-Surface Air Temperature – SAT

Net Tropical Cyclone Activity – NTC

North Atlantic Oscillation – NAO

North Carolina State University – NC State

North Pacific Oscillation – NPO

Ordinary Least Squares – OLS

Pacific North American Patter – PNA

Power Dissipation Index – PDI

Quasi-Biennial Oscillation – QBO

Sea Ice – SI

Sea Ice Area – SIA

Sea Ice Extent – SIE

Sea Level Pressure – SLP

Sea Surface Temperature – SST

Siberian High Oscillation – SHO

Snow Cover – SC

Snow Cover Extent – SCE

Southern Oscillation Index – SOI

Thermohaline Circulation – THC

Total season length – TSL

Tropical Cyclone – TC

Tropical Cyclone Parameter – TCP

Tropical Storm – TS

Tropical Storm Risk Group – TSR

Tropical Upper Tropospheric Trough – TUTT

CHAPTER 1

INTRODUCTION

1.1 Background

Atlantic tropical cyclones (TCs) are among the costliest natural disasters that threaten the United States resulting in annual damages of $10 billion (Pielke et al., 2008). Atlantic TCs also feature the largest interannual variability of any ocean basin making seasonal forecasts an important area of research (Klotzbach and Gray, 2004). The first regularly issued seasonal forecasts for the Atlantic were issued on 1 June and 1 August in 1984 by Dr. William Gray (Gray, 1984a, b). Dr. Gray discovered that large-scale atmospheric and oceanic features like El Niño-Southern Oscillation (ENSO) and the Quasi-Biennial Oscillation (QBO) were linked to Atlantic TC activity through their effects on the environmental conditions within the Atlantic's TC main development region [MRD: 10-20°N, 20-70°W] (Gray, 1968; 1984a, b). In the time since Gray's first forecasts, seasonal forecasting research has increased considerably. Forecasts are now being issued for all seven TC producing ocean basins at lead-times greater than 6 months (Camargo et al., 2007). Though our understanding of the large-scale features that govern overall TC activity has improved, additional forecast improvements are needed. In particular, the predictors used by many forecasting groups often incorporate complex model projections of atmospheric and oceanic modes of climate variability (Klotzbach and Gray, 2012c; Saunders and Lea, 2005) that can increase the amount of uncertainty within the final forecast and these predictors can also be difficult to comprehend by the forecast readers (e.g., general public). Having a forecasting scheme that relies upon more simple, straight-forward predictors could allow for reduced forecast uncertainty and greater understanding for the forecast readers.

The average global near-surface air temperature (SAT) increased by 0.74 $^{\circ}$C between 1906-2005 (IPCC, 2007), with especially pronounced warming in the high latitudes of the northern hemisphere. The Arctic has seen a 2 to 3 $^{\circ}$C increase in SATs since 1950 (ACIA, 2005), making this region particularly important for climate research. This enhanced regional warming, often referred to as "polar amplification," has been mainly linked to the ice-albedo feedback (Johannessen et al., 2004), where reductions in the highly reflective surfaces of sea ice (SI) and snow cover (SC) have led to decreases in surface albedo and consequently increases in solar radiation absorption by the much darker (i.e., less reflective) surfaces of open ocean and bare ground causing an increase in SATs, which then ultimately leads to more reductions in SI and SC (Robock, 1980). Polar amplification in the Arctic is manifesting itself regionally through drastic increases in SAT and reductions in SI and SC (Screen and Simmonds, 2010), but these changes also have serious consequences for regions outside of the Arctic due to the Arctic's ability to influence the global energy budget (IPCC,2007).

Regions outside of the Arctic are being affected by polar amplification through changes to large-scale atmospheric and oceanic features like the Arctic Oscillation (AO) and North Atlantic Oscillation (NAO: Budikova, 2009; Bader et al., 2011) and ocean currents (Holland and Bitz, 2003). These large-scale features may able influence the weather and climate of regions outside of the Arctic by altering atmospheric and oceanic circulation patterns (Kushnir, 1994; Hurrell and Van Loon, 1997). Variability in these atmospheric and oceanic oscillations, referred to as climate modes (CMs), have been associated with the rapid changes experienced within the Arctic (IPCC, 2007). Since Arctic SI and SC variability are associated with changes in CMs, further investigation into the role the cryosphere plays in atmospheric and oceanic variability is

warranted. Especially, if many of the CMs used within seasonal TC forecasting are the same ones known to be associated with cryospheric variability.

If many of the CMs being used for TC forecasting (Camargo et al., 2007) also interact with SI and SC (Deser et al., 2000; Bartolini et al., 2010), then why hasn't the inclusion of SI and SC data within seasonal forecast models been thoroughly investigated? Only three studies have incorporated either SI data (Ke, 2007), SC data (Yan et al., 2012), or both (Choi et al., 2010) when investigating seasonal TCs. Of these studies, Chio et al. (2012) and Ke (2007) investigated the link between cryospheric variability and overall TC frequency within the Western North Pacific, while Yan et al. (2012) investigated this link for the Atlantic. Though, these studies investigated the link between the cryosphere and TC activity none of them investigated the potential forecast application of this relationship.

These three studies did not directly investigating the potential forecast application of this cryosphere-TC relationship nor did they investigate:

- both SI and SC variations as they relate to the Atlantic TC season,
- how SI and SC variations in multiple regions throughout the Northern Hemisphere are related to Atlantic TC activity,
- using sea ice area (SIA) as opposed to SIE as a predictor (since SIA is a more representative measure of the actual SI present in a specific region,) and
- combining CM and cryospheric data within a statistical forecasting scheme.

This study will directly address this lack of research by investigating the inclusion of SI and SC data in seasonal Atlantic hurricane forecasts.

1.2 Problem Statement and Research Questions

SI and SC are completely absent from current Atlantic TC seasonal forecasting schemes even though many schemes use CMs that have been linked with variability in SI and SC. For example, the AO (Bamzai, 2003; Rigor et al., 2002), ENSO: Seager et al., 2010; Mysak et al., 1996), the Pacific North American Pattern (PNA: L'Heureux et al., 2008; Cohen and Entekhabi, 2001) and the NAO (Seager et al., 2010; Mysak et al., 1996) all exhibit significant correlations during years with anomalous SI and SC. These covariations between SI and SC during different phases of these CMs have been known for many years, but there is still some uncertainty regarding the exact causal mechanisms governing these relationships. Much of this uncertainty is centered on two key questions: 1) Do variations in SI and SC cause changes to CMs or do changes in CMs cause variations in SI and SC? and 2) What are the direct and indirect feedbacks between the cryosphere and CMs that enhance or suppress these variations? These questions and others are still not completely resolved and require further research. Most seasonal forecasting schemes for TCs use one or more of these CMs as predictors without considering the possible influence of the cryosphere.

For this study, the aim will be to quantify the cryosphere-TC relationship for the Atlantic by developing a new statistical seasonal forecasting scheme that utilizes SIA, SCE, and CM data to predict 13 different seasonal tropical cyclone parameters (TCPs). Unlike the three previously mentioned studies that only investigated the cryosphere in a particular geographic region, this study will consider a total of 13 separate geographic regions that encompass the entire Northern Hemisphere as well as indices of five CMs as predictors of TC activity. By including multiple geographic regions, specific locations within the cryosphere that lead to an enhanced or suppressed TC season can be identified. Additionally, by including both cryospheric and CM

data into the forecast model, quantifying the relationships between the cryosphere, the CMs and the TCPs will be possible. Analyzing these statistical relationships will allow for the identification of the geographic regions throughout the Northern Hemisphere that have associations with TC activity allowing for the physical mechanisms that govern these relationships to be explored.

This study is guided by four primary research questions:

1. Which components of the cryosphere have the strongest associations with North Atlantic TC activity?
2. What geographic areas within the cryosphere are the most influential to the statistical forecast models? How do these regions relate to the CMs?
3. What are the physical mechanism governing theses significant relationships?
4. How does the forecasting scheme incorporating cryospheric information compare to current operational forecasting schemes?

Answering these research questions will: a) lead to a better understanding of relationship between the cryosphere and the CMs known to influence Atlantic TC activity, b) allow for the identification of specific geographic regions within the cryosphere whose variability has an effect on CMs and TCs, and c) allow for the first quantitative comparison of forecast models with and without cryospheric predictors. Some initial hypotheses are that only a few regions within the cryosphere will have statistically significant relationships to the CMs and TCPs; those significant relationships will feature coinciding geographical regions; and that a forecasting scheme that includes cryospheric information will be comparable, if not superior, to current models at a variety of lead times.

This thesis will be divided into four remaining chapters. A literature review will be presented in Chapter 2 in which a brief history of Atlantic seasonal TC forecasting will be given, followed by a climatology of the Atlantic's TC season, a brief summary on each Atlantic TC forecasting groups and lastly an overview of the cryosphere-TC relationship. In Chapter 3 the methodology used in this study will be presented as well as the methodology used by current forecasting groups. In Chapter 4 the findings of this study will be presented as well as a comparative analysis of these findings to current forecasting groups. Finally, in Chapter 5 a summary of this study and future research directions will be presented.

CHAPTER 2

LITERATURE REVIEW

2.1 Introduction to Seasonal Forecasting of Tropical Cyclones

In tropical meteorology seasonal forecasting refers to the forecasts aimed at predicting the overall activity of a TC season compared to climatology (i.e., above- or below-normal activity). Overall TC activity can be assessed by a variety of measures. Some of the most popular being the total number of tropical storms (TSs) and TCs, the annual accumulated cyclone energy index value (ACE; Bell et al., 2000) or the power dissipation index value (PDI; Emanuel, 2005).This chapter aims to synthesize the research on Atlantic TC forecasting.

The first attempt to produce a seasonal forecast of TC activity was by Nicholls (1979) for the Australian TC basin in 1979 when he discovered a -0.6 correlation between winter pressure at Darwin, Australia and the subsequent TC frequency. The first Atlantic seasonal forecasts were issued in June and August of 1984 by Gray (1984a, b) using ENSO, Quasi-Biennial Oscillation (QBO), and Caribbean Sea level pressure (SLP) as predictors. Both Gray (1984a) and Nicholls (1979) used statistical methods to produce their forecasts, where statistical relationships between TC frequency and oceanic/atmospheric conditions were used to predict the TC season. There are also dynamical forecasts that use general circulation models (GCMs) and regional climate models to predict TC activity. Statistical forecasts are still the most frequently utilized forecast type and the most accurate, though dynamical forecasts (Camargo and Zebiak, 2002; LaRow et al., 2008) are showing improvements (Camargo et al., 2007). See Table 2.1 for a list of many of the top forecasting groups. This chapter will be divided into four remaining subsections: 1) a general climatology of the Atlantic TC season (A climatology of the study period will be presented in Chapter 4) including a description of tropical cyclogenesis requirements, 2) a brief

overview of current forecasting groups, 3) a description of various forecast/hindcast skill measures, and 4) an overview of the cryosphere-TC relationship including summaries of current studies investigating this relationship.

Table 2.1 List of current forecasting groups issuing seasonal tropical cyclone forecasts for the North Atlantic by forecast type (Adapted from Camargo et al., 2007 Table I).

Forecasting Group	Type	Website
Colorado State University, USA (CSU)	Statistical	http://hurricane.atmos.colostate.edu
Tropical Storm Risk, UK (TSR)	Statistical	http://tsr.mssl.ucl.ac.uk
National Oceanic and Atmospheric Administration, USA (NOAA)	Statistical	http://www.cpc.noaa.gov
Cuban Meteorological Institute (INSMET)	Statistical	http://www.met.inf.cu
North Carolina State University, USA (NCSU)	Statistical	http://cfdl.meas.ncsu.edu/index.html
European Centre for Medium-Range Weather Forecasts (ECMWF)	Dynamical	http://www.ecmwf.int (collaborating agencies only)
International Research Institute for Climate and Society (IRI)	Dynamical	http://iri.columbia.edu/forecast/tc_fcst/
Meteorological Office, UK (MetOffice)	Dynamical	http://www.metoffi ce.gov.uk/weather/ tropicalcyclone/northatlantic

2.2 Atlantic Basin Climatology

The North Atlantic TC Basin includes the Atlantic Ocean north of the equator, the Caribbean Sea, and the Gulf of Mexico. Its TC season officially runs between 1 June and 31 November, with 90% of the activity occurring being between mid-August and late October (See Figure 2.1). The term tropical cyclone is a generic term for a warm core low-pressure system with organized convection and defined cyclonic surface winds that form in barotropic environments over tropical and subtropical waters (Holland, 1993). TCs are described by a variety of terms depending on the ocean basin in which they form. For example, in the western North Pacific the term typhoon is used, while in the North Indian Ocean the term very severe cyclonic storm is used, and in the Atlantic the term hurricane (H) is used (Neumann et al., 1993).

Since this study is focused on the Atlantic the terms describing TCs will be those that are regionally specific to the Atlantic. In the Atlantic when a TC has winds less than 17 ms^{-1}, greater than 17 ms^{-1}, greater than 33ms^{-1}, and greater than 50ms^{-1} it is called a tropical depression, tropical storm (TS), hurricane (H), and major hurricane (MajH), respectively (Neumann et al., 1993). Hs that have winds greater than 33ms^{-1} and less than 50ms^{-1} are often termed minor hurricanes (MinHs) while Hs that have wind speeds greater than 50ms^{-1} are termed MajHs. Since 1950, TCs that meet TS wind speed criteria are given a name. The term "TC activity" will represent all TSs, Hs, MinHs, and MajHs in a given season. For the period of 1966-2009 there were on average 11.3, 6.2, and 2.3 TSs, Hs, and MajHs, respectively (NOAA, 2012a).

There are six environmental conditions that are required for TC formation (tropical cyclogenesis): 1) warm ocean waters of at least 26.5ºC throughout a depth of least 50m, 2) an atmosphere that rapidly cools with height leading to conditional instability, 3) abundant mid- to low-level tropospheric moisture, 4) a minimum distance of at least 500 km from the equator so that the Coriolis force becomes non-negligible, 5) a pre-existing near-surface disturbance with sufficient vorticity and low-level convergence, and 6) low values of vertical wind shear of typically less than 10ms^{-1} between the upper and lower troposphere (Gray, 1979). The aim of any forecasting group is to predict one or more of these environmental conditions for an upcoming TC season in order to gauge the likelihood of tropical cyclogenesis.

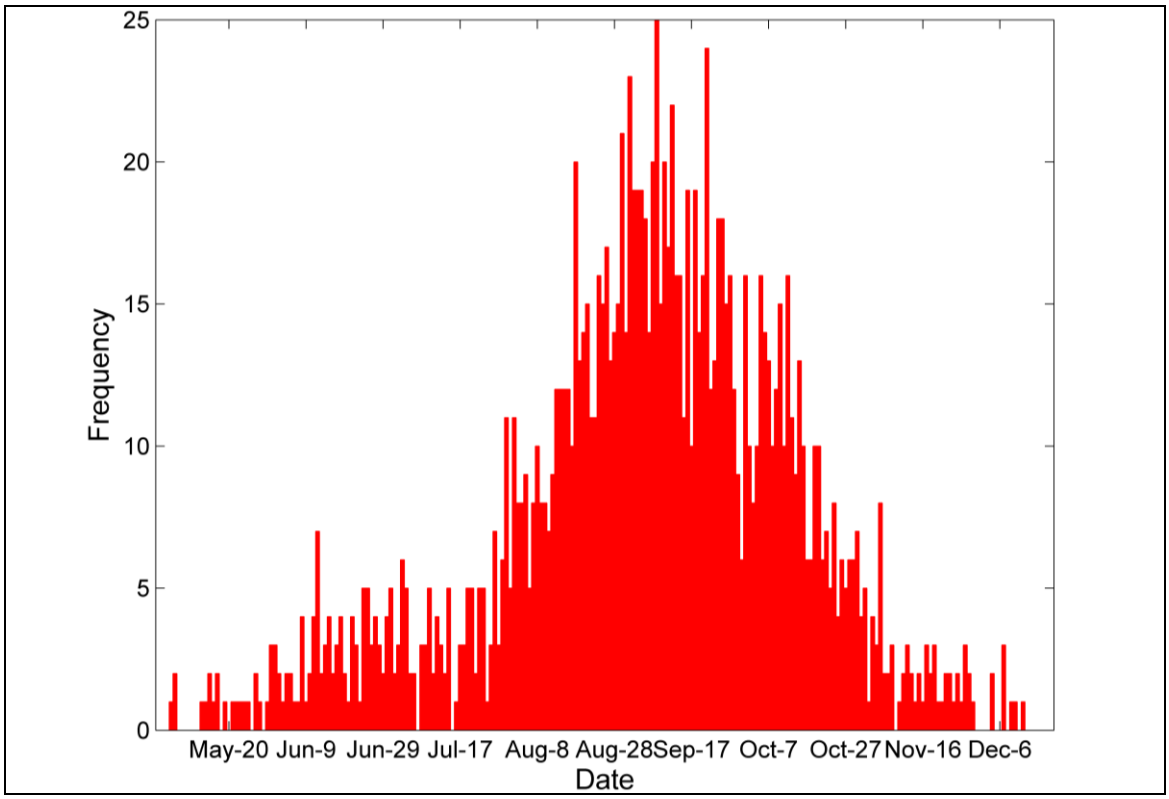

Figure 2.1 Number of tropical cyclones that have occur since 1851 by date of cyclogenesis. The Atlantic's tropical cyclone season officially runs from June 1 to November 31.

2.3 Seasonal Forecasting Groups

In this subsection an overview of the top statistical forecasting groups for the Atlantic will be presented. Many of these groups are university research groups or government agencies. Regardless of the forecasting group, the process of producing a forecasting scheme is very similar from group to group. Each group uses multiple regression techniques in order to develop their models with some groups using an analog approach to further refine their model output. Predictors for their models are can either be past or forecasted environmental conditions with known associations with TC activity. Based on their forecasting scheme, groups will either produce forecasts every month, generally starting in the December prior to the TC season, or

every few months leading up to the TC season. Regardless of forecasting scheme, each group produces a forecast at the start of the TC season in June.

2.3.1 Colorado State University

Colorado State University (CSU) currently issues quantitative forecasts at four issuance dates – early December, April, June, and August. Early June and August forecasts have been issued since 1984 (Gray 1984a, b) and the extended-range forecasts of December and April have been issued since 1992. The quantitative December forecast was discontinued in 2011 and replaced with a qualitative forecast due to a lack of operational skill (Gray et al., 1992; Klotzbach 2008; Klotzbach and Gray, 2010). The CSU group uses multiple OLS regression equations to produce their forecasts. CSU use a tropical cyclone parameter (TCP) called Net Tropical Cyclone (NTC) activity in order to predict how active a TC season will be. NTC is an aggregate measure of the following six parameters: named storms (NSs [Same as the term TCs]), named storm days (NSD), hurricanes (H), hurricane days (HD), intense hurricanes (IH [Same as the term MajHs]), and intense hurricane days (IHD; Gray et al., 1994). These six parameters are normalized by their climatologies resulting in a normal annual NTC being 100. Above (below) average TC seasons will have an NTC of greater (less) than 100. NTC is forecasted by CSU instead of the six individual TCPs because modeled NTC has shown greater agreement with observations than the individual TCPs (Gray et al., 1994). Once an NTC is forecasted the six parameters are then derived empirically from the NTC value.

The most recent quantitative early December forecast was issued in 2010 (Klotzbach and Gray, 2010) and had three predictors (See Table 2.2 and Figure 2.2). Predictors were selected by using the National Centers for Environmental Prediction/National Center for Atmospheric Research (NCEP/NCAR) reanalysis dataset (Kistler et al., 2001). A time series from 1950-2007

for NTC was created and then the reanalysis fields of SLP, sea surface temperature (SST) and 500-mb height were correlated against the observed NTC values from 1950-1989. The years 1990-2007 were left out in order the test the hindcast skill of the model. Predictors had to meet four criteria for selection: 1) predictors had to be significantly correlated at the 95% confidence level with NTC over the period 1950-1989, 2) the correlation between the predictors and NTC had to remain at the 95% level for the left out 1990-2007 period, 3) the predictors had to be significantly correlated with physical features known to effect Atlantic Basin TC activity through alterations to wind shear, SLP, and SST patterns during the following August-October period, and 4) when the predictors were added into the stepwise regression model they had to increase the variance explained by 3% over the three time periods of 1950-1989, 1990-2007, and 1950-2007 (Klotzbach, 2008). The NTC hindcasts are then ranked from highest (1) to lowest (58), and then the corresponding observed NTC values are assigned to the predicted NTC ranks. Using these three predictors the ranked hindcasts were able to explain 54% of the variance in the observed NTC record (Klotzbach, 2008).

October-November SSTs (December predictor 1: DP1) was selected because warm fall North Atlantic SSTs are correlated ($r > 0.5$) with the following August-October SSTs throughout the North Atlantic, and warm North Atlantic SSTs are indicative of an active AMO and a strong Atlantic thermohaline circulation (Goldenber et al., 2001). With an active AMO in place the Atlantic's MDR generally experiences anomalously low vertical wind shear and low SLP, and anomalously warm STTs. The reduced wind shear is not only linked to the phase of the AMO but also to a weakened Tropical Upper Tropospheric Trough (TUTT) in the central Atlantic, which leads to reductions the upper-level westerlies and low-level easterlies further enhancing the

likelihood of anomalously low vertical wind shear being experienced during the peak TC peaks (Klotzbach, 2008).

Table 2.2 List of predictors and their locations for the CSU quantitative forecasts at the four lead times (Adapted from Klotzbach and Gray, 2010,2012a,b,c).Acronyms used are : SLP (sea level pressure) and SST (sea surface temperature).

December Predictors And Locations	
1. October-November SST 2. November 500 mb geopotential height 3. November SLP	1. (55-65˚N, 60-10˚W) 2. (67.5-85˚N, 50˚W-10˚E) 3. (7.5-22.5˚N, 175-125˚W)
April Predictors And Locations	
1. January-March Atlantic SST 2. March SLP 3. February-March SLP 4. ECMWF 1 March SST Forecast for September Nino 3	1. (5˚S-35˚N, 10-40˚W) 2. (20-40˚N, 20-35˚W) 3. (5-20˚S, 85-120˚W) 4. (5˚S-5˚N, 90-150˚W).
June Predictors And Locations	
1. April-May SST 2. April-May 200-mb zonal winds 3. ECMWF 1 June SST Forecast for September Nino 4. May SLP	1. (15-55˚N, 15-35˚W) 2. (0-15˚S, 150˚E-120˚W) 3. (5˚S-5˚N, 90-150˚W) 4. (20-40˚N, 30-50˚W)
August Predictors And Locations	
1. July Surface zonal Wind 2. July Surface Temperature 3. July 200-mb zonal Wind	4. (10-17.5˚N, 60-85˚W) 5. (20-40˚N, 15-35˚W) 6. (5˚-15˚N, 0-40˚E)

November 500 mb geopotential height (December predictor 2: DP2) was selected because DP2 correlates highly with AO values at r = -0.73 (Thompson and Wallace, 1998) and with NAO values at r = -0.55 (Barnston and Livezey, 1987). When the AO and NAO are in their negative phase, reductions in the strength of the westerlies across the central Atlantic occur because more blocking/ridging is experienced throughout the central Atlantic. Additionally, a negative NAO is associated with a weaker Azores High causing positive SSTs anomalies and reduced easterly trade winds in the tropical Atlantic (Marshall et al., 2001). Finally November 500-mb heights are

also correlated with anomalously low summer and early fall Caribbean SLPs and easterly anomalies at the 200mb level. Both of which reduce vertical wind shear in the tropical Atlantic.

November SLP (December predictor 3: DP3) was selected because high SLP in the subtropical Northeast Pacific usually occurs during the fall and winter prior to a La Nina event because the higher SLP strengthens the trade winds in the East Pacific leading to more upwelling in the East Pacific, increasing the likelihood of La Nina (Larkin and Harrison, 2002). When a La Nina event is in place TC activity is expected to increase because the majority of Pacific tropical convection is shifted westward causing more vertical wind shear to be present in the Pacific and less in the Atlantic (Gray, 1984a). Low vertical wind shear is crucial for tropical cyclogenesis in any tropical ocean basin (Gray, 1968).

As of December 2011 CSU has been providing a qualitative rather than a quantitative forecast due to the lack of real-time forecast skill between 1992-2011 (Klotzbach and Gray, 2011). The quantitative forecast was discontinued because there was a breakdown of several long-term relationships that worked on hindcast data but not in real-time forecasting and because no statistical or dynamical models have shown any skill at predicting ENSO at the 9-12 month lead times needed at the early December timeframe. The current 2012 December forecast is issued with four possible TC activity scenarios dictated by the strength of the Atlantic thermohaline circulation (THC) and the phase of ENSO and how likely changes to those physical parameters are for the upcoming TC season.

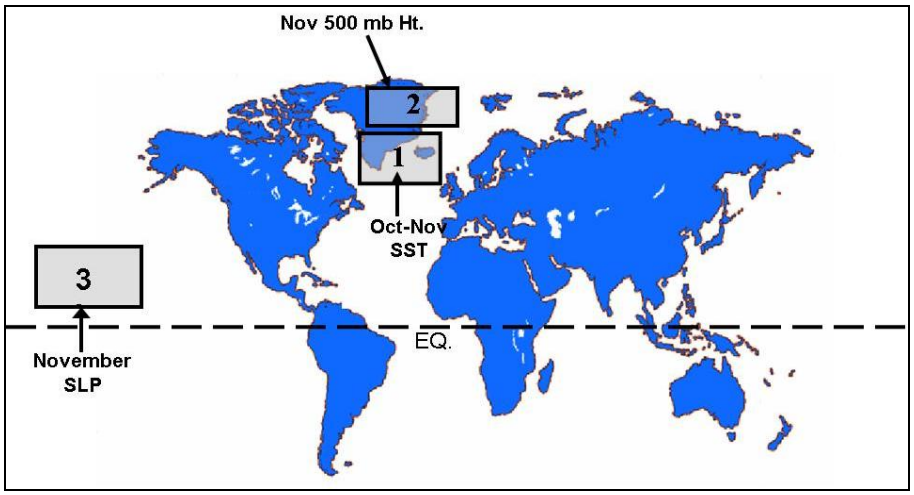

Figure 2.2 Locations of the predictors used in the early December quantitative forecast for the 2011 TC season issued by CSU (From Klotzbach and Gray, 2010).

The April forecast model is built using data from 1982-2010 and utilizes four predictors from the NCEP/NCAR reanalysis dataset (See Table 2.2 and Figure 2.3). The validated hindcast of NTC is correlated with observations at r = 0.68 (Klotzbach and Gray, 2012a).

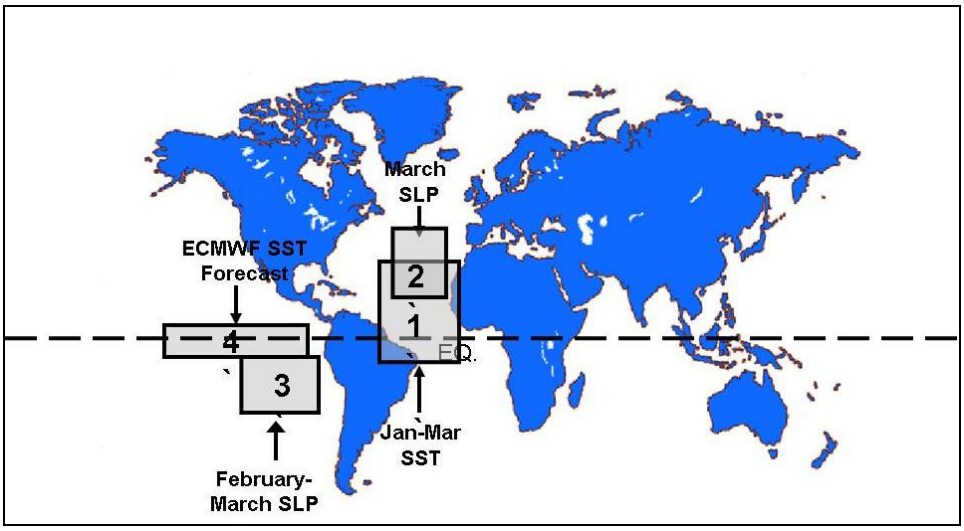

Figure 2.3 Locations of the predictors used in the early April quantitative forecast for the 2012 TC season issued by CSU (From Klotzbach and Gray, 2012a)

January-March Atlantic SST (April predictor 1: AP1) was selected because above average SSTs in the tropical and subtropical eastern Atlantic during January-March are correlated strongly (r = 0.65) with August-October values of the Atlantic Meridional Mode (AMM; Kossin and Vimont 2007). The AMM impacts Atlantic TCs by altering the position and intensity of the Inter-Tropical Convergence Zone (ITCZ) and in doing so causing changes to vertical and horizontal wind shear patterns and SST patterns throughout the tropical Atlantic.

March SLP (April predictor 2: AP2) was selected because March SLP in the subtropical Atlantic is used to evaluate the strength of the Azores High. It has been observed that a strengthened Azores High corresponds with increased trade winds across the Atlantic causing increased ocean surface mixing and upwelling leading to cooler-than-normal SSTs. These SST anomalies cause a positive feedback that results in higher SLP and stronger trade winds and further SST cooling (Knaff 1998). All these changes lead to a less active TC season.

February-March SLP (April predictor 3: AP3) was selected because above average February-March SLP in the southeastern tropical Pacific is correlated with a positive Southern Oscillation Index (SOI) and stronger trade winds across the eastern Pacific leading to an increased likelihood of La Nina conditions in August-October.

ECMWF 1 March SST forecast for September Nino 3 (April predictor 4: AP4) is the first time that CSU has used a dynamical model prediction as a predictor in their forecasts. The ECMWF forecast of September Niño 3 by 1 March has shown considerable skill in predicting the phase of ENSO several months in advance with ensemble averages for the September Niño 3 region and observations correlating at r =0.63 (Stockdale et al., 2011).

Along with these four predictors CSU now includes an analog approach within their April forecast. The analog approach analyzes prior environmental conditions back to 1949 that show

similarities to current February and March conditions. Years that feature similar environmental conditions are analyzed and their TC activity compared to model output. The current model output is then refined using the historical analogs.

The early June forecast uses a new forecasting scheme that has been in use since 2010. It has four predictors (See Table 2.2 and Figure 2.4) that are chosen from the newly developed Climate Forecast System Reanalysis dataset (CFSR: Saha et al., 2010) over the period 1982-2010. Hindcast correlation between model and observed NTC are r = 0.74 after cross validation (Klotzbach and Gray, 2012b). All four predictors are associated with affecting wind shear throughout the troposphere across the Atlantic's MDR.

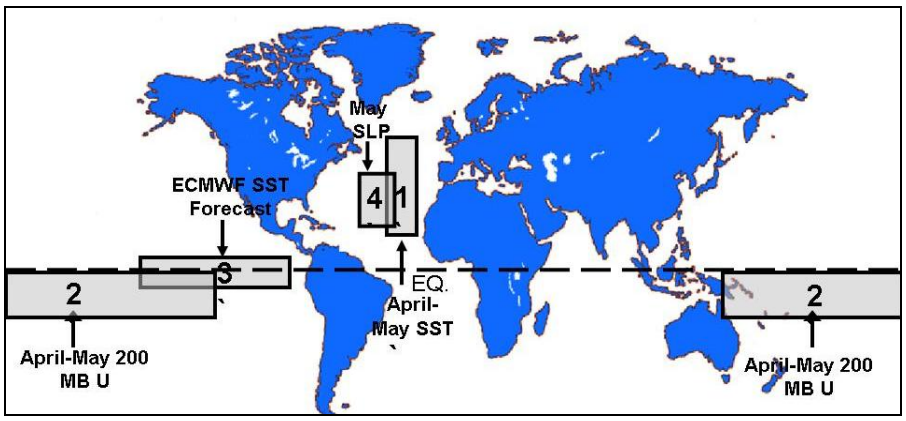

Figure 2.4 Locations of the predictors used in the early June quantitative forecast for the 2012 TC season issued by CSU (From Klotzbach and Gray 2012b).

April-May SST (June predictor 1: JP1) is very similar to AP1 with only slight temporal and spatial differences. Above average April-May SSTs in the eastern Atlantic are correlated with a weakened subtropical high throughout the spring, which is correlated with weaker trade winds and upper tropospheric westerlies, below-normal SLP, and above-normal SSTs in the MDR in the following August-October period. JP1 is also correlated with August-October values

of the AMM over the 1982-2010 period with the AMM primarily influencing TC activity through changes in the position and intensity of the ITCZ.

April-May 200-mb zonal winds (June predictor 2: JP2) was selected primarily because increased April-May 200-mb zonal winds in the south-central tropical Pacific are typically associated with La Nina conditions and decreased odds of having a La Nina transition to an El Niño event. With the odds of La Nina conditions likely, above-average SSTs, and below-average SLPs and zonal wind shear throughout the Atlantic during the August-October period are expected.

ECMWF 1 June SST forecast for September Nino 3 (June predictor 3: JP3) was selected because, much like AP3, the ECMWF seasonal forecast system has shown considerable forecast skill as evident by correlations ($r = 0.81$) between model Niño 3 Region SSTs and observations. Knowing SST values in the eastern tropical Pacific during the August-October TC period will allow for ENSO conditions during that period to be included in the forecast.

May SLP (June predictor 4: JP4) was selected because anomalously low SLP in the central Atlantic in May is associated with reduced trade winds across the Atlantic, which promotes reduced oceanic upwelling and sustains warm SST anomalies in the tropical Atlantic. Low SLP in May also tends to persist into the peak TC months. Much like the early April forecast scheme, early June uses an analog approach to refine the statistical model output.

The early August forecast is developed from ERA-Interim Reanalysis data using the years 1979-2011. The current forecast scheme uses three predictors (See Table 2.2 and Figure 2.5) and has shown a correlation of 0.91 between hindcast and observed NTC model validation (Klotzbach and Gray, 2012c).

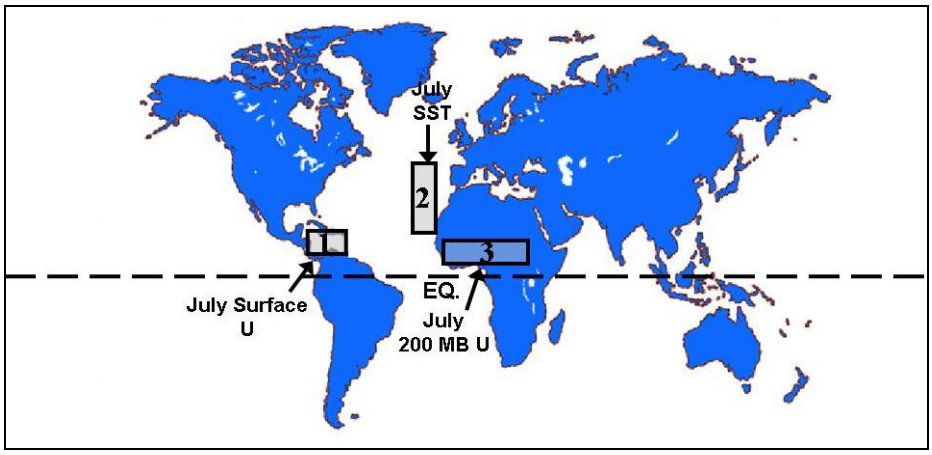

Figure 2.5 Locations of the predictors used in the early August quantitative forecast for the 2012 TC season issued by CSU (From Klotzbach and Gray 2012c).

July surface zonal wind (August predictor 1: AP1) was selected because reduced surface zonal winds in the Caribbean are associated with weakened trade winds in the Atlantic leading to a larger-than-normal Atlantic Warm Pool (AWP: Wang and Lee, 2007) This change to the trade winds and AWP lead to less vertical wind shear increasing the likelihood of tropical cyclogenesis, and anomalously warm SSTs lead to more latent heat being available for the intensification of TCs into MajHs (Goldenberg and Shapiro, 1998).

July SST (August predictor 2: AP2) was selected because anomalously warm SSTs in the northeastern subtropical Atlantic are associated with the positive phase of the AMM leading to an altered ITCZ and consequently reduced trade winds across the tropical Atlantic (Kossin and Vimont, 2007) and warmer SSTs during August-October.

July 200-mb zonal wind (August predictor 3: AP3) was selected because anomalously eastern flow at the 200-mb level over northern tropical Africa creates an environment conducive to easterly wave development. These easterly waves are very important for tropical cyclogenesis, especially in MajHs (Gray 1968). This anomalous eastern flow tends to persist into August-October leading to reduced wind shear over the MDR and AP3 also correlates well with ENSO

conditions. Much like the early April and June forecast schemes, early August also uses an analog approach to refine the statistical model output.

All of the CSU quantitative forecast schemes utilize pressure, temperature, and wind fields from reanalysis datasets, apart from the April and June forecasts also utilizing the ECMWF Niño Region 3 predictions. All the forecasting schemes have shown good agreement between modeled NTC and observations with correlations at 0.68, 0.74, and 0.91 for April, June, and August hindcasts, respectively. Since 2011 the early December forecast has been qualitative rather than quantitative due to the lack of real-time forecast skill. All the quantitative forecasts also feature landfall probabilities for 11 U.S. coastal regions and every island in the Caribbean based on the principle that during a more active TC season there is a greater probability of landfall (Klotzbach and Gray, 2012a, b, c).

2.3.2 Tropical Storm Risk

The Tropical Storm Risk (TSR) group is based out of the Benfield Hazard Research Centre within University College London and has been issuing forecasts of the following TCPs for the Atlantic since 2000: 1) ACE, 2) number of TCs, 3) Hs, and 4) MajH, 5) ACE of land falling TCs, 6) number of land falling TSs, 7) Hs, and 8) MajHs (Camargo et al., 2007). Monthly leads out to 10 months from 1 August are considered. Forecasts are developed using linear OLS regression modeling with predictors being updated at each new monthly issuance. The forecast model is constructed using NCEP/NCAR reanalysis data from 1950-2011. The two predictors are July-September forecast 925-mb zonal wind over the Caribbean and the North Atlantic and, secondly, August-September forecast SST for the MDR (Saunders and Lea, 2005).

July-September forecast 925-mb zonal wind is predicted by using August-September forecasts of ENSO SSTs from the consolidated 18-member ensemble version of the ENSO-

CLIPER model (Llyod-Hughes et al., 2004). 925-mb zonal wind was selected because it reflects the speed of the trade wind over the Caribbean and North Atlantic and because it is a good proxy for vertical wind shear over these same regions. If 925-mb zonal wind is predicted to weaken then vertical wind shear will be reduced causing a greater likelihood of an enhanced TC season. August-September SST is forecasted using the same model as aforementioned with warmer-than-normal SSTs in the MDR being linked to high ACE values. The forecast skill of the ENSO-CLIPER model for these two predictors at the early August issuance are 73% and 86%, respectively (Saunders and Lea, 2012). Modeled and observed ACE from 1950-2003 are significantly correlated ($r = 0.78$) at the early August issuance (Saunders and Lea, 2004). Since 2005 TSR has also issued landfall probabilities for the US coastline using winds patterns at heights between 750 and 7,500 meters across six regions of North America, the East Pacific and Atlantic Oceans during July for the August forecast (Klotzbach et al., 2011).

2.3.3 National Oceanic and Atmospheric Administration

The National Oceanic and Atmospheric Administration (NOAA) has been issuing seasonal forecasts, which they call seasonal outlooks, since 1998 with outlooks being issued in late May and early August each year (Klotzbach et al., 2011). Their outlooks include predictions of the total number of TSs, Hs and MajHs, and ACE for the upcoming TC season. Their statistical model is based on four predictors: 1) an August-October ENSO forecast, 2) the tropical multi-decadal signal, 3) a forecast of August-October Atlantic basin SSTs, and 4) a forecast of August-October vertical wind shear across the tropical Atlantic (Klotzbach, 2007). The August-October ENSO forecast takes into account the model predictions of ENSO from the following dynamical models: NOAA's Coupled Forecast System (CFS), NOAA's Geophysical Fluid Dynamics Laboratory (GFDL), the European Centre for Medium-Range Weather Forecasting

(ECMWF), the United Kingdom Meteorology office (UKMET), and the European Seasonal to Interannual Prediction ensemble (EUROSIP). The tropical multi-decadal signal is determined by incorporating the observations of the AMO and the magnitude of the West African monsoon (NOAA, 2012b). When the AMO is in its positive phase vertical wind shear is reduced, above-average SSTs, and below-average SLP are experienced throughout the Atlantic leading to greater instability and enhanced low-level convergence (Goldenberg et al., 2001). Both the August-October SSTs and vertical wind shear forecasts come from the CFS model. The forecast model output is then qualitatively refined by incorporating an analog forecasting approach and gathering the consensus of forecasters from the following NOAA climate and weather centers: the Climate Prediction Center (CPC), the National Hurricane Center (NHC), and the Hurricane Research Division (HRD).

2.3.4 Cuban Meteorological Institute

The Cuban Meteorological Institute (INSMET) has been issuing seasonal forecasts since 1996 (Camargo et al., 2007). Their forecasts include predictions of: 1) number of TSs and TCs in the Atlantic MDR, Caribbean and Gulf of Mexico (separately), 2) first date of TC genesis, 3) last day with TC activity, and 4) number of TCs that form in the Atlantic MDR and impact the Caribbean (Camargo, et al., 2007). These predictions are based on five environmental parameters: 1) North Atlantic winds, 2) observed and predicted ENSO, 3) intensity of the Atlantic subtropical ridge, 4) North Atlantic SSTs, and 5) observed QBO (Camargo et al., 2007, Klotzbach, 2007). As with many of the other forecasting groups INSMET also utilizes an analog method in combination with their statistical regression model outputs to refine their forecasts.

2.3.5 North Carolina State University

North Carolina State University (NC State) has been issuing seasonal forecasts since 2006 (Camargo et al., 2007) for predictions of the total number of TSs, Hs, and MajHs for the Gulf of Mexico, Caribbean, and Atlantic basins separately, as well as the total number of landfalls for the Gulf, Southeast, and Northeast coasts of the USA (Xie et al., 2012). All the predictors except for the ENSO index are gathered from the CPC while the ENSO index is a forecast value from the CFS model (See Table 2.3). The statistical model utilizes a log-linear OLS regression approach, which works under the assumption that the log of the prediction parameters are linearly related to the selected climate indices.

Table 2.3 NC State's list of indices and their monthly averages that were used as predictors in their seasonal forecast of the 2012 TC season (Adapted from Xie et al., 2012).

Index	Months Averaged Over
1) Atlantic Meridional Mode	**January-March**
2) Atlantic Multidecadal Oscillation	**January-February**
3) Dipole Mode	**January-March**
4) North Atlantic Oscillation	**January-March**
5) Forecasted El-Niño-Southern Oscillation Region 1 & 2	**July-September**
6) Tropical North Atlantic	**January-February**
7) Tropical Southern Atlantic	**November-January**
8) Western Hemisphere Warm Pool	**August-November**

2.3.6 Florida State University

Florida State University (FSU) does not issue any operational seasonal forecasts for the Atlantic but FSU researchers developed some pioneering methods in the statistical modeling of Atlantic TC activity and landfall. In 1993 FSU researchers showed that using a nonlinear Poisson regression model instead of the linear model when modeling MajH occurrences had a 40% increase in hindcast skill when compared to a linear model (Elsner and Schmertmann, 1993).

FSU researchers also discovered that the phase of the NAO influenced the tracks of TCs showing that when the NAO is positive (excited) TCs tended to recurve into the higher latitudes of the North Atlantic making the US East Coast more susceptible to TC strikes while in its negative (relaxed) phase TCs tended to be nonrecurving and stay in lower latitudes making the US Gulf Coast more susceptible to strikes (Elsner et al., 2000). FSU researchers were also the first to build a Bayesian model of seasonal TC activity and landfalls over the USA using May-June values of the NAO, SOI, and the AMO as predictors (Elsner and Jagger, 2004; 2006).

2.4 Forecast Skill Metrics

Testing the skill of the various forecasts produced by the different groups is of critical importance in order the show the accuracy of their models. Models that have good skill are validated models that consistently make correct TCP predictions. Validated models are those that have been tested against historical data, referred to as hindcasting, to assess how well the model has predicted past TC seasons. If a model's hindcast is similar to historical TC observations, then the model is said to have skill. Models that show substantial hindcast skill allow for greater confidence in future TCP predictions. In recent years, there has been a call for a standardization of model output (i.e., TCPs) and verification skill measure used to judge model performance (Camargo et al., 2007; WMO, 2002). Camargo et al. (2007) proposed seven possible verification skill scores that could be used for deterministic model assessment: 1) mean root square error skill score, 2) Pearson correlation coefficient, 3) Spearman rank correlation coefficient, 4) uncentered correlation coefficient, 5) bias compared to climatology, 6) percentage improvement over trend, and 7) normalized natural categories skill score. Table 2.4 summarizes all the statistical forecasting groups by their TCPs predicted, predictors, and validations methods.

Table 2.4 Statistical forecasting groups' predictors, predictands, and validation and skill methods used to provide their Atlantic seasonal tropical cyclone forecasts. (Table adapted from Camargo et al., 2007 Table II).

GROUP	PREDICTORS	PREDICTANDS	VALIDATION/SKILL METHODS
CSU	• Sea surface temperatures in the North and South Atlantic • Sea level pressure at Atlantic and Pacific Oceans • Upper- and low-level zonal winds over the Pacific and Atlantic Oceans • ENSO forecasts	• Tropical storm count • Tropical storm day count • Tropical cyclone count • Tropical cyclone day count • Intense tropical cyclone count • Intense tropical cyclone day count • Accumulated cyclone energy • Net tropical cyclone activity	• Jackknife cross-validation • Pearson correlation between modeled and observed NTC • Improvement over climatology
INSMET	• North Atlantic winds • ENSO • Intensity of the Atlantic subtropical ridge • SST North Atlantic • Quasi Biennial Oscillation	• Number of named TCs • Number of hurricanes • Number of TCs in the Atlantic Main Development Region, Caribbean, and Gulf of Mexico (separately) • First day with a TC formation • Last day of TC formations	• Cross validation • Pearson correlation between modeled and observed? • Comparison to climatology

Table 2.4 (Continued)

NC STATE	• Atlantic Meridional Mode • Atlantic Multidecadal Oscillation • Dipole Mode • North Atlantic Oscillation • Forecasted El-Niño-Southern Oscillation region 1 & 2 • Tropical North Atlantic • Tropical Southern Atlantic	• Number of tropical storms, hurricanes, and major hurricanes in the Atlantic, Caribbean, and gulf of Mexico (separately) • Number of landfalls for the gulf, southeast, and northeast coasts of the USA	• Cross validation • Comparison of the 95% prediction intervals to climatologies at >50, 20, 15 year values
NOAA	• ENSO forecast • Tropical Multi-Decadal Signal • Atlantic sea surface temperatures • Forecast of vertical wind shear over tropical Atlantic	• Number of tropical storms, hurricanes, and major hurricanes • Accumulated Cyclone Energy	• Cross-validation • Mean absolute error • Comparison to climatology • Contingency tables
TSR	• Forecast of sea surface temperatures in the Atlantic main development region • Forecasts of 925 mb zonal wind over the Caribbean and North Atlantic	• Accumulated Cyclone Energy • Number of tropical storms, hurricanes, and major hurricanes • ACE of land falling Tropical cyclones • Numbering of land falling tropical storms, hurricanes, and major hurricanes	• Cross validation using block elimination • Pearson correlation coefficient with p-value between hindcast and observations • Mean square error • Improvement over climatology

All six of the forecast groups presented used predictors that were taken from continental and/or oceanic temperature, pressure, and/or wind fields that relate back to large-scale atmospheric and oceanic CMs such as AMO, ENSO, or NAO. Many of these CMs are based on atmosphere-ocean interactions. SI and SC are both capable of e\affecting these interactions by altering the energy fluxes between the surface types. With rapid changes in SI (Stroeve et al., 2012) and SC (Dery and Brown, 2007) being experienced throughout the Northern Hemisphere

some researchers have started to investigate the possible linked between SI and SC variability and TCs (Ke, 2007, Choi et al., 2010, Yan et al., 2012).

2.5 The Cryosphere and Tropical Cyclones

The cryosphere is the frozen part of the climate system consisting of: snow cover, river and lake ice, sea ice, glaciers and ice caps, ice shelves and sheets, and frozen ground, but for the purpose of this study the cryosphere will only refer to SI and SC since their interactions with CMs and TCs are of primary interest. Fresh SC has a very high albedo (0.8-0.9) that leads to a direct snow-albedo feedback that influences the surface energy budget and Earth's total radiative balance (IPCC, 2007) as well as indirect feedbacks on atmospheric circulation at varying timescales (Bojariu and Gimeno, 2003; Bartolini et al., 2010). SI plays an important role in the cryosphere because: 1) its direct ice-albedo feedback is crucial to the climate response at high latitudes, 2) it modifies the exchange of heat, gases, and momentum between the atmosphere and the ocean, and 3) it alters ocean buoyancy by redistributing freshwater via the movement and melting of SI through the polar oceans (IPCC, 2007).

Beyond having multiple direct and indirect feedbacks on the atmosphere and the ocean the cryosphere also exhibits high annual and decadal variability. Since 1979 when satellite observations became available, Arctic SI has shown an average maximum areal extent of approximately $15.86\times10^6\,km^2$ in March (NSIDC, 2012a) and an average minimum of approximately $6.14\times10^6\,km^2$ in September (NSIDCb, 2012). In recent years though, minimums have been closer to $4\times10^6\,km^2$ with $3.41\times10^6\,km^2$, $4.33\times10^6\,km^2$, and $4.17\times10^6\,km^2$ being experienced in 2012, 2011, 2007, respectively (NSIDCb, 2012). Figure 2.7 reveals that September SI minimums have experienced a rapid downward trend of 12.4% per decade between 1979-2010 (Stroeve et al., 2012). Maximums are also on the decline with the last nine years

(2004-2012) being the lowest on satellite record (NSIDC, 2012a). SC features even more variability than SI with an average maximum of approximately 46.7×10^6 km^2 in December and a minimum of approximately 3.1×10^6 km^2 in August (Robinson, 2012). SC not only features greater variability then SI but also a greater decline with Northern Hemisphere June SC between 1979 and 2012 declining at -17.6% per decade (NOAA, 2012c). The cryosphere exhibits large variability (NSIDIC, 2012a; Robinson, 2012) and has known impacts on surface energy fluxes that lead to changes in temperature, pressure, and wind fields (IPCC, 2007; Budikova, 2009; Bartolini et al., 2010). As previously mentioned, these three atmospheric fields are the primary predictors in seasonal forecasts of TCs, so further research into the cryosphere's influence on these fields is required

Currently there are three studies that investigate the link between the cryosphere and TCs (Ke, 2007, Choi et al., 2012, Yan et al., 2012). Of these studies Ke (2007) and Choi et al. (2010) investigated the cryosphere and TC activity only for the western North Pacific, while Yan (2012) provided the only study that investigated the Atlantic. A brief description of each study and their findings will be given.

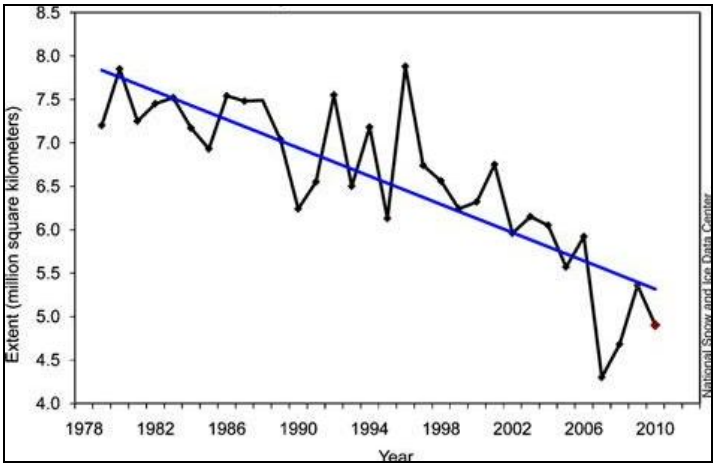

Figure 2.6 A -12.4% linear trend in the average minimum Arctic sea ice extent that occurs annually in September (adapted from Stroeve et al., 2012 Figure 1).

Ke (2007) investigated North Pacific SIE in March-April-May (MAM) and how it related to subsequent annual TC counts in the tropical western North Pacific (TWNP) between 1965-2004. Correlation analysis between MAM-SIE and annual TCs revealed a correlation coefficient of -0.49. Correlation analysis was also used to investigate high and low SIE years and how they relate to SLP, SST, and atmospheric circulation anomalies. Years with ENSO events featuring ±0.5˚C SST anomalies and lasting for six months during December through May were removed from the correlation analysis in order to better isolate the SIE signal on these three atmospheric fields. High MAM-SIE years were shown to reduce the TC activity through increases in SLP and vertical wind shear, and reductions in SSTs through the TWNP's MDR. Low MAM-SIE years were shown to exhibit the opposite pattern with decreases in SLP and vertical wind shear and increases in SSTs within the MDR. These patterns correspond well with the North Pacific Oscillation (NPO) with a positive phase occurring during low MAM-SIE years and the negative phase occurring during high MAM-SIE years.

The Choi et al. (2010) study was the first to develop multiple regression models for seasonal forecasting of TC frequency in the western North Pacific using three CMs for the period 1951-2007 while incorporating cryospheric data. The three predictors chosen for the models were April 500 hPa meridional wind and 850 hPa zonal wind, and May 200 hPa zonal wind. Each of these predictors correspond to a different CM with April 500 hPa meridional wind, April 850 hPa zonal wind, and May 200 hPa zonal wind corresponding to the Siberian High Oscillation (SHO), Antarctic Oscillation (AAO), and the NPO, respectively. The hindcast model output correlate well ($r = 0.65$) with observed TC frequency. The 17 highest and lowest TC frequency years were then synoptically analyzed by looking at large-scale environmental features present during the April and May proceeding the TC season. During high TC frequency years the SHO

and NPO tended to be in their positive phase and the AAO in its negative phase. Low TC years experience the opposite conditions. The strength of the SHO can be influenced by SC anomalies across eastern Asia with anomalous anticyclonic circulation (positive SHO) over eastern Asia being experienced during boreal springs with above-average SC and the opposite condition during below-average SC. Atmospheric circulation anomalies were also seen in the North Pacific, where SI has been shown to influence the strength of the NPO during winter and spring by altering the strength of the Aleutian low (Tachibana et al., 1996). When spring SI is more (less) expansive the Aleutian low tends to be stronger (weaker) resulting in a positive (negative) NPO.

Lastly, Yan et al., (2012) investigated North American SCE in January-February and Atlantic TC activity between 1950-2009 with the ENSO signal detrended from the data. North American SCE was chosen due to previous studies looking into SCE variability as it relates to the intensity of the North American monsoon (Hawkins et al., 2002) and atmospheric circulation anomalies over the tropical and subtropical Americans and adjacent oceans during monsoon seasons (Ellis and Hawkins, 2001). Correlation coefficients between January SCE and North Atlantic TCs and January SCE and ACE are -0.29 and -0.24, respectively. During high and low SCE years different atmospheric circulation anomalies were present during the peak TC months of August and September across the Atlantic's MDR. When anomalously low SCE was present during January and February an increase in TC activity was observed due to the following: 1) an amplified subtropical ridge, 2) weaker TUTT, 3) anomalous 200 hPa easterly winds, 4) weaker low-level easterly trade winds, along with an anomalous cyclonic circulation, 5) below-average 1000 hPa geopotential heights, 6) warmer SSTs, 7) decreased vertical wind shear, and 8) a strengthening and northward shift of the ITCZ across the eastern tropical Pacific and Atlantic

Oceans. Conversely, when anomalously high SCE was present a decrease in TC activity was expected due to the following: 1) near average strength of the TUTT, 2) increased low-level easterly trade winds, 3) below-average SSTs, 4) near normal vertical wind shear, and 5) an overall weaker ITCZ confined to the deep tropics. Many of these environmental conditions have been linked to the persistence of the AO from spring into summer. Walland and Simmonds (1996) showed that anomalous snow boundary conditions can lead to a change in meridional temperature gradients over the North Atlantic Ocean thereby influencing the phase of the AO through alterations to baroclinic zones and upper-level circulation anomalies.

Of the three studies that investigated cryosphere-TC relationship only Choi et al. (2010) developed statistical models using wind field data at various heights. However, Choi et al. (2010) only indirectly related the cryosphere to these predictors, while Fe (2007) and Yan et al., (2012) directly investigated the cryosphere-TC relationship, but without developing a statistical model. Though only looking at the cryosphere indirectly, Choi et al. (2010) conducted the only study that analyzed both SC and SI data as they pertain to the strength of various CMs, while Fe (2007) only investigated North Pacific SI and Yan et al. (2012) investigated only North American SCE. There are no statistical modeling studies directly investigating the link between SC and SI throughout the entire Northern Hemisphere to Atlantic TC activity. Both Ke (2007) and Yan et al. (2012) mentioned that further modeling, both statistical and dynamical, would be helpful in improving our understanding of how the cryosphere can influence atmospheric circulation that conducive to tropical cyclogenesis. A better understanding of the physical mechanisms linking the cryosphere and TCs may lead to the inclusion of cryospheric data into current operational seasonal forecasting schemes.

CHAPTER 3

METHODOLOGY

3.1 Introduction to Methodology

This study utilizes multiple datasets and analytical methods in order to investigate the cryosphere-CM-TC relationships. This chapter will present the datasets, analytical methods, the statistical forecasting scheme, and the model evaluation techniques used for this study.

3.2 Datasets and Study Period

There were a total of four datasets used in this study. The TC data came from the HURDAT "best track" dataset, which is maintained by NOAA's National Hurricane Center (NHC: Jarvinen et al., 1984). HURDAT has observational data on each Atlantic TC from 1851 to 2010 (NHC, 2012). HURDAT features 6-hourly (0000, 0600, 1200, 1800 UTC) observations of storm center location given in latitude and longitude, the intensity of the storm as measured by its maximum 1-minute surface wind speed in knots, and the storm's minimum central pressure in millibars. Additionally, starting in 1950, each storm is given a name according to the naming convention specified for that given year. Monthly CM indices since 1950 for the AO, ENSO, NAO, PNA, and QBO were downloaded from NOAA's Earth System Research Laboratory (ESRL) – Physical Science Division (ESRL, 2012).

SIA and SIE data came from the National Snow and Ice Data Center's (NSIDC) Sea Ice Trends and Climatologies dataset (Stroeve, 2003). The NSIDC dataset features SIA and SIE for 10 geographic regions (See Figure 3.1) throughout the Northern Hemisphere for each month between November 1978 and December 2010. SIA is defined as the actual amount of SI present on the surface of the ocean. It is calculated by determining the concentration of SI within a given satellite data pixel. The NSIDC uses a 15% concentration threshold within each pixel, which

means that if 15% or more SI is present in a pixel then that percentage is multiple by the total area of that pixel. For example, if a pixel covers 1000 km^2 and has an observed SI concentration of 64% then the resulting SIA for that pixel would by 640 km^2, but if pixel has a concentration less than 15% than that pixel is considered ice-free. Conversely, SIE is defined simply as if the pixel is ice covered or not. The threshold again is 15%, so a 1000 km^2 pixel is covered by 64% then that entire pixel is considered ice covered, meaning the SIE value would be 1000 km^2. SCE data came from Rutgers University's Global Snow Lab's (GSL) Monthly Area of Extent dataset and features SCE for four geographic regions in the Northern Hemisphere for each month since November 1966 (GSL, 2013). SCE is defined in a similar manner as SIE (e.g., in that the pixel is considered snow covered or not, but with a 50% concentration threshold instead of 15% (Robinson et al., 1993). See Table 3.1 for a summary of all datasets and parameters derived.

Since the datasets described above have different observation periods, a common period was chosen to encompass all the datasets – 1980-2010. 1980 is the start of the study period because the 1980 TC season was the first that had complete SIA and SIE data for the preceding year (i.e., 1979). 2010 is the last year of the study period because 2010 is the latest available year in the HURDAT and NSIDC datasets.

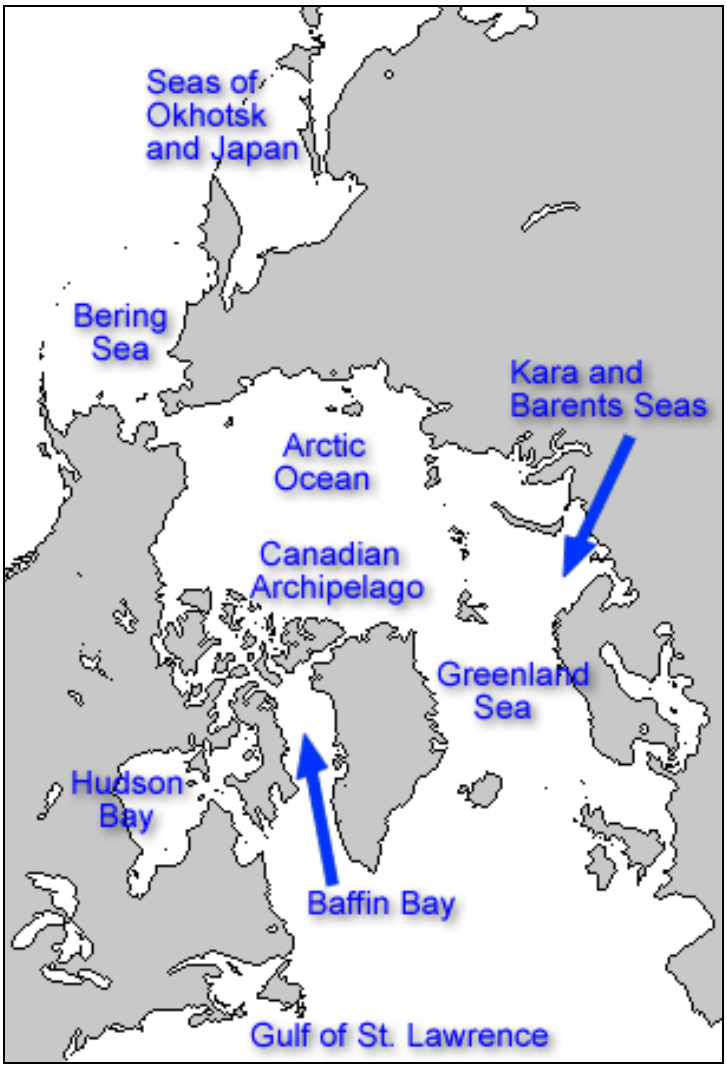

Figure 3.1 The nine geographic regions for which sea ice area and sea ice extent data are available. The 10th geographic region is the total Northern Hemisphere sea ice (NSIDC, 2013b).

Table 3.1 Summary of the datasets used in this study and the parameters derived from them. Acronyms are: ESRL (Earth System Research Laboratory), GSL (Global Snow Lab), HURDAT (hurricane database), NSIDC (National Snow and Ice Data Center), TCs (tropical cyclones), and TSs (tropical storms). The term seasonal mean stands for the four meteorological seasons (DJF, MAM, JJA, SON).

Datasets			
HURDAT	ESRL: Climate Modes	NSIDC: Sea Ice Area and Extent	GSL: Snow Cover Extent
TC season parameters	3 month seasonal mean derived from datasets		
• Annual TCs • TSs • Hurricanes • Minor TCs • Major TCs • Accumulated Cyclone Energy • Power Dissipation Index • Landfalls • Annual mean peak wind • Lifetime mean duration of storm • First cyclogenesis • Last cyclogenesis • Total Season Length	• Arctic Oscillation • El Niño-Southern Oscillation • North Atlantic Oscillation • Pacific North American Pattern • Quasi-Biennial Oscillation	• Arctic Ocean • Baffin Bay • Barents and Kara Seas • Bering Sea • Canadian Archipelago • Greenland Sea • Gulf of St. Lawrence • Hudson Bay • Seas of Okhotsk and Japan • Total Northern Hemisphere	• Eurasian • North American and Greenland • Total Northern Hemisphere
Total number of parameter derived from each dataset			
13	20	80	12

3.3 Predictors and Predictands

From the datasets listed in Table 3.1, 13 TCPs were calculated from HURDAT and four seasonal averages for the CMs, SIA/SIE, and SCE from ESRL, NSIDC, and GSL data, respectively. The 13 TCPs were chosen in order to comprehensively describe TC climatology and to allow for comparison between current forecasting groups (Klotzbach and Gray, 2012c; Saunders and Lea, 2005). Seasonal averages were calculated using the meteorological definition of the seasons (DJF, MAM, JJA, and SON). Seasonal averages were chosen instead of shorter time scales (e.g., monthly or weekly) because the goal was to analyze the overall seasonal

environmental characteristics preceding a given TC season. To further justify the use of seasonal averages, Overland and Wang (2010) showed that seasonal changes in summer SIE are associated with changes in the phase of the AO that tended to persist into late fall and winter, suggesting that environmental changes in one season can influence subsequent seasonal climate variations. In the statistical forecast scheme the 13 TCPs are the predictands (i.e., dependent variables) while the seasonal averages of each CM and of the 13 cryospheric regions are the predictors (i.e., independent variables). The statistical forecast scheme therefore included 13 predictands and 112 possible predictors.

3.4 Analytical Methods and Forecasting Scheme

Cross correlation and linear correlation coefficient tables have appeared in numerous statistical forecasting studies in the past (Klotzbach and Gray, 2004; Gray et al., 1994). Therefore, before the forecasting scheme was developed, cross correlation analysis was conducted between the seasonal SIE values, SIA values, seasonal CMs values, and 13 TCPs, with the aim of identifying relationships among the predictors and predictands. Following the cross correlation analysis, hindcasts were developed at four lead times before and within the Atlantic TC season based on the passing of each season. Thirteen separate statistical models, one for each TCP, were developed after each season's averages were derived leading to a hindcast issued in December, March, June, and September as the fall, winter, spring , and summer averages became available. For example, for any given TC season (1 June through 31 November) three hindcasts (December, March, and June) were issued before the start of the TC season while one was issued during the season (September).

Each forecast was created using of multiple linear OLS regression within the statistical software program MATLAB 2007a. In order to develop the regression equations that governed

each model, a stepwise procedure was used to select the most statistically significant predictors from the various subsets of seasonal averages determined by the hindcast issuance. The stepwise selection procedure used a statistical significance value of $\alpha = 0.05$ in order to determine which predictors were going to be included within the models. Within the 1980-2010 study period three groups of models were constructed based on the available predictors (See APPENDIX D for MATLAB code). These groups were the CM-only models, CRYO models, which only had SIE, SIA, and SCE data, and CM-CRYO models, which had both the CM and cryospheric data available during the stepwise selection procedure. These three model groups were chosen to indentify which variables best predicted the TCPs. The number of predictors available for the selection procedure at each hindcast varied from 20 (four seasonal averages of five CMs) for the CM models to 92 predictors (four seasonal averages of 23 cryosphere regions) for the CRYO models to 112 (four seasonal averages of five CMs and four seasonal averages of 23 cryosphere regions) for the CM-CRYO models. For each model group's hindcasts, the number of predictors the stepwise procedure was able to choose from increased by five for the CM models, by 23 for the CRYO models, and by 28 for the CM-CRYO models (See Table 3.2). For example, the March hindcast of the CM-CRYO models utilized both fall and winter seasonal averages of the 23 regional cryospheric values and five CM values giving the stepwise procedure a maximum number of 56 predictors to choose from, but for the March forecast of the CM models only the fall and winter averages of the five CMs would be available allowing for a maximum of ten possible predictors. Regardless of the model group, a total of 52 models were developed one for each TCP and at each of the four lead times resulting in 156 total models.

Table 3.2 Forecast scheme in terms of month of hindcast issuance and maximum possible seasonal predictors included for a particular hindcast. Acronyms are: CM (climate modes), SC (snow cover), SIA (sea ice area), and SIE (sea ice extent).

SEASONAL MEANS OF PREDICTORS	1980-2010 STUDY PERIOD FORECAST ISSUANCE			
	December	March	June	September
Fall	CM: 5 SIA: 10 SIE:10 SC: 3	CM: 5 SIA: 10 SIE:10 SC: 3	CM: 5 SIA: 10 SIE:10 SC: 3	CM: 5 SIA: 10 SIE:10 SC: 3
Winter		CM: 5 SIA: 10 SIE:10 SC: 3	CM: 5 SIA: 10 SIE:10 SC: 3	CM: 5 SIA: 10 SIE:10 SC: 3
Spring			CM: 5 SIA: 10 SIE:10 SC: 3	CM: 5 SIA: 10 SIE:10 SC: 3
Summer				CM: 5 SIA: 10 SIE:10 SC: 3
Total possible predictors	28	56	84	112

3.5 Model Evaluation

Before the models were evaluated, their hindcast skill was assessed using a cross validation technique (see Elsner and Schmertmann, 1994), which is standard practice in statistical forecasting (see Xie et al., 2012; Klotzbach and Gray, 2012b; Klotzbach et al., 2011; Klotzbach, 2007; Camargo et al., 2007; Saunders and Lea, 2005). For this study, cross validation was performed using a leave-one-out (i.e., jackknifing) approach, so that one year worth of data were left out and the remaining years' data were used to build the model and produce a hindcast for the year that was left out. This process was then repeated until data for each year were left out producing a final hindcast for each of the 156 models. The evaluation techniques used to test

model performance were the Pearson correlation coefficient, R^2 value, mean absolute error value, and mean square error skill score (MSSS) in addition to comparing each model with climatology. After model evaluation, the best performing models were then compared to the current, operational models to analyze the effects of including cryospheric data into a statistical forecasting scheme. Once the top performing models were identified the top eight most frequently selected predictors were analyzed to determine the physical mechanisms driving the relationship.

3.6 Physical Mechanism Investigation

The top eight predictors were analyzed in order to determine their role in TCP variability. The top eight predictors included of the four top CM predictors and the four top cryospheric predictors. These predictors were chosen because a comparison between CM and cryospheric predictors was necessary to investigating the role CMs and the cryosphere played in the TCPs variability. The top eight predictors were comprised of roughly the top 20% of the total chosen predictors from the best performing model group. To further analyze these key predictors, each predictor were analyzed through NOAA's Earth System Research Laboratory – Physical Sciences Division's interactive plotting and analysis tool, which allowed for maps of linear correlations between the key predictors and gridded NCEP reanalysis data to be created (ESRL, 2013). The interactive plotting and analysis tool was very user friendly allowing the user to specify correlations between 24 predefined atmospheric variables at 24 levels and 45 predefined time series. Users are also able to upload their own custom time series. Correlation maps could be produced for any study period between January 1948 and February 2013 for any user defined month or season with the user being able to plot correlations on three map projections for any region of the globe.

This interactive plotting tool allowed for spatial correlation plots to be created between the key predictors and seasonal environmental factors known to influence TC activity, such as SSTs, SLP, and wind speed/wind shear. If any of the key predictors showed strong correlations with any of these environmental variables within the Atlantic's MDR, then composite maps were constructed, again, using the interactive plotting tool. The top seven lowest and highest years [Roughly the top third and bottom third of the study period] of these key predictors were used to construct the composite maps. Composite maps were constructed using the same environmental variables as the correlation plots, which allowed for the determination of differing environmental conditions present in the Atlantic's MDR between the lowest and highest years. The key predictors that showed both strong correlation plots and agreement between the composite maps were then further analyzed to determine why these key predictors might be causing these correlations plots and composite maps to highlight the environmental conditions leading to an enhanced or suppressed TC season.

3.7 Chapter Summary

In this chapter the methodology that was used for this study was presented. NOAA's HURDAT and ESRL datasets were used for the calculation of the 13 TCPs and four seasonal averages for each of the 5 CMs, respectively. The NSIDC and GSL datasets were used in the calculation of the four seasonal averages of each of the ten regional SIA/SIE values and three regional SCE values, respectively. Stepwise multiple OLS regression was used to select the most statistically significant CM, SIA/SIE, and SCE parameters as predictors for the models. A total of 156 models were built – one for each of the 13 TCPs, at each of the four hindcast issuance dates (December, March, June, September), and for the three model groups (CM, CRYO, CM-CRYO). Models were then validated using a jackknife approach to create hindcasts for each of the TCPs.

These hindcasts were evaluated using a variety of hindcast skill measures (e.g., R^2 values, MSSS values, comparison to climatology) to identify the best performing models. The eight most frequently selected predictors were analyzed using an interactive plotting tool from NOAA's ESRL to construct correlation plots and composite maps of environmental variables known to influence TC activity to determine possible physical mechanisms that are causing these key predictors to influence TC activity. These models were then compared to current operational statistical models to assess the effects of including cryospheric data in a forecasting scheme.

CHAPTER 4

RESULTS

4.1 Introduction to Results

In this chapter the results of the statistical models, outlined in the previous chapter, will be presented along with an interpretation of the results. This chapter is divided into six subsections: 1) climatology of the study period, 2) model diagnostics and key predictors, 3) correlation analysis between the key predictors and environmental conditions known to influence TC activity in the Atlantic, 4) composite analysis of the key predictors and the environmental conditions identified in the previous subsection, 5) possible physical mechanisms governing the SIA and TC relationship, and 6) model comparison against current operational statistical models.

4.2 Climatology of Study Period

A climatology of the study period is provided in Table 4.1 as a frame of reference for the relative skill of the models. Statistical models of seasonal TC activity are frequently compared to climatology in order to gauge whether models provide more information about the upcoming TC season then a simple average (climatology). Statistical models of TC activity are considered helpful when, for example, the known climatology (Table 4.1) of the total number of TCs for the upcoming Atlantic TC season is 12, and the model predicts 16 but the actual number of TCs the season observed was 15. This prediction of 16 by the model is very close to the observed number of TCs of 15, which means the model accurately predicted above-normal activity for TCs for that particular season. Predicting TCPs is extremely difficult due to the highly nonlinear behavior of the climate system, but being able to predict the likelihood that a TCP will be above- or below-average is possible and is very important to coastal city planners, government agencies, the economy, and community members. Knowing the likelihood of TC activity allows decision

makers to appropriately allocate resources before and during the TC season. Because of the destructive nature of TCs, modeling of TC activity will continue to be an active area of research, and with increasing global near SATs the relationship between global warming and TC activity is of critical importance.

Table 4.1 Climatology for each of the seasonal tropical cyclone parameters between 1980-2010. Acronyms and units for each of the 13 TCPs are: ACE (Accumulated Cyclone Energy; $10^4 kt^2$), H (hurricanes), LF (landfalls), LMD(lifetime mean duration; days), MAD (maximum day of year), MajH (major hurricanes), MID (minimum day of year), MinH (minor hurricanes), PDI (Power Dissipation Index; $10^6 kt^3$), PW (mean peak wind, ms^{-1}), TC (tropical cyclones), TS (tropical storms), and TSL (total season length: days).

TC	TS	H	MinH	MajH	ACE	PDI	LF	PW	LMD	MID	MAD	TSL
12	5.4	6.6	3.9	2.7	121.8	94.3	1.6	37.8	8.4	177.8	304.8	127.4

4.3 Model Diagnostics

This subsection investigates the performance of the models for each of the seasonal TCPs at the four hindcast issuance dates based on the variance explained (R^2) and mean squared skill score (MSSS) of the models. MSSS is the percentage reduction in mean square error of the model hindcasts compared to the hindcasts made with the climatology values, meaning higher values of MSSS represent larger reductions in mean square error over climatology and a more accurate model.

Figures 4.1 and 4.2 are examples of the hindcasts created by the models for total number of TCs and MajHs, respectively, at the four issuance dates [For the hindcasts of the other TCPs see Appendix – A). There are three hindcasts present at each lead time, one for each model group (i.e., CM, CRYO, and CM-CRYO). The hindcasts show that the CM-CRYO and CRYO models produced identical hindcasts at all issuances for MajHs and at the December and March

issuances for TCs, which shows that the stepwise procedure identified the same predictors for the CRYO and CM-CRYO models. Another feature of the hindcasts is that the CRYO and CM-CRYO models do not have similar hindcasts to that of the CM models. This highlights the fact that differences in the predictors greatly influence the resulting hindcasts.

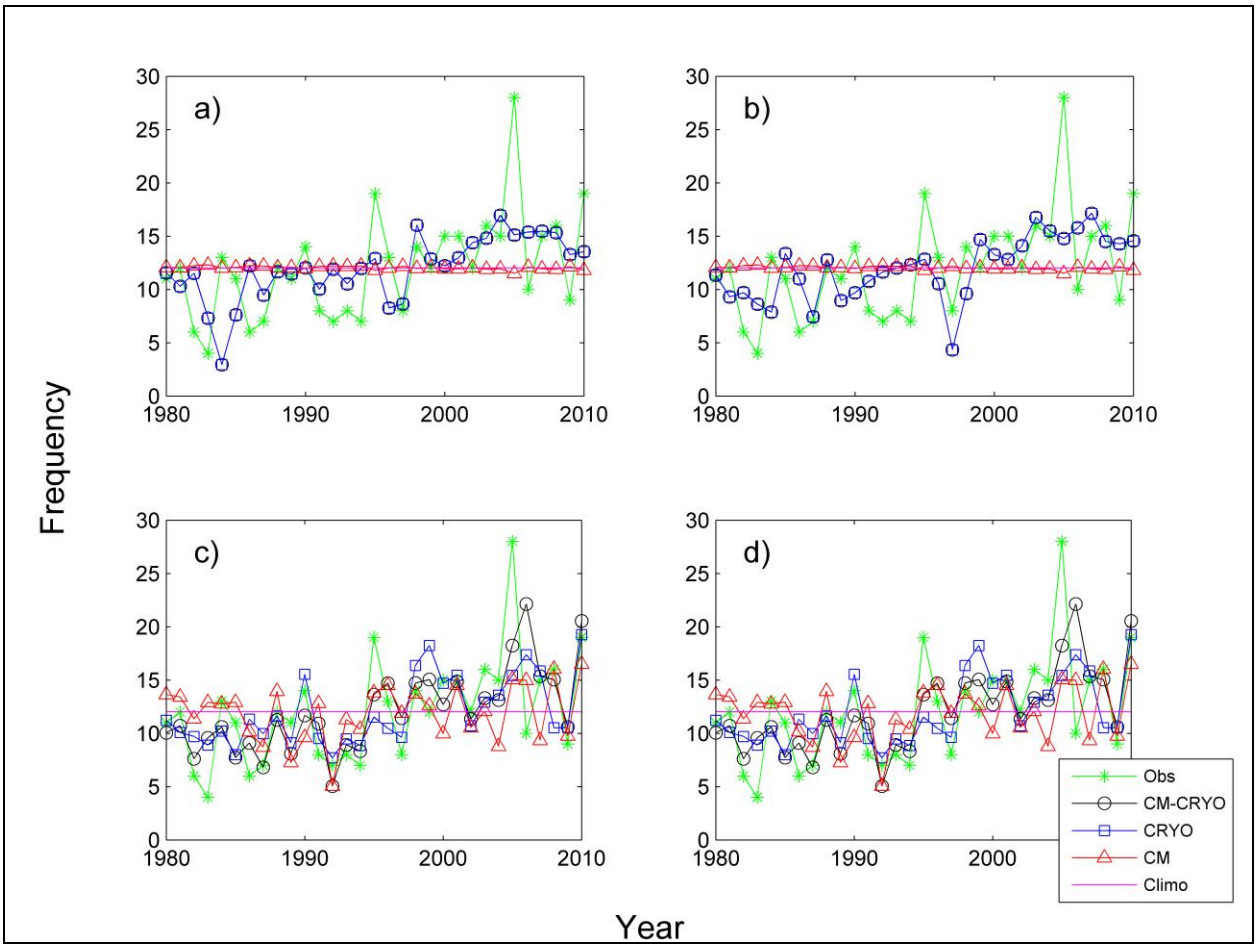

Figure 4.1 December (a), March (b), June (c), and September (d) hindcasts of the three model groups compared to historical observations and climatology for tropical cyclone frequency. The three model groups are climate mode only (CM), cryosphere only (CRYO), and both datasets (CM-CRYO).

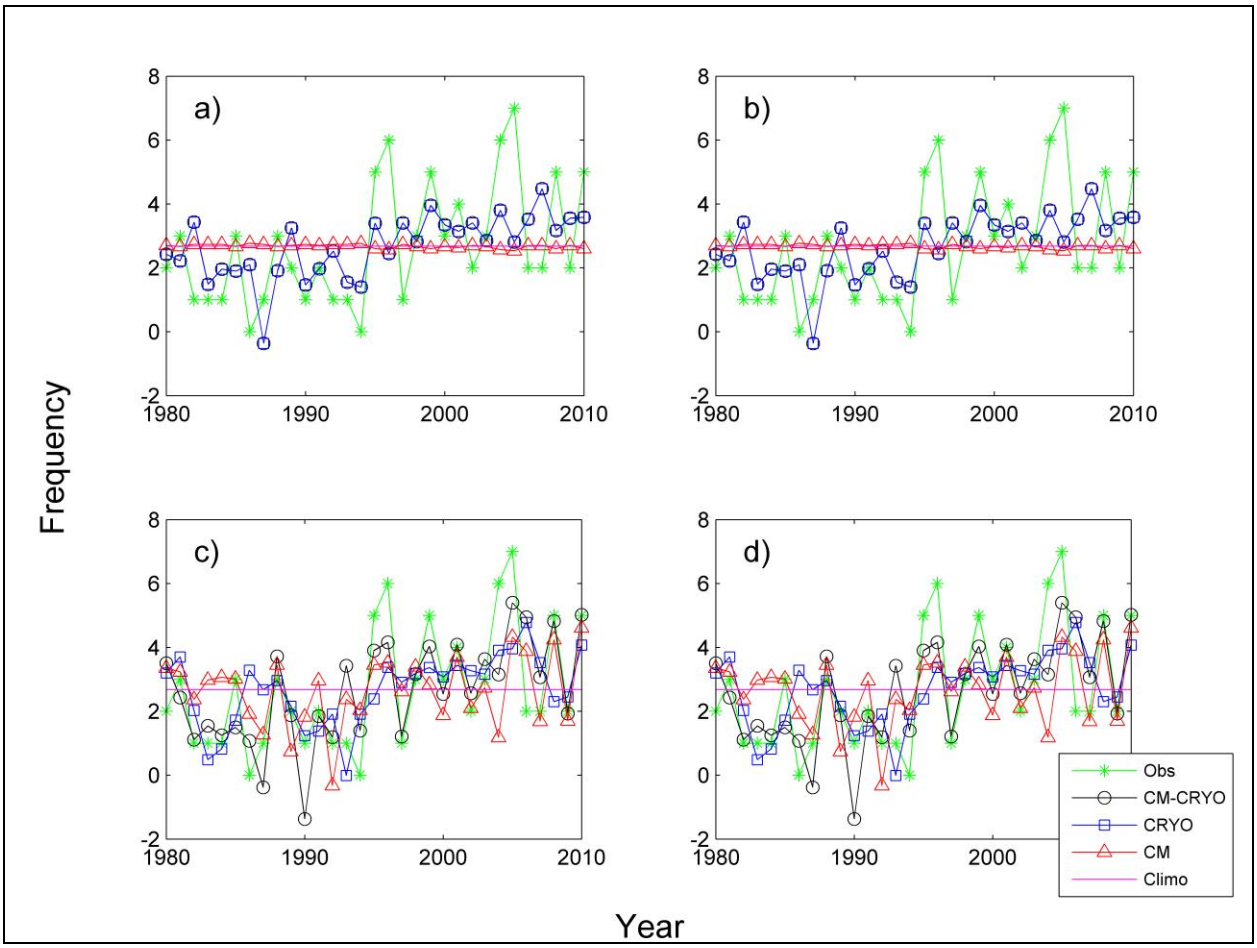

Figure 4.2 December (a), March (b), June (c), and September (d) hindcasts of the three model groups compared to historical observations and climatology for major hurricanes. The three model groups are climate mode only (CM), cryosphere only (CRYO), and both datasets (CM-CRYO).

Figures 4.1 and 4.2 also clearly reveal the large interannual variability of the TCPs with the TCPs never exhibiting climatology. This variability in the TCPs clearly highlights the importance of seasonal forecasts in providing additional information regarding above- or below-normal activity of these TCPs with respect to climatology. Hindcasts are useful for quickly evaluating years when models did well predicting the observed TCPs by locating when hindcasts overlapped observations (e.g., June forecast of MajH in 2001 [Figure 4.1] and June forecast of TCs in 2008 [Figure 4.2]). Hindcasts can also show when models correctly predicted seasons with below- or above-average values of the TCPs by locating when the hindcasts and

observations are both above or below the climatology marker (e.g., June forecast of MajH between 1982-1984 [Figure 4.1] and March forecast of TCs between 2003-2005 [Figure 4.2]). Though analyzing hindcasts against observations and climatology markers can be useful in determining specific periods when the models did well, verification measures must be computed in order to quantify the overall accuracy of the models and allowing for confidence in the models for operational forecasting.

Figure 4.3 shows the variance explained by the models, based on R^2, for 12 TCPs. The TCP lifetime mean duration of storm (LMD) was not included because no significant relationships were present during the stepwise procedure resulting in no regression coefficients to build a model (See Appendix –A). Figure 4.3 highlights one of the key challenges in seasonal forecasting, which is accurate forecasting at long lead times. This challenge is clearly demonstrated when examining the R^2 of the MinH models. There are no data points for all three model groups at the December and March hindcasts because no significant relationships between the possible predictors and MinH variability exist at these lead times resulting in no regression coefficients. Even when models are built, R^2 values are low at the longer lead times of December and March and tend to increase as the start of the TC season approaches as evidenced by the increasing R^2 values at the June and September hindcasts. Also evident in Figure 4.3 is that CRYO and CM-CRYO models often have the same R^2, which shows, (just like in the hindcasts Figures 4.1 and 4.2), that the CRYO and CM-CRYO models are frequently using the same predictors. The R^2 of the CM models are almost always lower than those of the other models highlighting the fact that the CM models are the poorest performing models of the three model groups when only R^2 is considered, and that CMs, alone, are not good predictors for the TCPs.

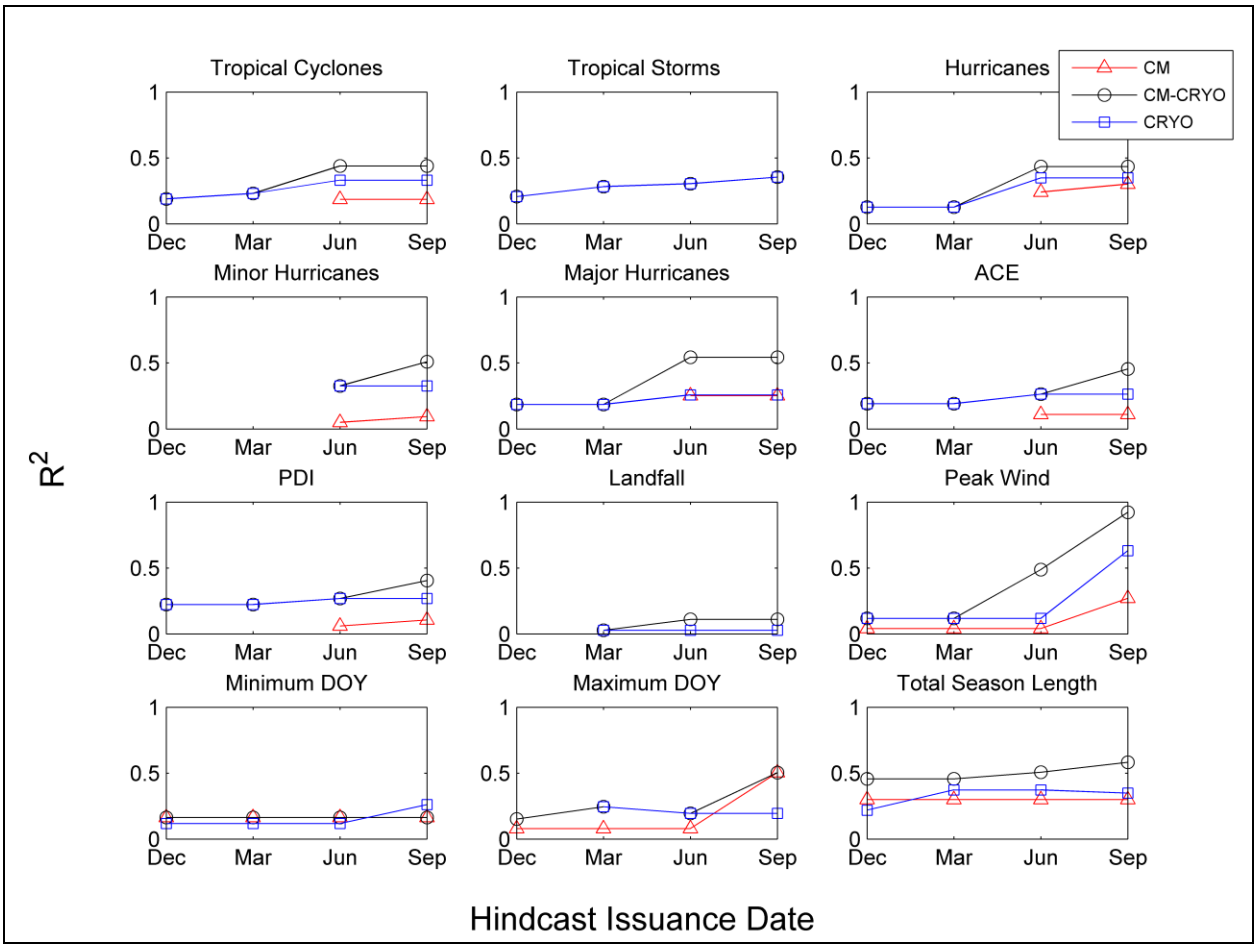

Figure 4.3 Variance explained, based on R^2, by the model groups for 12 tropical cyclone seasonal parameters at the four issuance dates. Missing data points indicate that no models were created. Acronyms are: ACE (accumulated cyclone energy), CM (climate mode only models), CM-CRYO (cryospheric and climate mode models), CRYO (cryospheric predictors only models), DOY (day of year), and PDI (power dissipation index).

Figure 4.4 shows the MSSS of the models at the four lead times for the 12 TCPs. Again, the CRYO and CM-CRYO models perform identically in most cases, while the CM models have lower values. The power of evaluating MSSS instead of R^2 is that MSSS quantifies the skill of models relative to climatology. MSSS values also increase as the lead times become shorter with the highest MSSS values occurring during the September hindcasts.

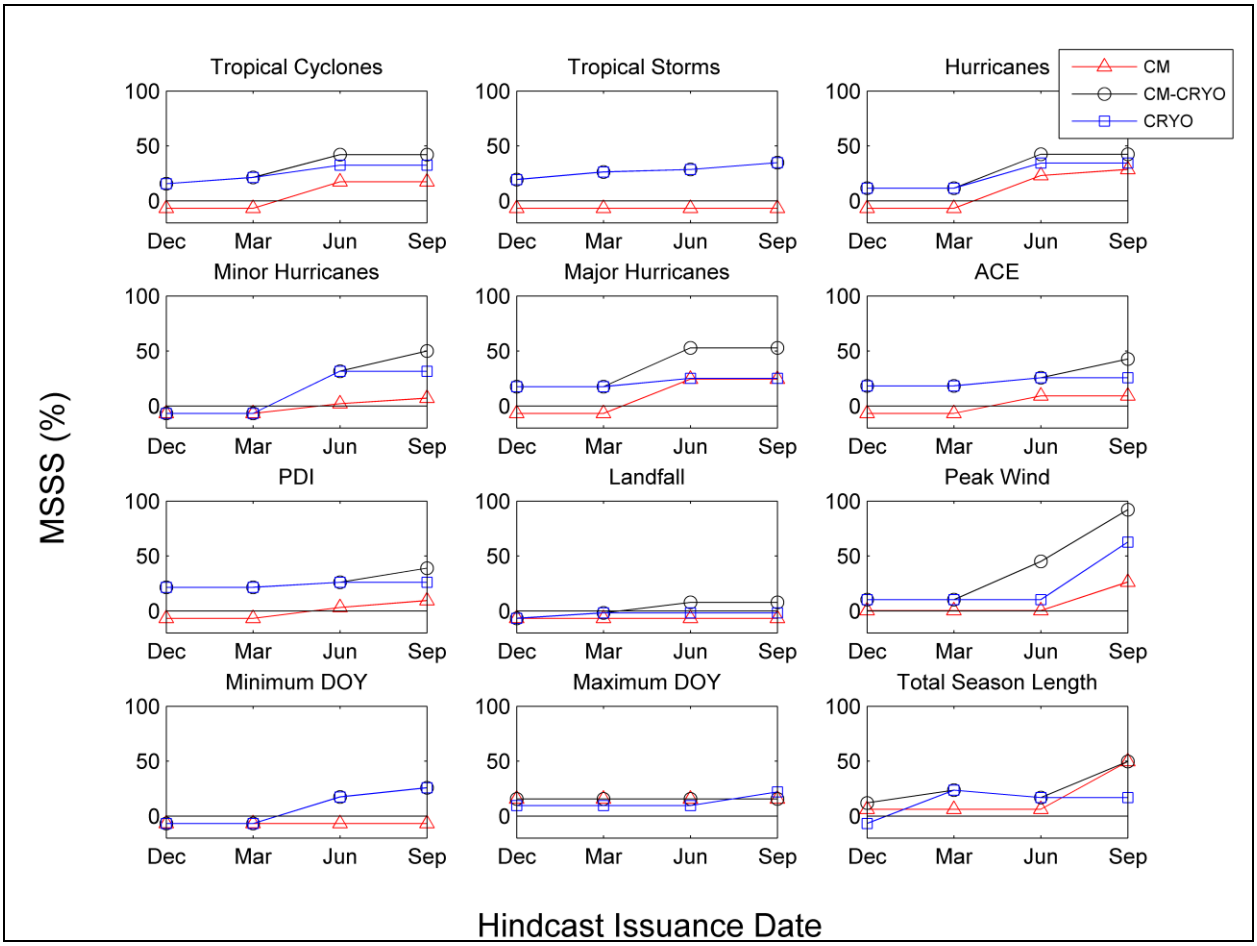

Figure 4.4 Mean squared skill score (MSSS) of the model groups for 12 tropical cyclone seasonal parameters across the four issuance dates. Solid black line represents the skill of climatology. The acronyms are: ACE (accumulated cyclone energy), CM (climate mode only models), CM-CRYO cryospheric and climate mode models), CRYO (cryospheric predictors only models), DOY (day of year) and PDI (power dissipation index).

When analyzing the June hindcast MSSS values, the CM-CRYO models were the best performing group, followed by the CRYO models, and then the CM models. Within the CM-

CRYO models, MajHs had the highest MSSS value with the models performing 54% better than the mean square error of climatology followed by TSL at 50%, Pwind at 45% and TCs and Hs both having MSSS values of 42%. These models also have the largest R^2 values at the June hindcast with 0.54, 0.51, 0.49, 0.44, and 0.43 for MajHs, TSL, Pwind, TCs, and Hs, respectively. When comparing these top performing models to the other model groups for the same TCPs, the CRYO (CM) models had, on average, MSSS values 19% (28%) lower than those of the CM-CRYO models. These results clearly show that a combination of CM and cryospheric information is essential for a model to produce an accurate hindcast while models using information from only one of the predictor categories leads to greater model error and uncertainty.

In order to better understand the specific predictors involved in producing a more accurate model, the frequency of predictor occurrence was analyzed. Within each model group a model was constructed for the 13 TCPs at the four lead times causing there to be a total of 52 models. Key predictors were identified by analyzing the number of times each predictor was chosen by a model with key predictors being those chosen most frequently. Figure 4.5 shows all the predictors that were chosen by at least one of the 52 models within the CM model group and the percentage of occurrence for each of the chosen predictors. The CM models only had seven predictors from a possible total of 25 that had statistically significant relationships between at least one of the TCPs based on the stepwise procedure. Of these seven predictors the Fall NAO seasonal mean was chosen by 21% of the 52 total models while Spring NAO was chosen by 19% of the models followed by Summer ENSO at 8%. Knowing the key predictors within the three model groups helps direct the investigation into the underlying physical mechanisms that are causing these key predictors to be selected.

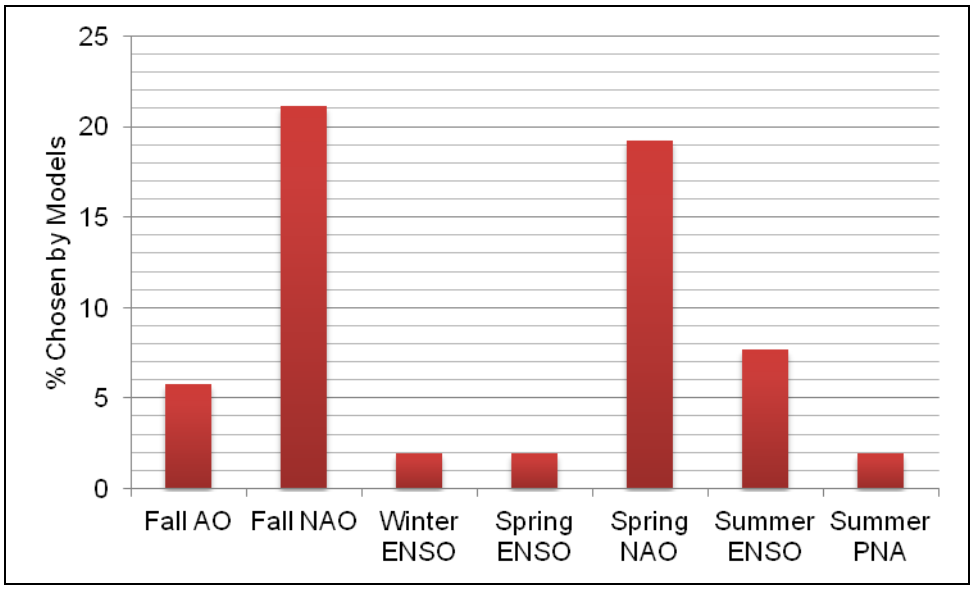

Figure 4.5 The most frequently chosen predictors that where included within the CM models. Acronyms are: AO (Arctic Oscillation), ENSO (El Niño-Southern Oscillation), NAO (North Atlantic Oscillation), and PNA (Pacific-North American Pattern).

Figure 4.6 shows the frequency of the 22 selected predictors within the CRYO models from the possible 92 total predictors with Winter Bering Sea SIA being chosen most frequently at 21% followed by Spring Baffin Bay SIA at 15% and Fall Baffin Bay SIE at 13%. Even with 92 possible predictors at the September hindcast, only 22 predictors showed significance and even fewer of these 22 predictors were included within multiple models indicating that there must be some underlying physical mechanisms that cause these predictors to be frequently chosen, and since the CM-CRYO models were the best performing model group their key predictors will be thoroughly investigated.

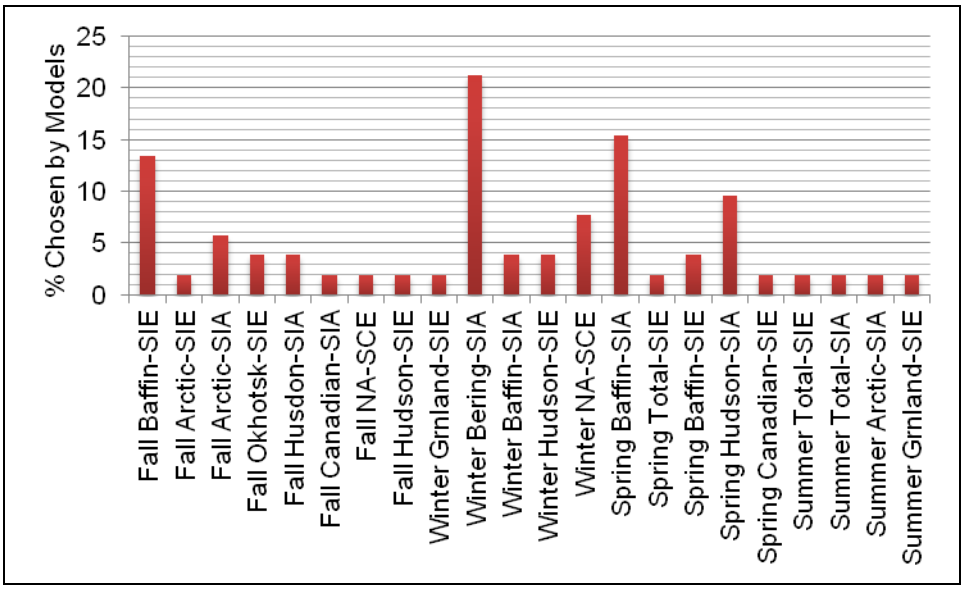

Figure 4.6 The most frequently chosen predictors that where included within the CRYO models. Acronyms are NA (North America), SCE (snow cover extent), SIA (sea ice area), and SIE (sea ice extent).

The key predictors within the CM-CRYO models showed similarities to the key predictors chosen within the two other model groups leading to higher confidence that the chosen key predictors do have some sort of underlying physical mechanisms that cause the different model groups to consistently chose the same predictors. Figure 4.7 shows that of the 112 possible predictors available for the September hindcasts only 37 predictors were selected. The top four CM predictors are Fall NAO (19%), Spring NAO (13%), Spring AO (8%), and Summer ENSO (8%), which is consistent with the top two predictors of the CM models. The top four cryospheric predictors in the CM-CRYO models were Fall Baffin Bay SIE (19%), Fall Bering Sea SIA (13%), Spring Baffin Bay SIA (13%), and Spring Hudson Bay SIA (10%), which is fairly consistent with the key predictors of the CRYO models. The CRYO models had Winter Bering Sea SIA being the top predictor at 21% while that predictor was only chosen by 10% of the CM-CRYO models. Fall Bering Sea SIA, Spring Baffin Bay SIA, and Spring Hudson SIA were still top predictors in both the CM-CRYO model and CRYO models.

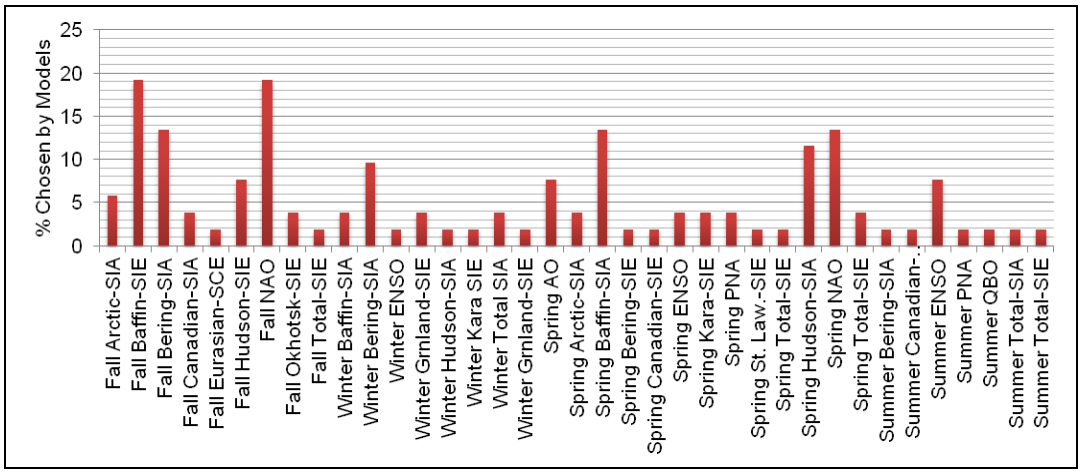

Figure 4.7 The most frequently chosen predictors that were included within the CM-CRYO models. Acronyms are: AO (Arctic Oscillation), ENSO (El Niño-Southern Oscillation), NA (North America), NAO (North Atlantic Oscillation), SCE (snow cover extent), SIA (sea ice area), SIE (sea ice extent), PNA (Pacific North American Pattern), and QBO (Quasi-Biennial Oscillation).

4.4 Correlation analysis

By analyzing the predictor histograms key CM and cryospheric predictors were identified. This began the investigation into the possible physical mechanisms that determined why these predictors were chosen. A correlation analysis was conducted on the top four CM predictors (i.e., Fall NAO, Spring AO and NAO, and Summer ENSO) and the top four cryospheric predictors (i.e., Fall Baffin Bay SIE, Fall Bering Sea SIA, Spring Baffin Bay and Hudson Bay SIA) within the CM-CRYO models. Correlation analysis was conducted by investigating the linear correlations between the key predictors and known environmental factors that influence TC activity, as well as between the key predictors and the TCPs themselves. Each of the eight key predictors was analyzed to see which ones showed the most significant statistical relationships between the 13 TCPs. They were also compared to the environmental factors known to influence TC activity such as anomalies in SSTs, SLP, and 1000 mb wind vector. Key predictors that were

well correlated with the environmental factors and exhibited multiple statistically significant relationships to the TCPs will now be analyzed.

Table 4.2 shows the linear correlations between the top eight predictors and the 13 TCPs in the CM-CRYO models with the significant relationships in bold. The predictors with the most significant relationships were Spring Baffin Bay SIA and Fall Baffin Bay SIE with nine followed by Summer ENSO with eight, Spring Hudson Bay SIA with seven, and Spring NAO with six. The remaining predictors Fall NAO and Spring AO only had three and two significant relationships, respectively, while Fall Bering Sea SIE had none. Correlation plots created using NOAA's ESRL further supported why the key predictors have significant relationships with the TCPs. The numerous atmospheric variables known to influence Atlantic TC activity were tested against the key predictors in order to determine if there are any correlations within the tropical Atlantic. Key predictors were tested against the SST, SLP, 500 mb geopotential height, and outgoing longwave radiation at the tropopause between 1980 and 2010 for the peak TC months of July, August, and September. The key predictors that showed strong correlations with multiple atmospheric variables within the tropical Atlantic will now be presented.

Table 4.2 Linear correlations between the top four climate mode and top four cryosphere predictors in the CM-CRYO models with significant correlations (α=0.05) in bold. Acronyms are: ACE (accumulated cyclone energy), AO (Arctic Oscillation), BB (Baffin Bay), BS (Bering Sea), ENSO (EL Niño-Southern Oscillation), H (hurricane), HB (Hudson Bay), LMD (lifetime mean duration of storm), MajH (major hurricane), MaxDOY (latest cyclogenesis day), MinDOY (earliest cyclogenesis day), MinH (minor hurricane), NAO (North Atlantic Oscillation), PDI (power dissipation index), Pwind (peak wind), SIA (sea ice area), SIE (sea ice extent), TC (tropical cyclone), TSL (total season length), and TS (tropical storm).

	Fall NAO	***Spring AO***	***Spring NAO***	***Summer ENSO***	***Fall BS SIA***	***Spring HB SIA***	***Spring BB SIA***	***Fall BB SIE***
TC	-0.28	-0.35	**-0.46**	**-0.44**	-0.20	**-0.58**	**-0.59**	**-0.52**
TS	-0.24	-0.03	-0.34	-0.12	0.06	**-0.46**	**-0.39**	**-0.40**
H	-0.14	-0.15	-0.12	-0.14	-0.32	-0.05	-0.23	-0.34
Minor	-0.05	-0.25	-0.10	-0.18	-0.19	-0.30	**-0.48**	-0.27
Major	-0.15	**-0.49**	**-0.59**	**-0.42**	-0.28	**-0.51**	**-0.56**	**-0.49**
ACE	-0.02	-0.11	**-0.39**	**-0.43**	-0.06	**-0.58**	-0.35	-0.27
PDI	-0.15	-0.30	-0.26	**-0.60**	-0.32	-0.32	-0.35	**-0.46**
Landfall	**0.50**	-0.17	0.02	-0.03	0.20	0.06	0.28	**0.46**
Pwind	**-0.42**	-0.09	-0.21	**-0.37**	-0.32	-0.29	**-0.42**	-0.35
LMD	**-0.62**	0.07	-0.15	-0.20	-0.34	-0.22	**-0.46**	**-0.56**
MinDOY	-0.31	-0.34	**-0.40**	**-0.42**	-0.26	**-0.55**	**-0.59**	**-0.55**
MaxDOY	-0.19	-0.25	**-0.55**	**-0.39**	-0.10	**-0.65**	**-0.54**	**-0.49**
TSL	-0.11	**-0.36**	**-0.58**	**-0.51**	-0.20	**-0.66**	**-0.54**	**-0.45**

Of 32 correlation plots created, only Spring Baffin Bay and Spring Hudson Bay SIA showed strong correlation with multiple atmospheric variables known to influence TC activity. Figures 4.8 and 4.9 show the correlation plots between Spring Baffin Bay and SST and Spring Hudson Bay SIA and SST, respectively (See Appendix – B for all the correlation plots). These plots show that these predictors are inversely correlated with SSTs throughout the tropical and North Atlantic. This inverse relationship is strong ($r < -0.5$) within the Atlantic's MDR. The direct thermodynamic effect of SST on TCs has been known since the 1960s with above average SSTs leading to enhanced convection and below average SSTs leading to suppressed convection

(Malkus and Riehl, 1960). As mentioned in Chapter 2, above average SSTs and preexisting convection are two of the six key environmental factors necessary for tropical cyclogenesis. The fact that these predictors are correlated with SST within the MDR is an indicator that these predictors are skillful, assuming seasonal persistence, of environmental factors known to influence TC activity at the start of the TC season. SST can also indirectly influence vertical wind over the MDR, also a key environmental factor for tropical cyclogenesis, through its strong inverse relationships with SLP (Sharpiro, 1982; Gray 1984b).This relationship is evident when comparing the strong inverse correlations present between the predictors and SST (Figures 4.8 and 4.9) to the strong positive correlations present between the predictors and SLP (Figures 4.10 and 4.11). In general, above average SSTs are accompanied with below average SLP, which leads to weaker trade winds and ultimately reduced wind shear (Landsea et al., 1998). The relationships between SSTs, SLP, and trade wind strength will be addressed more thoroughly in section 4.5.

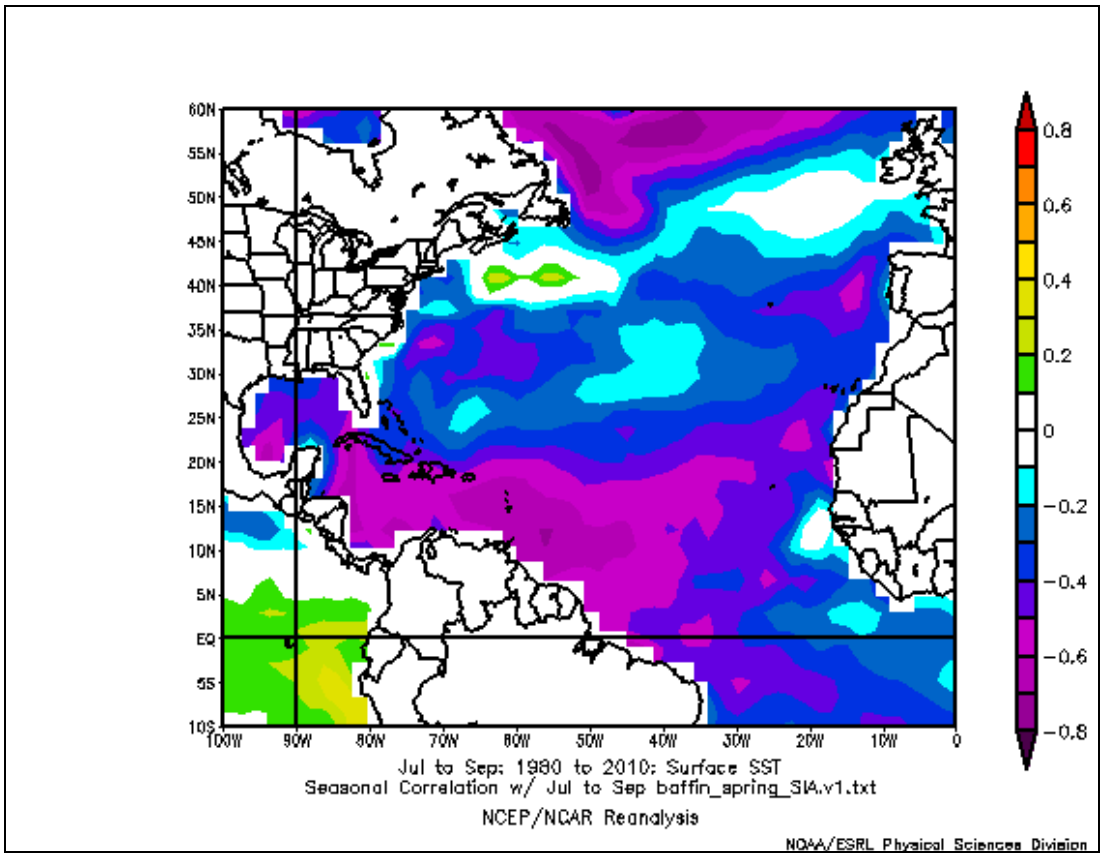

Figure 4.8 Correlation plot between July-September sea surface temperature and Spring Baffin Bay SIA from 1980 to 2010. Image provided by the NOAA/ESRL Physical Sciences Division, Boulder Colorado from their Web site at http://www.esrl.noaa.gov/psd/ (Kalnay et al., 1996).

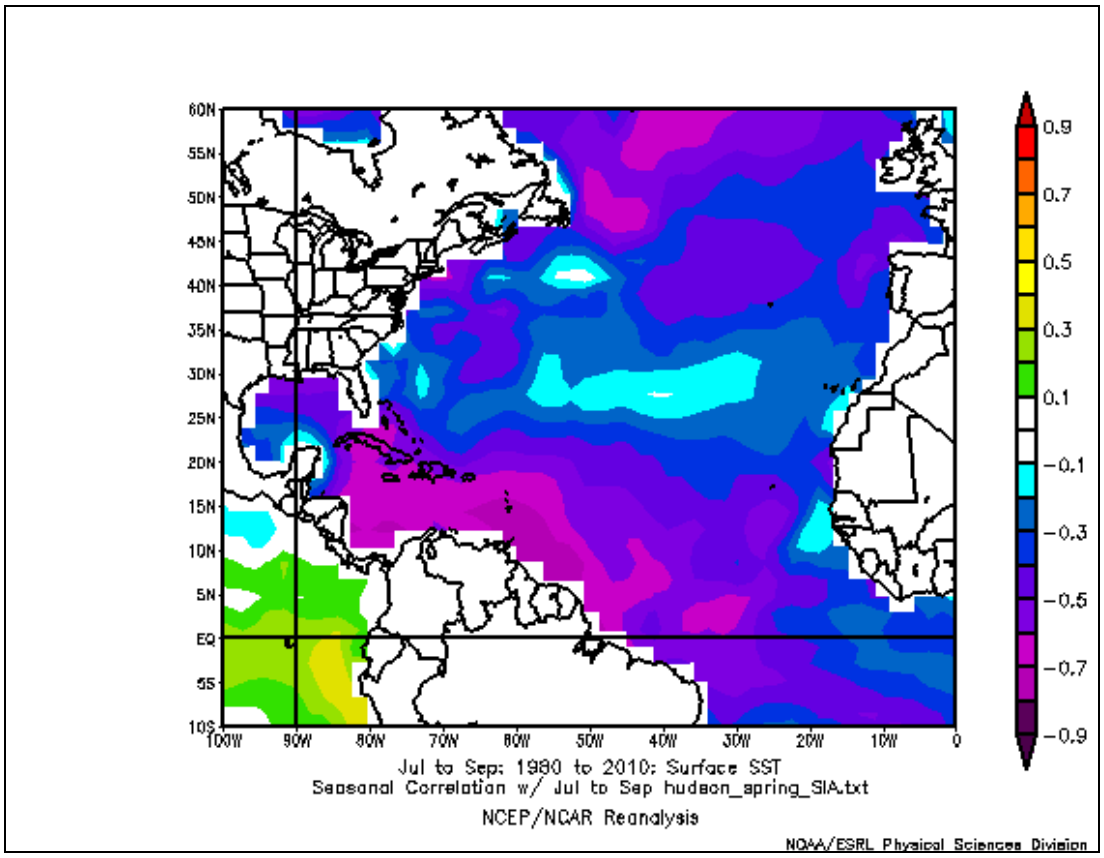

Figure 4.9 Correlation plot between July-September sea surface temperature and Spring Hudson Bay SIA from 1980 to 2010. Image provided by the NOAA/ESRL Physical Sciences Division, Boulder Colorado from their Web site at http://www.esrl.noaa.gov/psd/ (Kalnay et al., 1996).

Figures 4.10 and 4.11 show correlation plots for Spring Baffin Bay SIA and SLP and Spring Hudson Bay SIA and SLP, respectively. Both plots show strong ($r > 0.4$) positive correlations between the predictors and SLP throughout much of the MDR. As noted, above average SSTs and SLP have a strong inverse correlation, which is supported when comparing the correlation plots of SSTs (Figures 4.8 and 4.9) and of SLP (Figure 4.10 and 4.11). The SST plots have strong inverse (negative) correlations with the predictors while the SLP plots feature strong positive correlations. This implies an inverse relationship between SSTs and SLP. SLP variations across the Atlantic are known to influence TC activity with below average pressure being associated with an enhanced TC season and above average pressure associated with a suppressed

season (Gray, 1984b). In general, below average SLP in the MDR is associated with a weakening of the meridional pressure gradient between the MDR and equator, which leads to a weakening of the trade winds over the MDR while above average SLP is associated with the opposite conditions leading to strengthened trade winds (Gray et al., 1993). Additionally, it has also been hypothesized that below average SLP in the MDR indicate a poleward shift and/or strengthening of the ITCZ with either of these scenarios contributing to less subsidence and drying in the MDR (Gray et al., 1993). An enhanced ITCZ is also associated with increases in large-scale low-level cyclonic vorticity, often as westward moving easterly waves, which is a necessary component for tropical disturbances to form – the beginning stage of tropical cyclogenesis (Gray, 1968). With above average SLP in place, the ITCZ is closer to the equator thus causing more subsidence and drying within the MDR and reductions in large-scale low-level cyclonic vorticity. All of these factors being unfavorable for TC development and leading to a suppressed TC season. Finally, below average SLP is usually associated with more low- to mid-tropospheric moisture, which is essential to TCs since the energy that fuels TCs comes from the release of latent heat during the condensation of low- to mid-level tropospheric water vapor (Knaff, 1997).

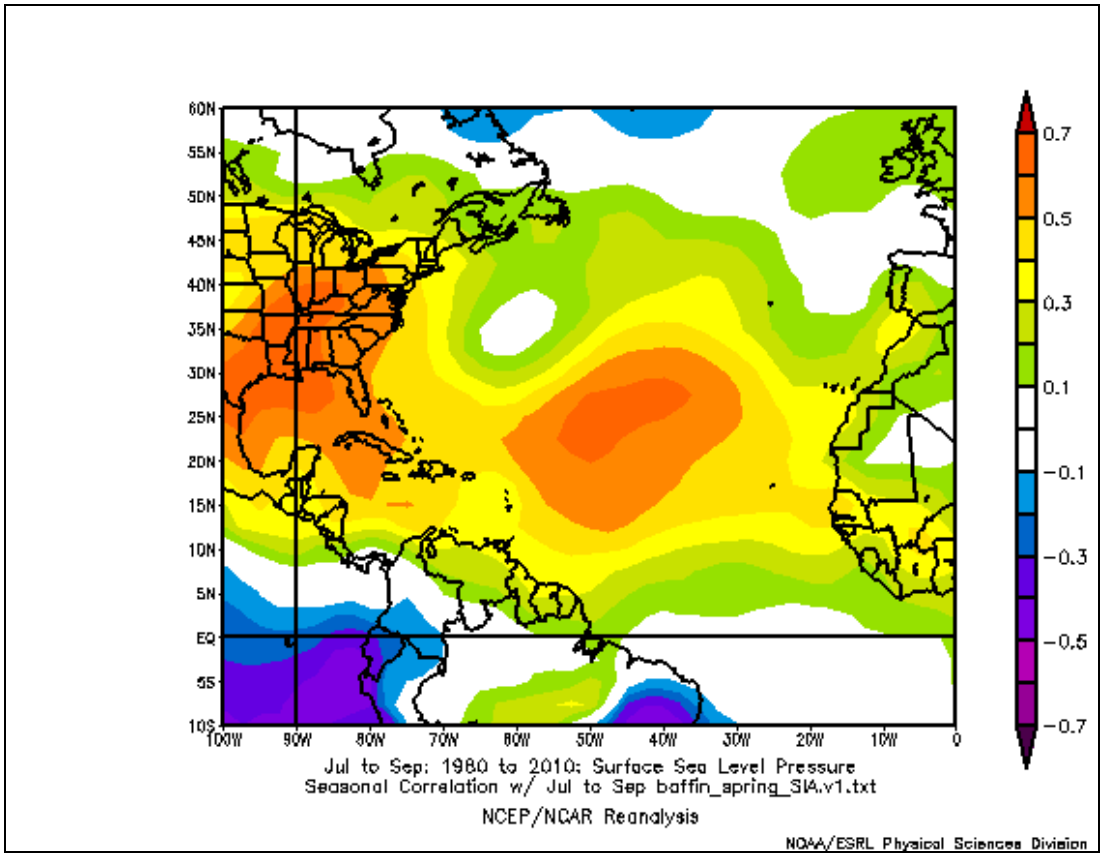

Figure 4.10 Correlation plot between July-September sea level pressure and Spring Baffin Bay SIA from 1980 to 2010. Image provided by the NOAA/ESRL Physical Sciences Division, Boulder Colorado from their Web site at http://www.esrl.noaa.gov/psd/ (Kalnay et al., 1996).

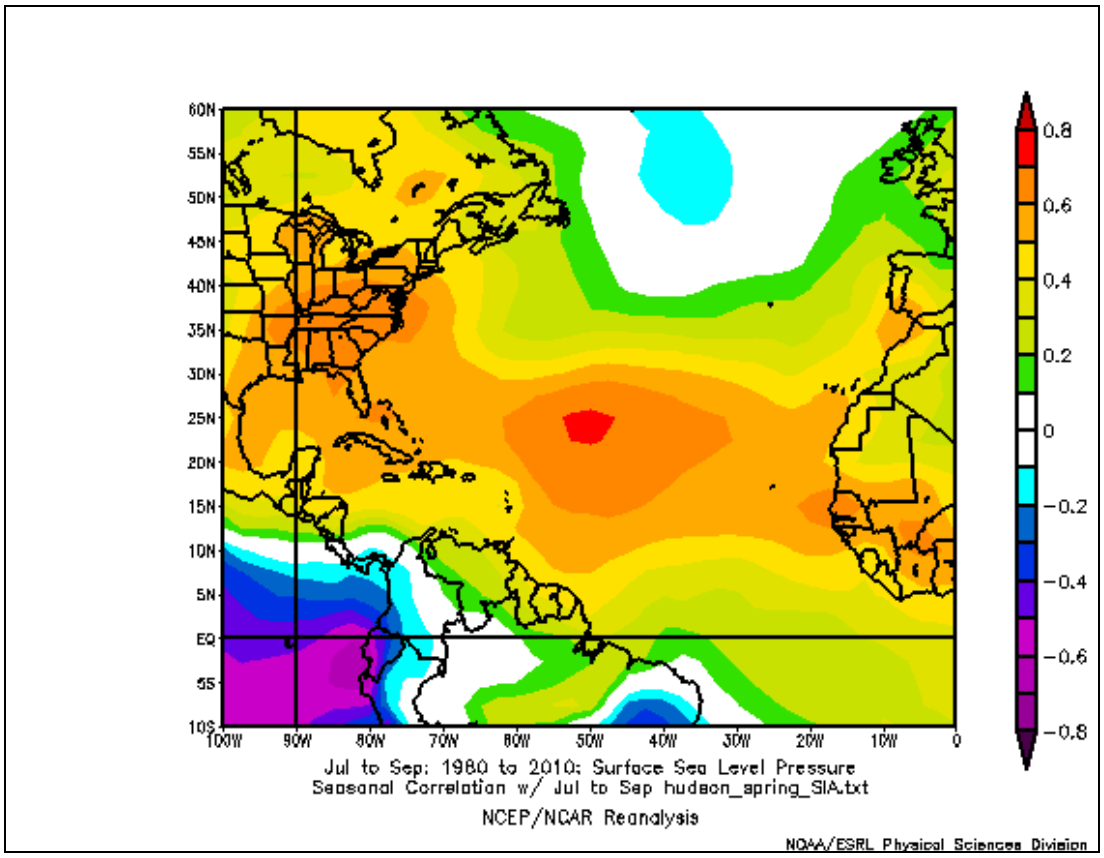

Figure 4.11 Correlation plot between July-September sea level pressure and Spring Hudson Bay SIA from 1980 to 2010. Image provided by the NOAA/ESRL Physical Sciences Division, Boulder Colorado from their Web site at http://www.esrl.noaa.gov/psd/ (Kalnay et al., 1996).

The correlation plots for SST and SLP indicate that Spring Baffin Bay SIA and Hudson Bay SIA have strong correlations with environmental factors known to be present during enhanced or suppressed TC activity. None of the other six key predictors had such strong correlation plots. This does not mean that these six predictors do not have environmental conditions associated with them that lead to changes in Atlantic TC activity, it simply means that these six predictors did not have significant correlations with the four NCEP reanalysis variables that were investigated.

All four of the key CM predictors have known effects on TC activity, which is most likely why they are included in the models. ENSO is currently used in almost every operational statistical forecasting scheme (Camargo et al., 2007) because of its large, well-documented,

impact on Atlantic TC activity. The state of ENSO influences the interannual variability of vertical wind shear throughout the MDR mainly through changes to the 200 mb westerlies over the tropical Atlantic brought on by changes in Pacific equatorial convection that influence upper-level flow (Gray, 1984a; Landsea et al., 1998). El Niño events are typically associated with increases in 200 mb westerlies and wind shear over the Atlantic causing suppressed TC activity while La Nina events are generally associated with reductions in the strength on the 200 mb westerlies and wind shear causing an enhanced TC season (Gray, 1984a; Goldenberg and Shapiro, 1996).

The NAO has also been used as a predictor in numerous statistical models, mainly being used for predicting the number of MajHs and number of US land falling TCs (Elsner et al., 2000; Elsner and Jagger 2006; Xie et al., 2012). These modeling studies have shown that the intensity of the NAO in spring and early summer influences of the amounts of ridging across the subtropical Atlantic and the position of the Bermuda high that leads to changes in the number and tracks of TCs. A strong (positive) NAO is associated with a more northeastward positioning of the Bermuda high which causes more TCs to recurve northward causing the East Coast of the US to be more susceptible to TC landfalls. A weak/neutral (negative) NAO is associated with a more southwestward positioning of the Bermuda high leading to less recurving causing TCs to track across the lower latitudes and causing the Gulf Coast of the US to be more susceptible to landfalls (Elsner et al., 2006).

The AO has been shown to be associated with overall TC activity and TC landfall counts through its effects on the zonal wind anomalies in the tropics (Larson et al., 2005). A positive AO is associated with enhanced midlatitude ridging across the North Atlantic and anomalies in the upper-level easterlies within the tropics. These easterly wind anomalies lead to reductions in

vertical wind shear that is associated with enhanced TC activity, while a negative AO leads to the opposite conditions and a suppressed TC season.

Although the top CM predictors do not have strong correlation plots they all have well documented effects on TC activity and landfall strike variability. Additionally, Fall Baffin Bay SIE and Fall Bering Sea SIA did not have strong correlation plots, but Fall Baffin Bay SIE is highly correlated ($r = 0.62$) with Spring Baffin Bay SIA, which does have strong correlation plots, meaning that some persistence from fall to spring can be inferred. Fall Bering Sea SIA does not feature the same seasonal persistence that fall and spring Baffin Bay SI does, but Bering Sea SIA has been shown to fluctuate according to the intensity of the North Pacific Oscillation (NPO), which is an SLP oscillation located within the Gulf of Alaska (Rogers, 1981). Changes in SLP in the Gulf of Alaska have been observed as precursors of a state change of ENSO with below average SLP occurring with a decaying El Niño event and above average SLP occurring with a weakening La Nino event (Larkin and Harrison, 2002). Fall Bering Sea SIA may be then associated with a changing state of ENSO causing it to be included within the top key predictors.

4.5 Composite analysis

Now that possible physical association between environmental conditions known to influence TC activity and the six other key predictors have been discussed the focus will shift back to the two predictors (Spring Baffin Bay and Hudson Bay SIA) that did show strong correlation plots for SST and SLP. Though these two predictors are well correlated with SST and SLP, these correlations do not suggest a physical mechanism that explains the relationship. To investigate the potential physical mechanisms causing these correlations a composite analyze was performed to better understand the relationship between these two predictors and TC activity.

Figure 4.12 compares the mean differences between the seven years of lowest and highest SIA for Spring Baffin Bay and Hudson Bay to the means of seven TCPs (See Appendix – C for additional comparison tables). Each of the means between the high and low SIA years were found to be statistically significant at $\alpha = 0.05$ based on a paired sample 2-tailed Student's T-test. A noteworthy feature of Figure 4.12 is that it indicates that even small variations to SIA in Hudson Bay during the spring are associated with large variations in the percentage change from climatology of the seven TCPs. The mean SIA of the seven highest years for spring Hudson Bay was only 3.5% above climatology while the mean of the lowest SIA years was 5% below climatology, but these small deviations are associated with large variations in the TCPs. During low SIA years a 45% increase in the number of MinHs is observed and a 42% increase in the PDI, while during high SIA years a 20% reduction in MinHs and a 46% lower PDI are observed compared to climatology. In fact all seven TCPs show higher (lower) seasonal averages during low (high) Spring Hudson Bay SIA years.

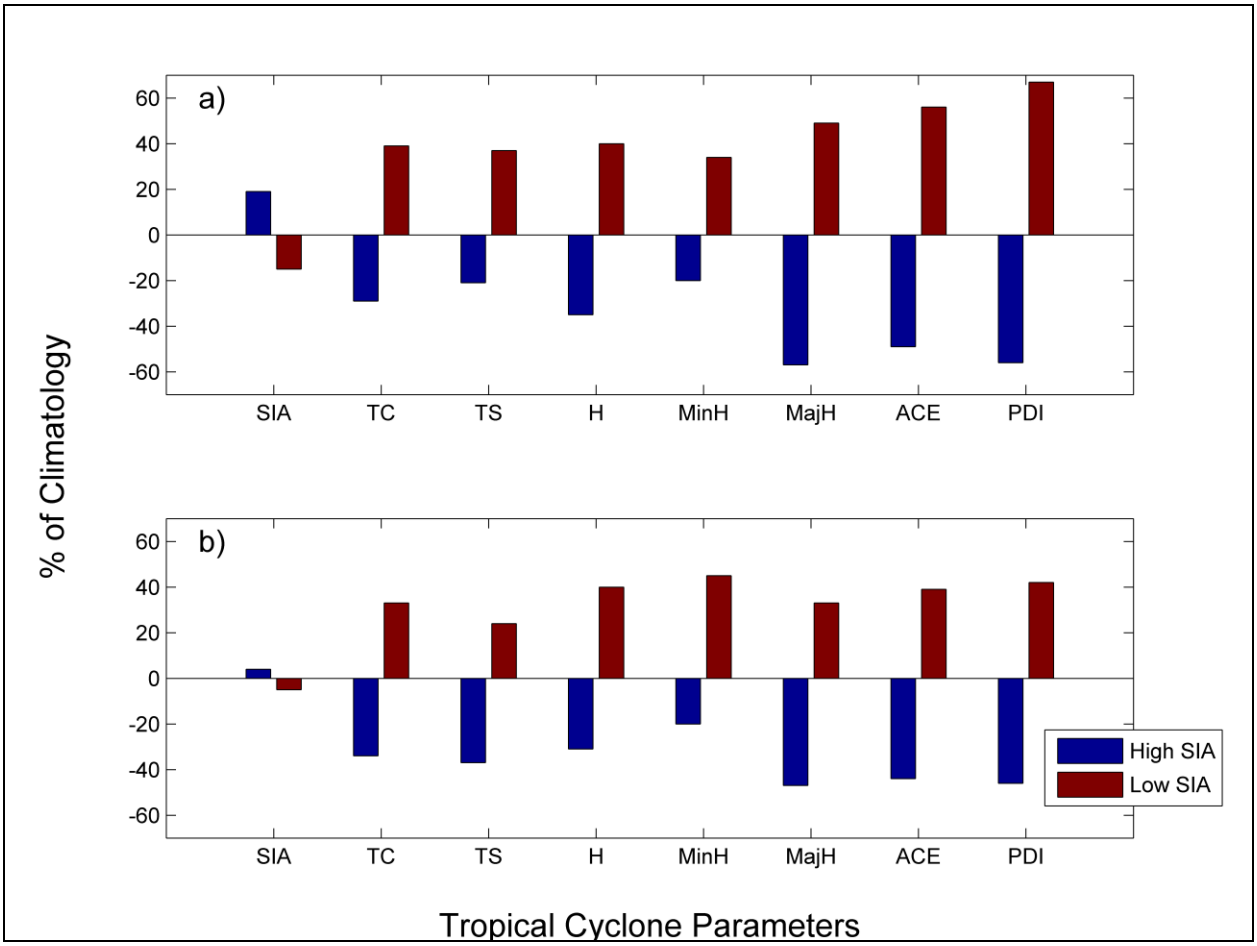

Figure 4.12 The percentage change from climatology (0 line) of means of seven tropical cyclone parameters between the top seven and bottom seven years of anomalous sea ice area (SIA) for Spring Baffin Bay (a) and Spring Hudson Bay (b). Acronyms are: ACE (accumulated cyclone energy), H (hurricane), MajH (major hurricane), MinH (minor hurricane), PDI (power dissipation index), TC (tropical cyclone), and TS (tropical storm),). Each of the parameter means were significantly different based on a paired sample 2-tailed T test at $\alpha = 0.05$.

Spring Baffin Bay SIA also shows significantly different seasonal means for the seven TCPs during high and low SIA years though variations in SIA are larger in Baffin Bay. SIA in Baffin Bay shows a mean reduction of 15% during low SIA years, and a 19% increase during high SIA years. These changes are associated with even large variations in the seven TCPs than those of Hudson Bay. During low SIA years increases of 67% and a 49% over climatology are observed for PDI and the number of MajHs, respectively, while during high SIA years a 56% and

57% reduction is observed for PDI and MajHs, respectively. Just like with Hudson Bay, increases in all the TCPs are observed during low SIA years and reductions during high SIA years. None of the other six key predictors revealed contrasts in the TCPs during low and high years. Spring Baffin Bay and Hudson Bay SIA reveal clear differences in TC activity which supports the findings in section 4.4 that the strong relationships between these predictors and SST and SLP are associated with changes in TC activity.

The correlation plots in section 4.4 revealed strong positive correlations between spring Baffin Bay and SLP and Hudson Bay and SLP across the tropical Atlantic meaning that low SIA values are generally associated with low SLP. As mentioned in the previous section, below average SLP is conducive to tropical cyclogenesis and tends to be present during high TC activity years. This established relationship between below average SLP and enhanced TC activity is supported by the findings in Figure 4.12 which reveals that during low SIA years increased TC activity is observed. When low (high) Baffin Bay and Hudson SIA is observed during the spring the subsequent July-September SLP across the tropics is also usually below (above) average leading a more (less) active TC season. During years with above average spring SIA, SLP will also be above average leading a reduction in TC activity because of the SLP-TC relationship, which is supported by the correlation plots and composite analysis.

The correlation plots in section 4.4 also reveal strong negative (inverse) correlations with July-September SSTs across the tropical Atlantic. Tropical SST is known to influence TC activity, just like SLP, with above average SSTs associated with enhanced TC activity. This inverse relationship between SIA and SST is evident in the composite analysis with low SIA years being associated with enhanced TC activity. When SIA is low in spring the subsequent peak TC months of July-September are correlated with above average SSTs leading to an

increased likelihood of experiencing an active TC season. During years with high spring SIA, the pattern is reversed with below average SSTs being experienced during July-September, which is associated with decreased TC activity. To further support these relationships between SIA, SST, SLP, and TC activity, composite maps of SST and SLP will be presented for the seven lowest and highest years in spring SIA across Baffin Bay and Hudson Bay in order to confirm that during years with low (high) spring SIA anomalously low (high) SLP and high (low) SSTs are experienced during the following July-September leading to years with high (low) TC activity.

Figures 4.13 and 4.14 show SLP anomalies for the seven lowest and highest Spring Baffin Bay SIA years, respectively, while Figures 4.15 and 4.16 show the seven lowest and highest Spring Hudson Bay SIA years, respectively. The strong positive correlation between spring SIA and July-September SLP is clearly supported by Figures 4.13-4.16 with the seven lowest SIA years for Baffin Bay and Hudson Bay revealing anomalously low SLP through the MDR and the opposite during the seven highest SIA years. This further supports the hypothesis that anomalously low Spring Baffin Bay and Hudson Bay SIA is associated with decreases in SLP throughout the tropical Atlantic, which can lead to a more active TC, while anomalously high spring SIA is associated with increases in SLP and less TC activity.

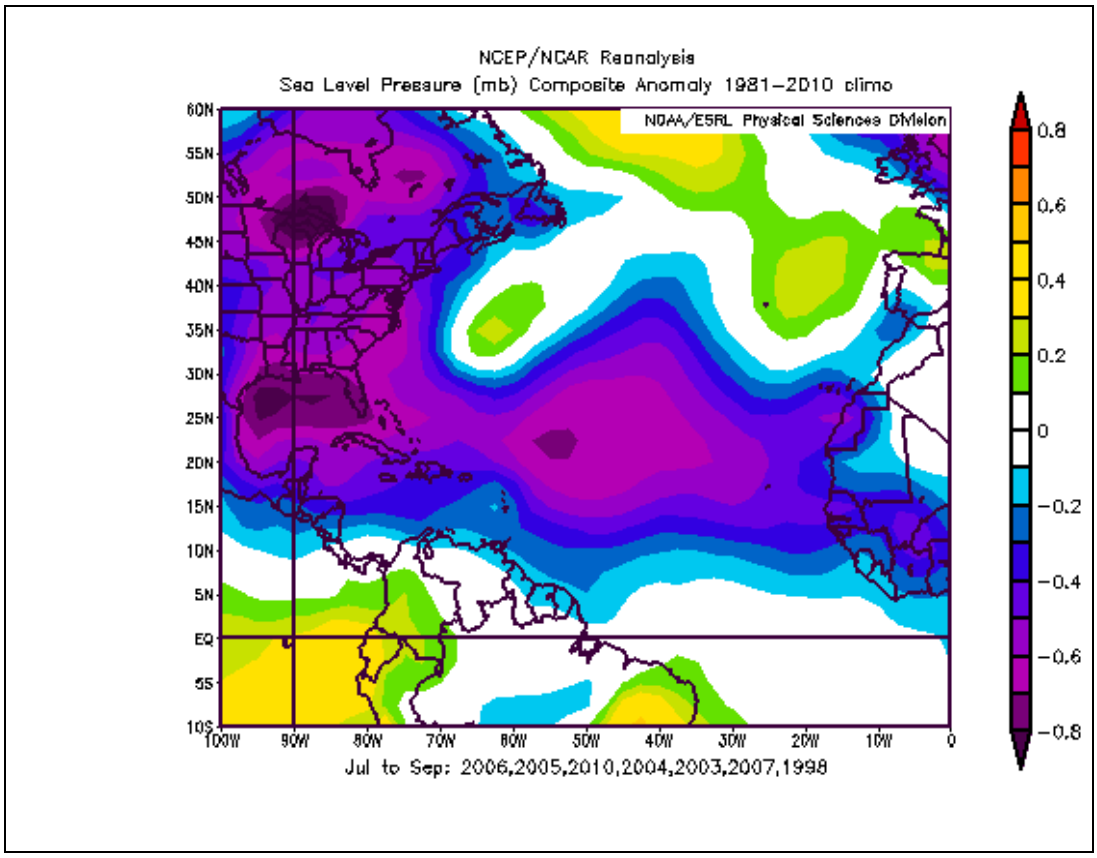

Figure 4.13 The anomalies in sea level pressure compared to 1981-2010 climatology during the seven lowest spring Baffin Bay sea ice area years. Image provided by the NOAA/ESRL Physical Sciences Division, Boulder Colorado from their Web site at http://www.esrl.noaa.gov/psd/ (Kalnay et al., 1996).

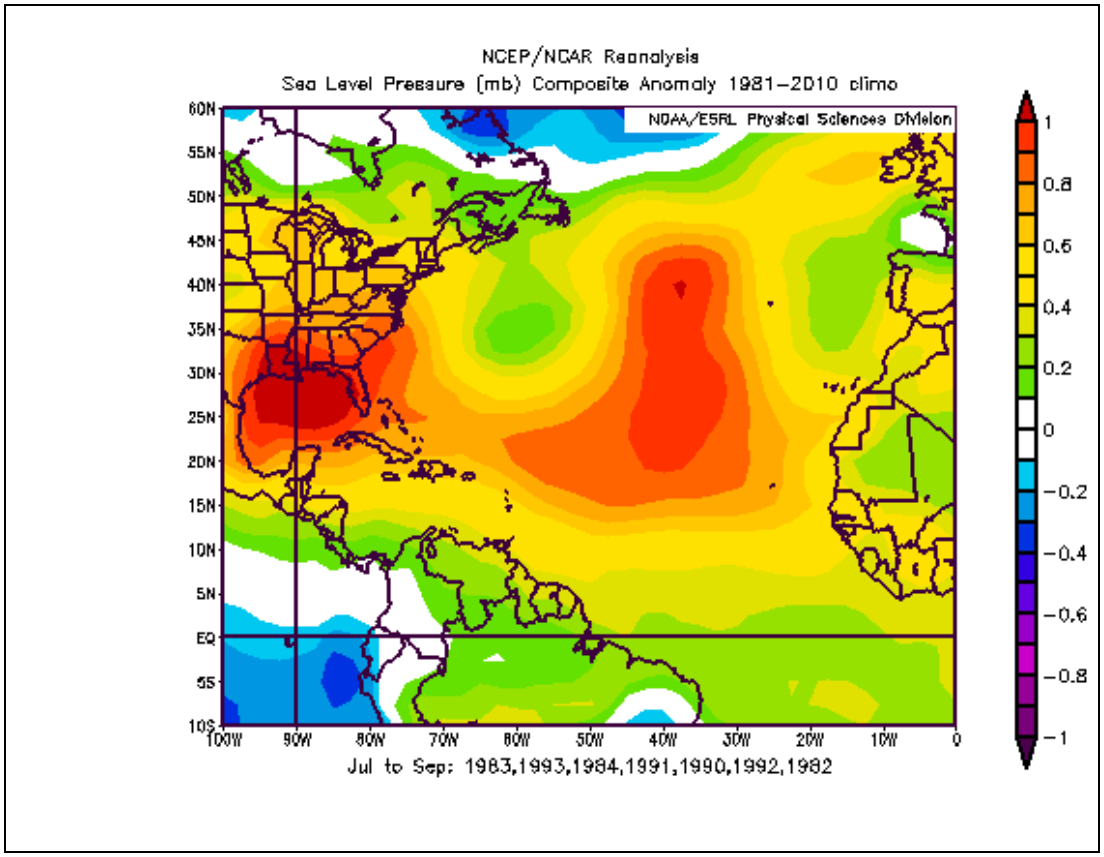

Figure 4.14 The anomalies in sea level pressure compared to 1981-2010 climatology during the seven highest spring Baffin Bay sea ice area years. Image provided by the NOAA/ESRL Physical Sciences Division, Boulder Colorado from their Web site at http://www.esrl.noaa.gov/psd/ (Kalnay et al., 1996).

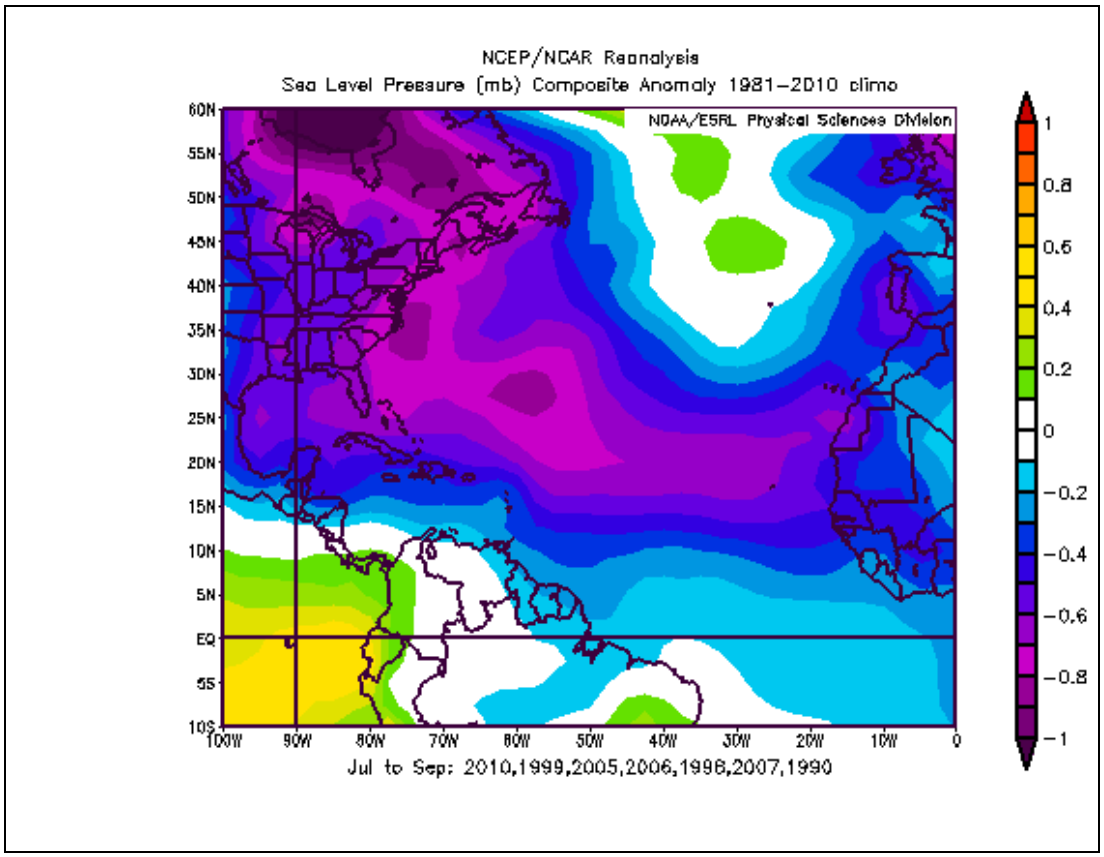

Figure 4.15The anomalies in sea level pressure compared to 1981-2010 climatology during the seven lowest spring Hudson Bay sea ice area years. Image provided by the NOAA/ESRL Physical Sciences Division, Boulder Colorado from their Web site at http://www.esrl.noaa.gov/psd/ (Kalnay et al., 1996).

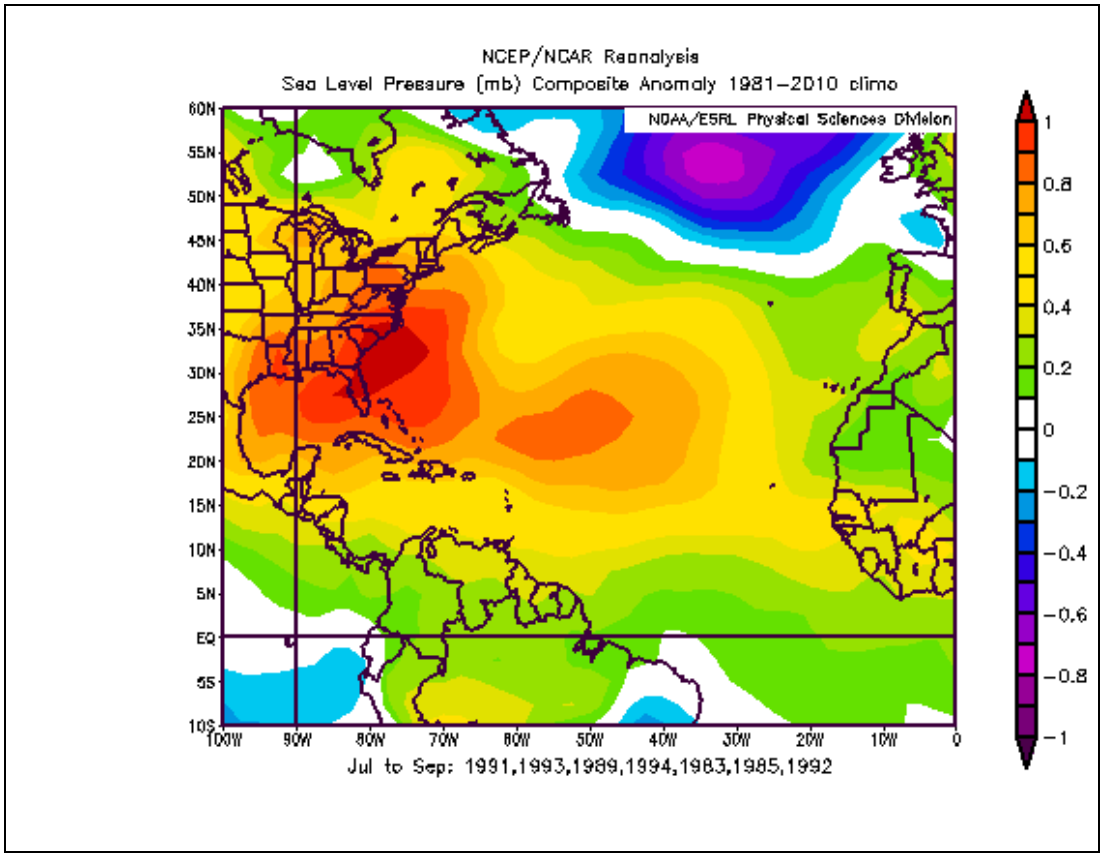

Figure 4.16 The anomalies in sea level pressure compared to 1981-2010 climatology during the seven highest Spring Hudson Bay sea ice area years. Image provided by the NOAA/ESRL Physical Sciences Division, Boulder Colorado from their Web site at http://www.esrl.noaa.gov/psd/ (Kalnay et al., 1996).

Figures 4.17 and 4.18 show SST anomalies for the seven lowest and highest Spring Baffin Bay SIA years, respectively, while Figures 4.19 and 4.20 show the seven lowest and highest Spring Hudson Bay SIA, respectively. Figures 4.17-4.20 show that during years of low spring SIA average to slightly above average SSTs are experienced throughout the MDR while during years of high SIA average to below average SSTs are experienced. Though these SST anomalies are not as widespread as those for SLP they are still consistent with the hypothesis that during years of low (high) spring SIA anomalously high (low) SSTs are present in the tropical Atlantic during July-September. Multiple environmental factors are necessary for the tropical

cyclogenesis, and since the SST composite did not reveal a strong SIA-SST relationship, 1000mb wind vector anomalies were investigated to test the hypothesis that Spring Baffin Bay and Hudson Bay SIA are related to changes in environmental factors conducive to tropical cyclogenesis. Wind vectors were also analyzes because of the SLP-trade wind strength relationship presented in section 4.4.

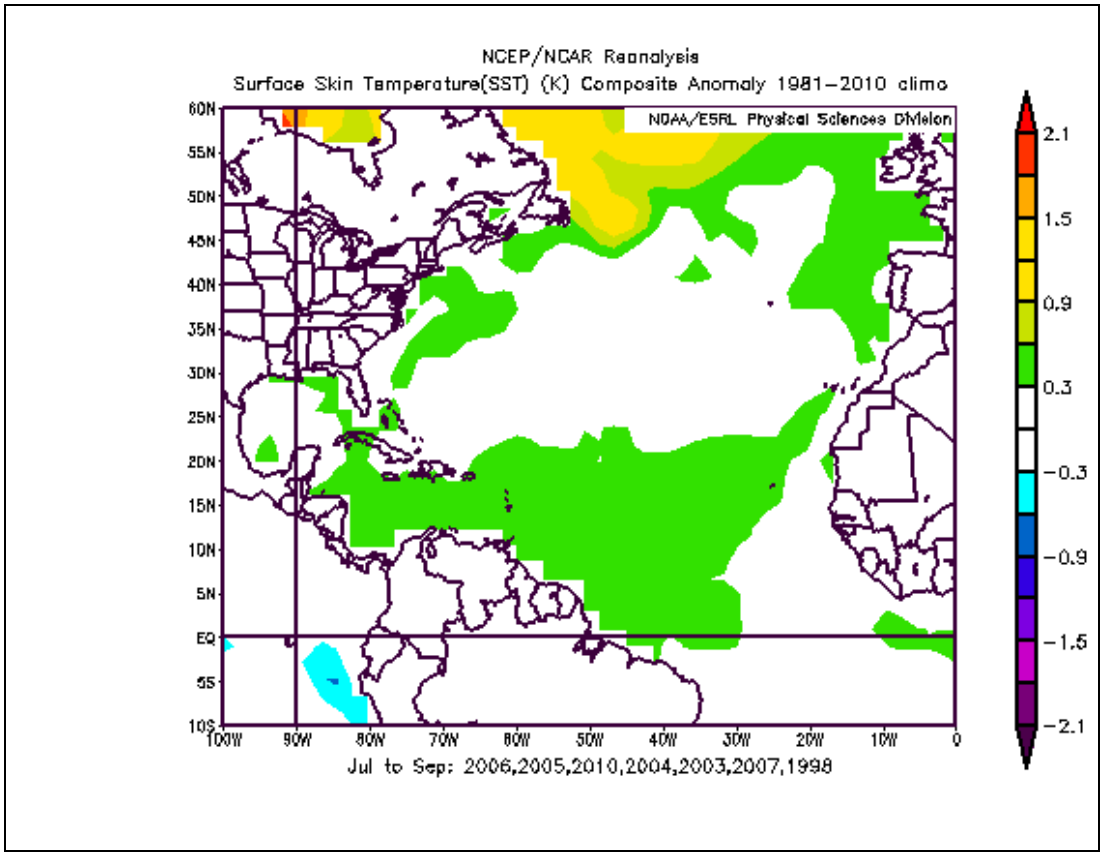

Figure 4.17 The anomalies in sea surface temperature compared to 1981-2010 climatology during the seven lowest Spring Baffin Bay sea ice area years. Image provided by the NOAA/ESRL Physical Sciences Division, Boulder Colorado from their Web site at http://www.esrl.noaa.gov/psd/ (Kalnay et al., 1996).

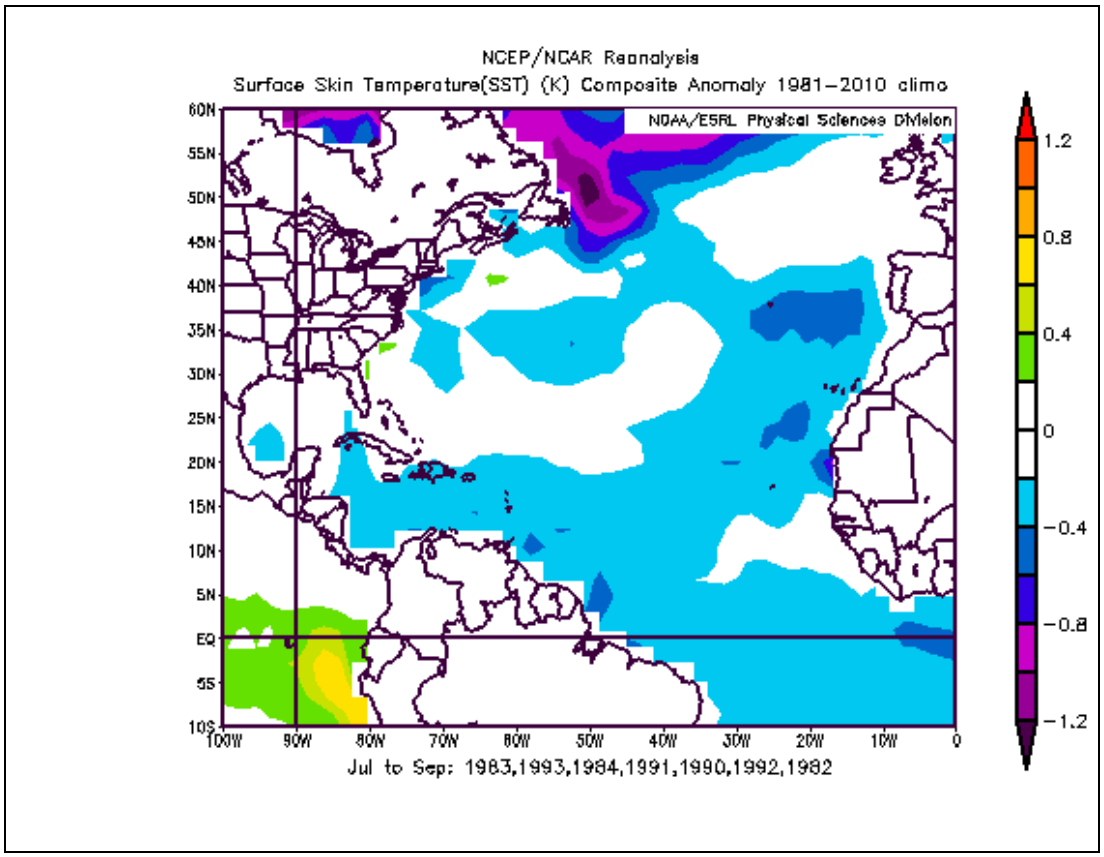

Figure 4.18 The anomalies in sea surface temperature compared to 1981-2010 climatology during the seven highest Spring Baffin Bay sea ice area years. Image provided by the NOAA/ESRL Physical Sciences Division, Boulder Colorado from their Web site at http://www.esrl.noaa.gov/psd/ (Kalnay et al., 1996).

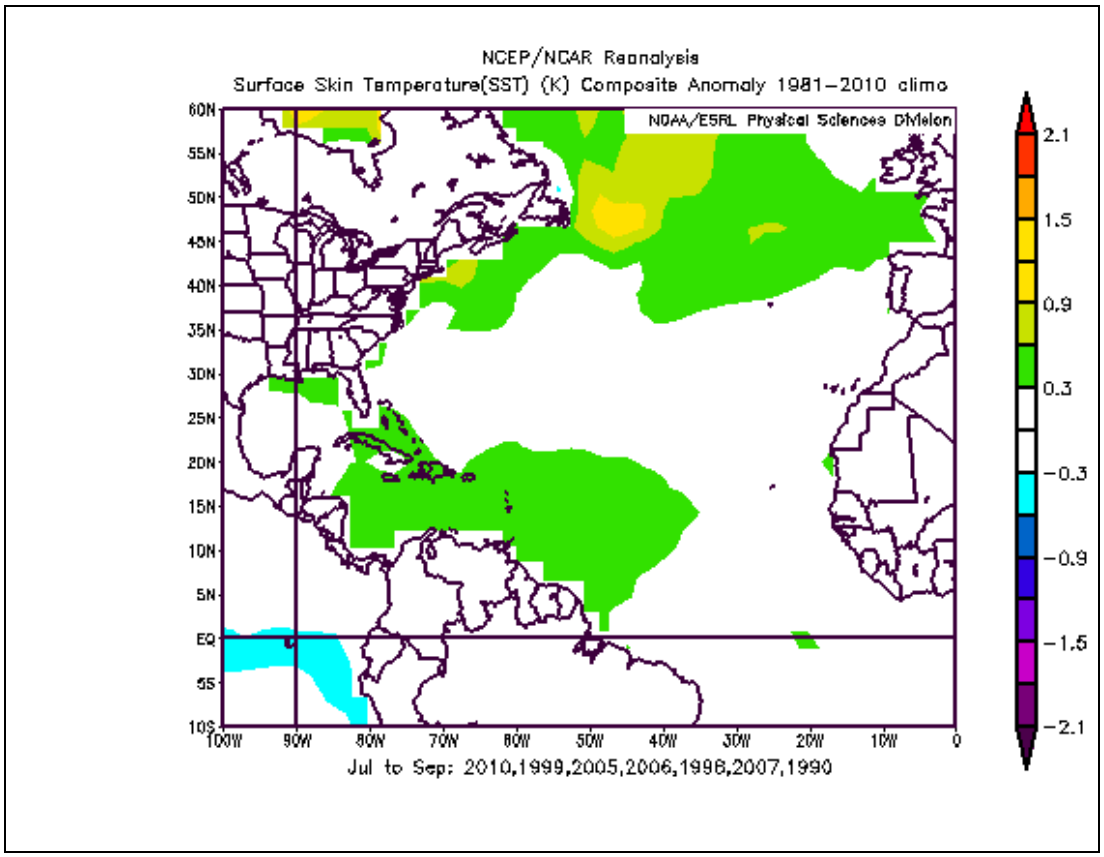

Figure 4.19 The anomalies in sea surface temperature compared to 1981-2010 climatology during the seven lowest Spring Hudson Bay sea ice area years. Image provided by the NOAA/ESRL Physical Sciences Division, Boulder Colorado from their Web site at http://www.esrl.noaa.gov/psd/ (Kalnay et al., 1996).

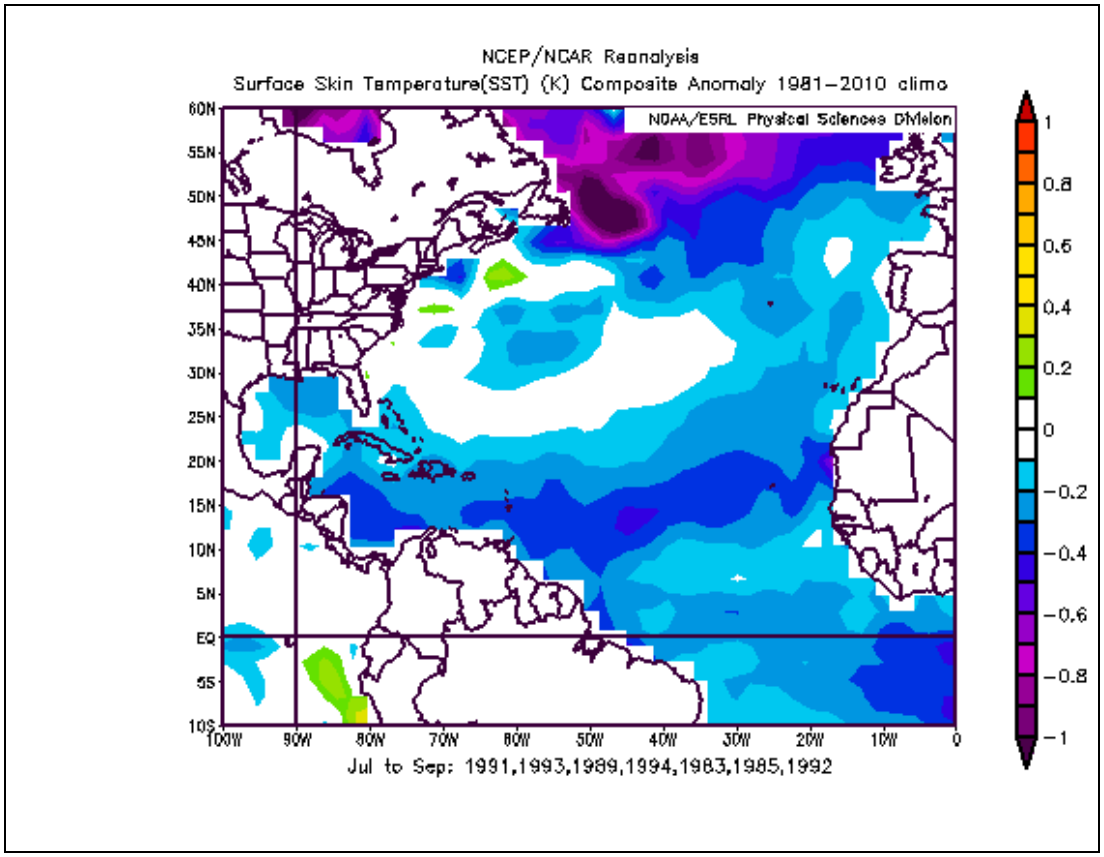

Figure 4.20 The anomalies in sea surface temperature compared to 1981-2010 climatology during the seven highest Spring Hudson Bay sea ice area years. Image provided by the NOAA/ESRL Physical Sciences Division, Boulder Colorado from their Web site at http://www.esrl.noaa.gov/psd/ (Kalnay et al., 1996).

Vertical wind shear across the MDR of the Atlantic is an extremely important factor in tropical cyclogenesis variability with the strength of the easterly trade winds being a large contributing factor in the amount of wind shear present in the MDR (Gray et al., 1993). The strength of the trade winds across the MDR is governed by the meridional pressure gradient between the MDR and the equator with below average SLP in the MDR leading to a decline in the pressure gradient and a weakening of the trade winds and ultimately less wind shear, while above average SLP leads to an increasing pressure gradient and a strengthening of the trade winds and more wind shear (Gray, 1994). Since the composite maps of SLP (Figures 4.13-4.16)

revealed strong changes in SLP between low and high SIA years, composite maps of the 1000 mb wind vector anomalies will aid in confirming that changes in SLP influence the strength of the trade winds across the MDR.

Figures 4.21 and 4.22 show the composite maps for 1000 mb vector wind anomalies for the seven lowest and highest Spring Baffin Bay SIA years, respectively, while Figures 4.23 and 4.24 show the composite maps for the seven lowest and highest Spring Hudson Bay SIA years, respectively. By analyzing the 1000 mb vector wind anomalies the relative strength of the easterly trade wind can be inferred with easterly vector wind anomalies indicating strengthened easterly trade winds and increased wind shear, while westerly vector wind anomalies indicate weakened trade winds. Figures 4.21 and 4.23 reveal that during years of low SIA westerly vector wind anomalies are present throughout the MDR indicating weakened trade winds. The composite maps of SLP indicate that a pattern of anomalously low SLP is present during low SIA years. This leads to the conclusion that low SLP is associated with weakened trade winds and reduced wind shear. Low SLP, weakened trade winds, and reduced wind shear are all key factors leading to an above average TC season. During years of high Spring SIA the opposite pattern is present with 1000 mb vector wind anomalies (Figures 4.22 and 4.24) being more easterlies meaning strengthened trade winds and increased wind shear. The composite maps of SLP support this finding by revealing that during years with high SIA SLP is anomalously high. This leads to an enhanced meridional pressure gradient resulting in strengthened easterly trade winds and increased wind shear in the MDR. All these conditions favor a suppressed TC season.

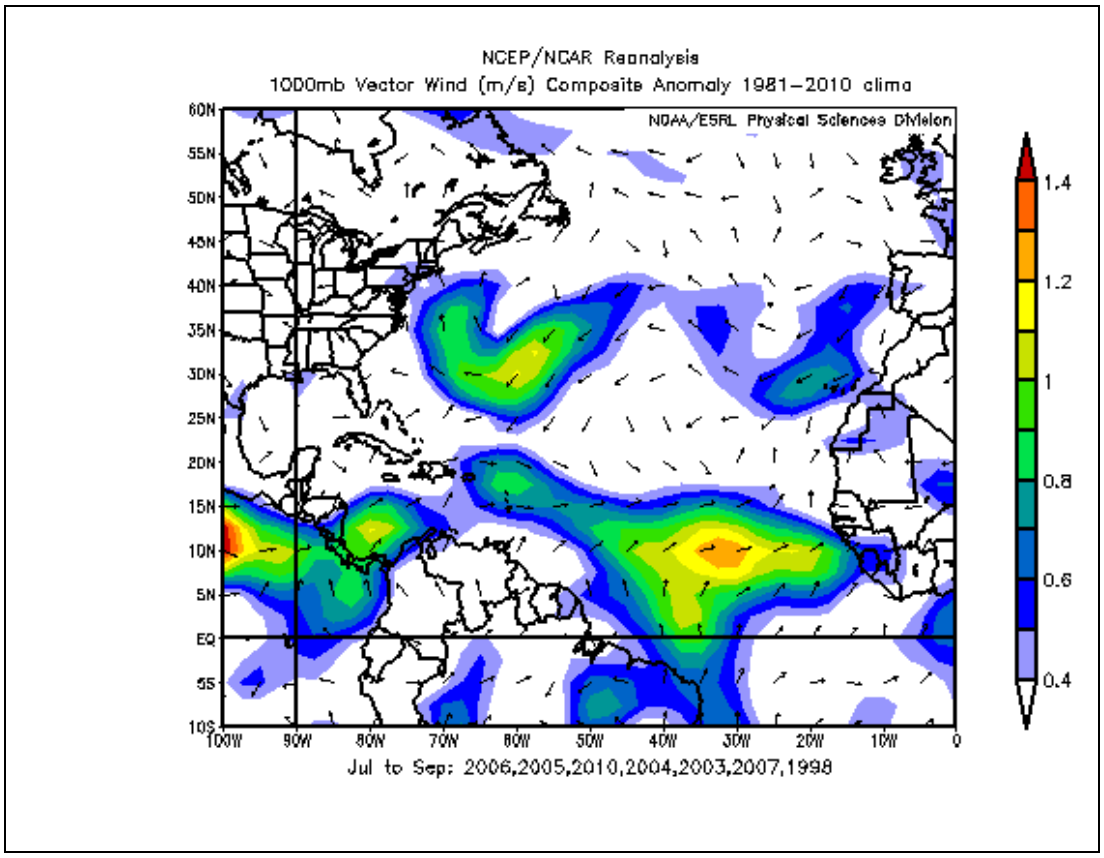

Figure 4.21 The anomalies in 1000 mb vector wind compared to 1981-2010 climatology during the seven lowest Spring Baffin Bay sea ice area years. Image provided by the NOAA/ESRL Physical Sciences Division, Boulder Colorado from their Web site at http://www.esrl.noaa.gov/psd/ (Kalnay et al., 1996).

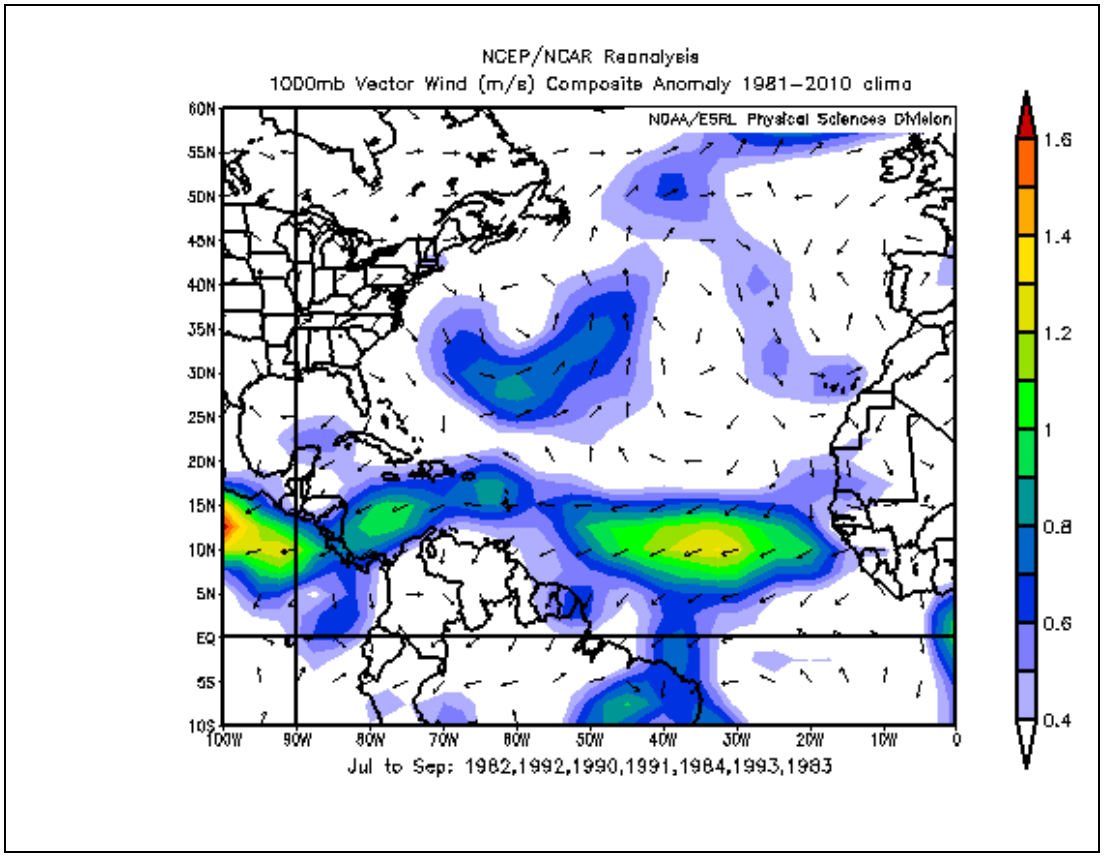

Figure 4.22 The anomalies in 1000 mb vector wind compared to 1981-2010 climatology during the seven highest Spring Baffin Bay sea ice area years. Image provided by the NOAA/ESRL Physical Sciences Division, Boulder Colorado from their Web site at http://www.esrl.noaa.gov/psd/ (Kalnay et al., 1996).

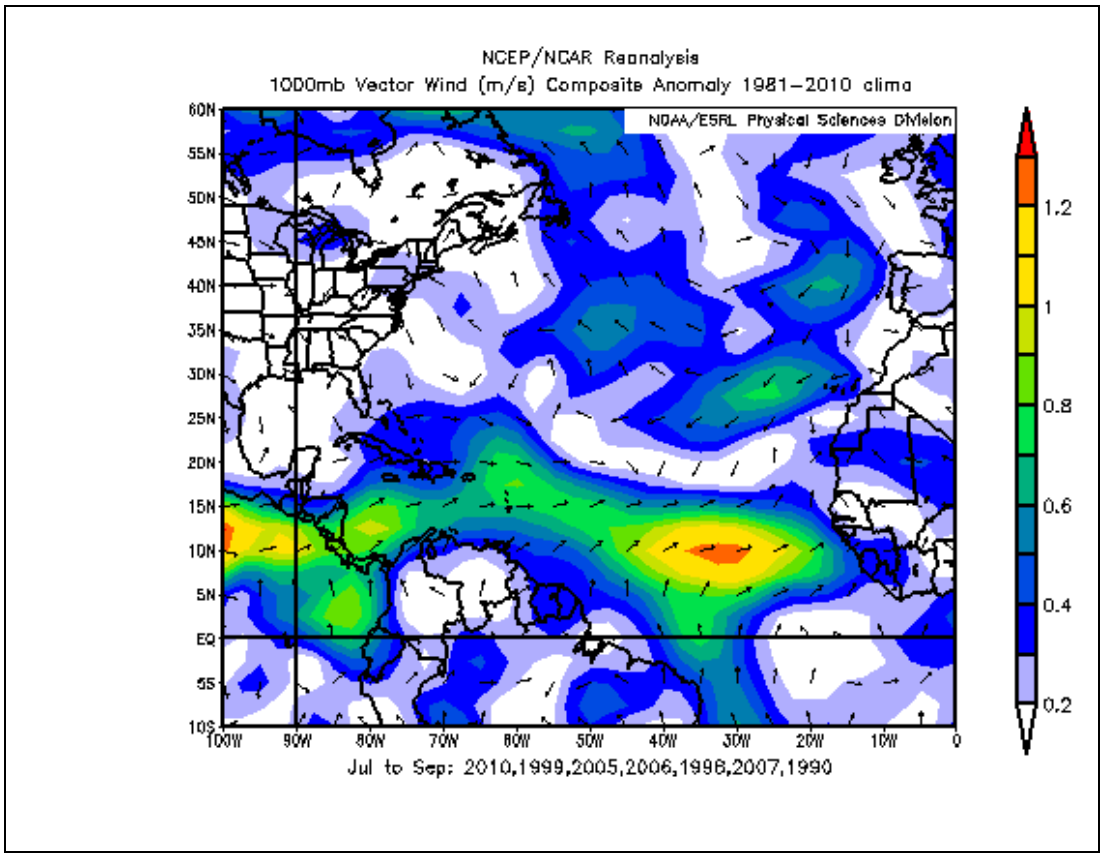

Figure 4.23 The anomalies in 1000 mb vector wind compared to 1981-2010 climatology during the seven lowest Spring Hudson Bay sea ice area years. Image provided by the NOAA/ESRL Physical Sciences Division, Boulder Colorado from their Web site at http://www.esrl.noaa.gov/psd/ (Kalnay et al., 1996).

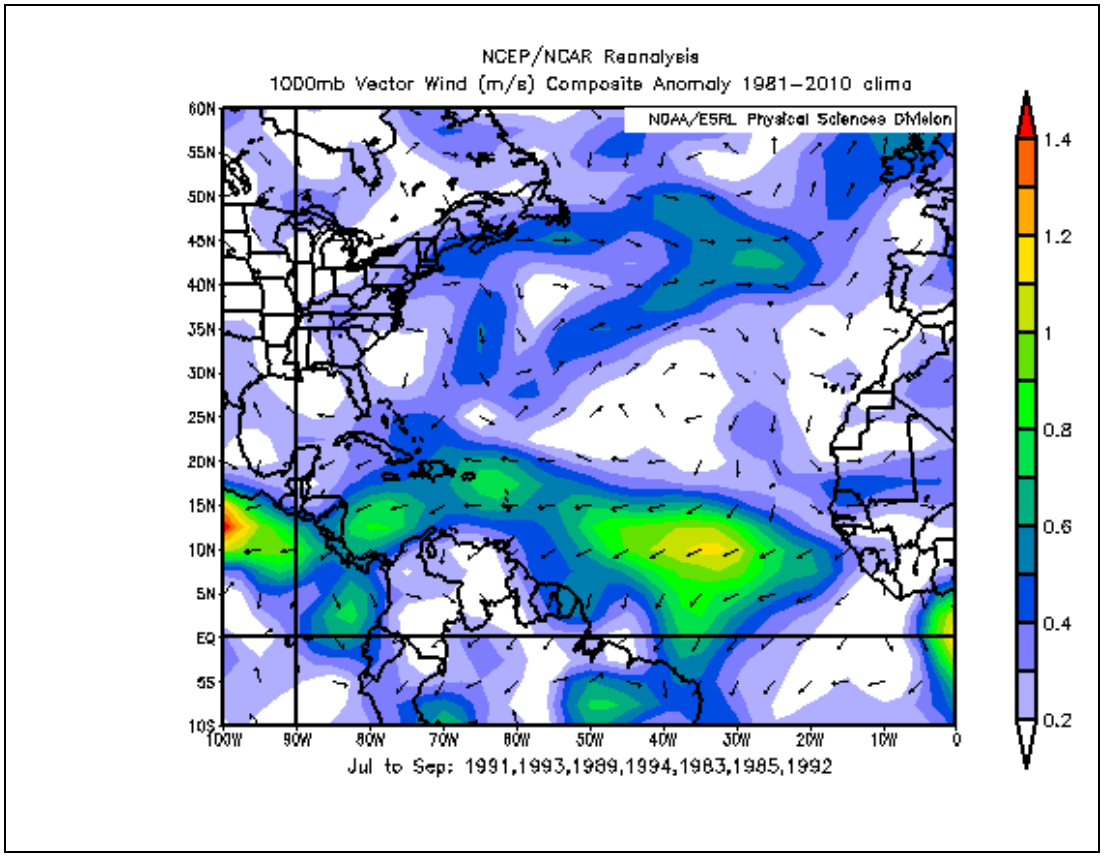

Figure 4.24 The anomalies in 1000 mb vector wind compared to 1981-2010 climatology during the seven highest Spring Hudson Bay sea ice area years. Image provided by the NOAA/ESRL Physical Sciences Division, Boulder Colorado from their Web site at http://www.esrl.noaa.gov/psd/ (Kalnay et al., 1996).

By using correlation plots and composite maps a clear relationship between Spring Baffin Bay and Hudson Bay SIA and the key factors known to influence TC activity in the Atlantic is revealed. Many of the environmental factors influencing TC activity are related to variations in SLP, SSTs, 1000 mb vector wind, and wind shear across the MDR. These changes directly influence tropical cyclogenesis by affecting the environmental conditions present during the peak months of the TC season. Though this relationship between Spring SIA and these key environmental factors is now well established, the exact physical mechanisms that allow

variations in the SI and SC across the high latitudes to influence atmospheric circulation in the tropics are still unresolved (Yan et al., 2012; Budikova, 2009).

4.6 Sea Ice Area and Tropical Cyclone Activity Relationship

Results from the correlation and composite analyze have shown that Spring Baffin Bay and Hudson Bay SIA have an association with changes to SST, SLP, and trade wind strength throughout the Atlantic's MDR that lead to TC variability from season to season. From other studies that have investigated the link between high-latitude climate changes and low-latitude climate variations a variety of physical mechanisms have been proposed. In this subsection two previously proposed physical mechanism regarding the high-low latitude climate link will be presented as well a newly proposed mechanism directly linking Baffin Bay and Hudson SIA to changes in TC activity.

4.6.1 Wind, evaporation, sea surface temperature feedback

It has been shown by modeling studies that a coupled feedback between wind, evaporation, and SST (WES feedback) could be a possible mechanism of energy transfer between high and low latitudes (Xie, 1999; Chiang and Bitz, 2005). The coupled feedback starts with anomalously high SI reducing local latent and sensible heat fluxes that leads to a drying and cooling of the air mass over the SI. The cooler and drier air is then advected into the mid-latitudes via extratropical cyclones, which in turn cause anomalous surface pressure gradients that strengthen surface easterlies. These surface easterlies then promote increased evaporation over the oceans thereby cooling the ocean surface. This cooled ocean surface is then pushed towards the equator via the trade winds. Once the cooled ocean waters reach the equator an anomalous meridional pressure gradient is induced, which displaces the ITCZ southward.

This mechanism is consistent with the hypothesis proposed by Gray et al. (1993) in which they suggest that an anomalous meridional pressure gradient across the Atlantic MDR is often associated with displacement of the ITCZ to the north (south) during enhanced (suppressed) TC activity. The composite maps (Figures 4.13-4.16) within this study also suggest this mechanism by revealing that during high SIA years anomalously high SLP is experienced in the MDR, which sets up a strengthened meridional pressure gradient force as evidenced by the enhanced easterly vector wind anomalies. The anomalies in SLP and vector wind imply that the ITCZ is in a more southward position, which leads to decreased TC activity. The composite analysis supports this SLP-vector wind-ITCZ relationship by showing statistically significant differences in the means of seven TCPs between high and low SIA year.

4.6.2 Wave Train Teleconnection

Ke (2007) also proposed a physical mechanism after investigating North Pacific SI as a predictor of western North Pacific TC activity. The author proposed that an atmospheric wave train teleconnection is responsible for the link between high latitude SIE changes and low latitude tropical atmospheric circulation. In his study the author found a correlation coefficient of -0.49 between March-May North Pacific SI and TC frequency in the western North Pacific. To isolate the March-May SI influence on TC frequency years with strong ENSO event were removed. Figure 4.25 shows the time series between Spring Baffin Bay SIA, TC, and ACE with values during years with strong ENSO events also removed. The correlation coefficients between SIA and TC and SIA and ACE are -0.56 and -0.64, respectively, showing that this study's and Ke's (2007) study produced similar results. Ke (2007) analyzed the March-May North Pacific SI in terms of its relationship to SLP anomalies and concluded that SI could be influencing tropical circulation through modulation of the NPO leading to a well-organized teleconnection wave

pattern in the 200 mb zonal wind field. Ke (2007) conducted composite and correlation analysis between March-May SI and environmental conditions linked to TC activity, similar to those conducted in subsections 4.4. and 4.5 of this study, and found that high (low) SI years are associated with cold (warm) SST, high (low) SLP, and enhanced (suppressed) vertical wind shear anomalies across the western North Pacific MDR all of which lead to decreases (increased) in TC activity. These results are consistent with the findings of this study, and since Spring Baffin Bay and Hudson Bay SIA are also associated with the NAO, an atmospheric wave train teleconnection could also be the physical mechanism linking SIA variations in Baffin Bay and Hudson Bay to changes in tropical atmospheric circulation

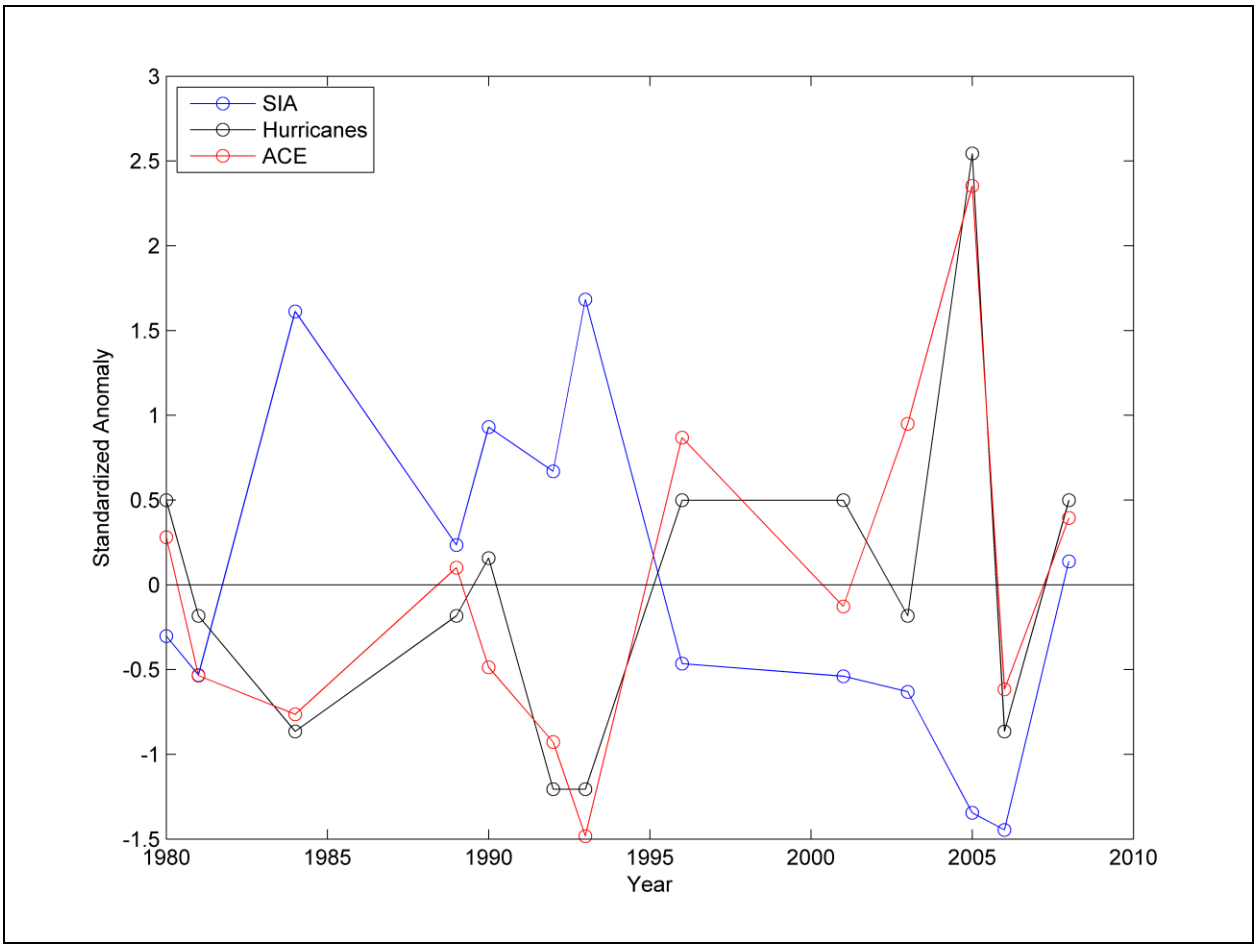

Figure 4.25 Time series of Spring Baffin Bay sea ice area, tropical cyclones, and accumulated cyclone energy with strong ENSO events removed.

4.6.3 Sea ice area as an indicator of climate mode states

Though the WES feedback has been found as the connection between high and low latitude climate within GCM studies, this mechanism usually takes around 12-15 months after the introduction of additional SI to displace the ITCZ southward (Hughen et al., 2000; Budikova 2009) making this mechanism an unlikely the link between spring SIA and the following July-September TC activity. The atmospheric wave train physical mechanism could operate at the timescales present between spring changes in SIA and subsequent July-September TC activity, but more analysis into the role of Baffin Bay and Hudson Bay SIA influencing the NAO's possible teleconnection wave train must be conducted in order to confirm this hypothesis. An alternative hypothesis is that spring SIA in Baffin Bay and Hudson Bay is not a physical mechanism governing tropical atmospheric circulation but rather is an indicator of current/near future atmospheric and oceanic oscillations, which is not captured by any one CM index. Wand et al. (1994) noted that Hudson Bay SI variability is almost completely due to atmospheric forcing because it exhibits features of an inland sea not influenced by ocean currents, while Baffin Bay experiences both oceanic and atmospheric forcings. Spring Hudson Bay SIA is significantly correlated with the key CM predictors of Summer ENSO ($r = 0.41$) and Spring NAO ($r = 0.43$), and since Spring NAO is correlated with Spring AO at $r = .64$ the two oscillations are often viewed as the same phenomenon with the NAO being a regional expression of the AO (Wallace, 2000).

Figures4.26 and 4.27 show the composite maps of SLP for March-May for the seven years of lowest and highest Spring Hudson Bay SIA, respectively. These figures clearly reveal the distinct dipole of the NAO pattern with a stronger NAO present during years of high SIA and weaker NAO during years with low SIA. The NAO pattern in the spring can persist into the

summer months meaning spring SIA can be an indicator of the spring state of the NAO that will likely persist into the summer months. Also August-October La Nina events occurred during four of the seven lowest Hudson Bay SIA years (La Nina events defined by Climate Prediction Center).In addition, Mysak et al. (1996) showed that simultaneously strong NAO and El Niño events lead to above average SI in Hudson Bay, Baffin Bay, and the Labrador Sea.

It has been shown that the states of the NAO, AO, and ENSO leading into a TC season influences TC variability through changes to the environmental factors influencing tropical cyclogenesis, such as SLP, SSTs, and wind shear across the MDR (Grey et al., 1984; Elsner et al., 2000; Xie et al., 2005). It has also been shown that Spring Baffin Bay and Hudson Bay SIA are often forced by these same CMs (Mysak et al., 1996), but since these CMs are not suggested by the correlation or composite analysis it can be hypothesized that SI may be a better indicator of these CMs than the CM index values themselves. CMs are often measured by a variety of methods causing the index values to differ greatly from one study to another, but the measurement of SIA is very straight forward and is very consistent (NSIDC, 2013a). CMs are also often expressed at a variety of timescales making them difficult to predict at lead times necessary for seasonal forecasting, but SI tends to be more predictable, due to its thermodynamic properties, possibly allowing SI to represent the seasonal state of CMs and their likely persistence into the following season. Observing seasonal changes in SI may allow for the future changes in CMs to be inferred, since the current state of many CMs can be captured by SI. This is the case for Spring Baffin Bay and Hudson Bay SIA, since these were among the top predictors for the CM-CRYO models and they are strongly correlated with environmental conditions known to influence the TC season. This capacity to record and future state of CMs may be why the CRYO models almost always outperformed the CM models and why the CYRO models were almost

always identical to the CM-CRYO models. Since the CYRO and CM-CRYO models were so similar in model performance, comparing the CM-CRYO models to current operational seasonal TC activity models will show how effect SI can be for the seasonal forecasting of TCs.

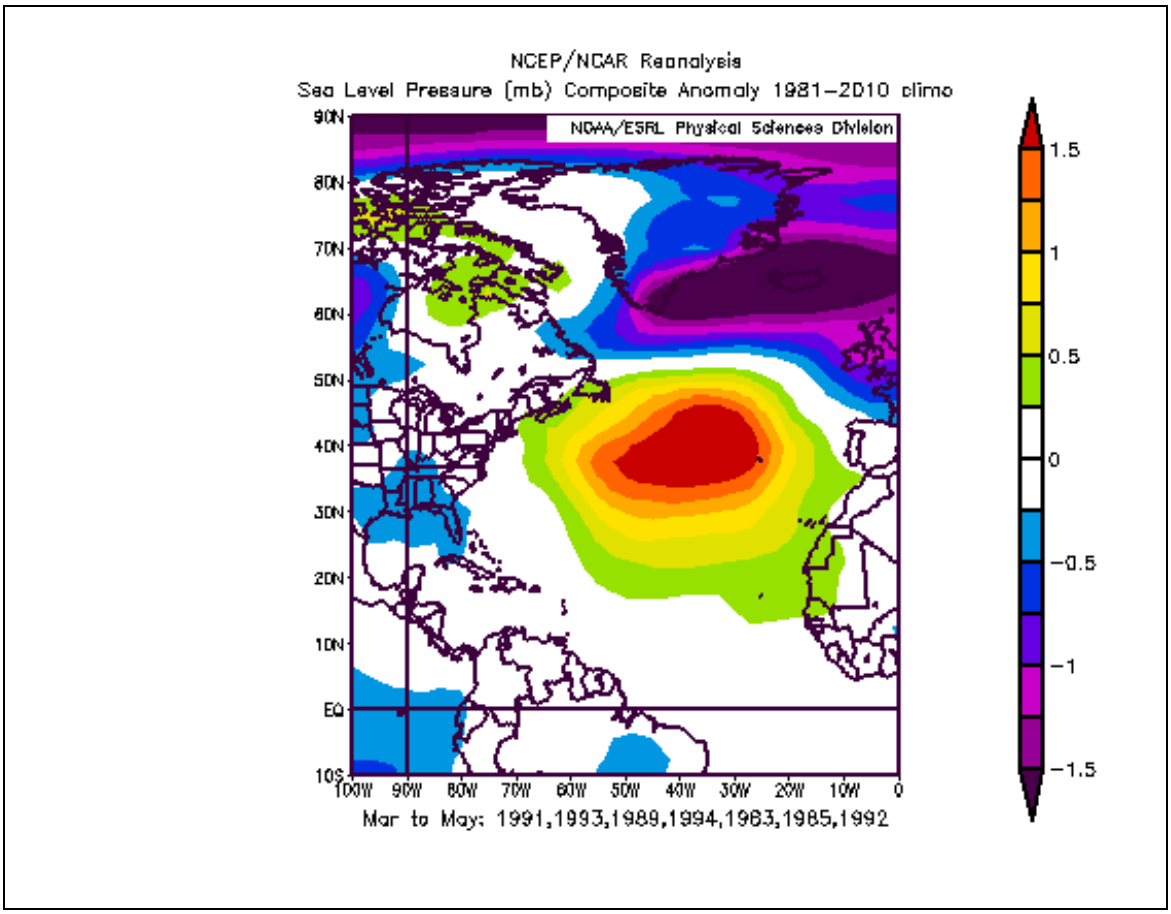

Figure 4.26 Composite map of sea level pressure anomalies for March-May for the seven years with the highest Hudson Bay sea ice area. Image provided by the NOAA/ESRL Physical Sciences Division, Boulder Colorado from their Web site at http://www.esrl.noaa.gov/psd/ (Kalnay et al., 1996).

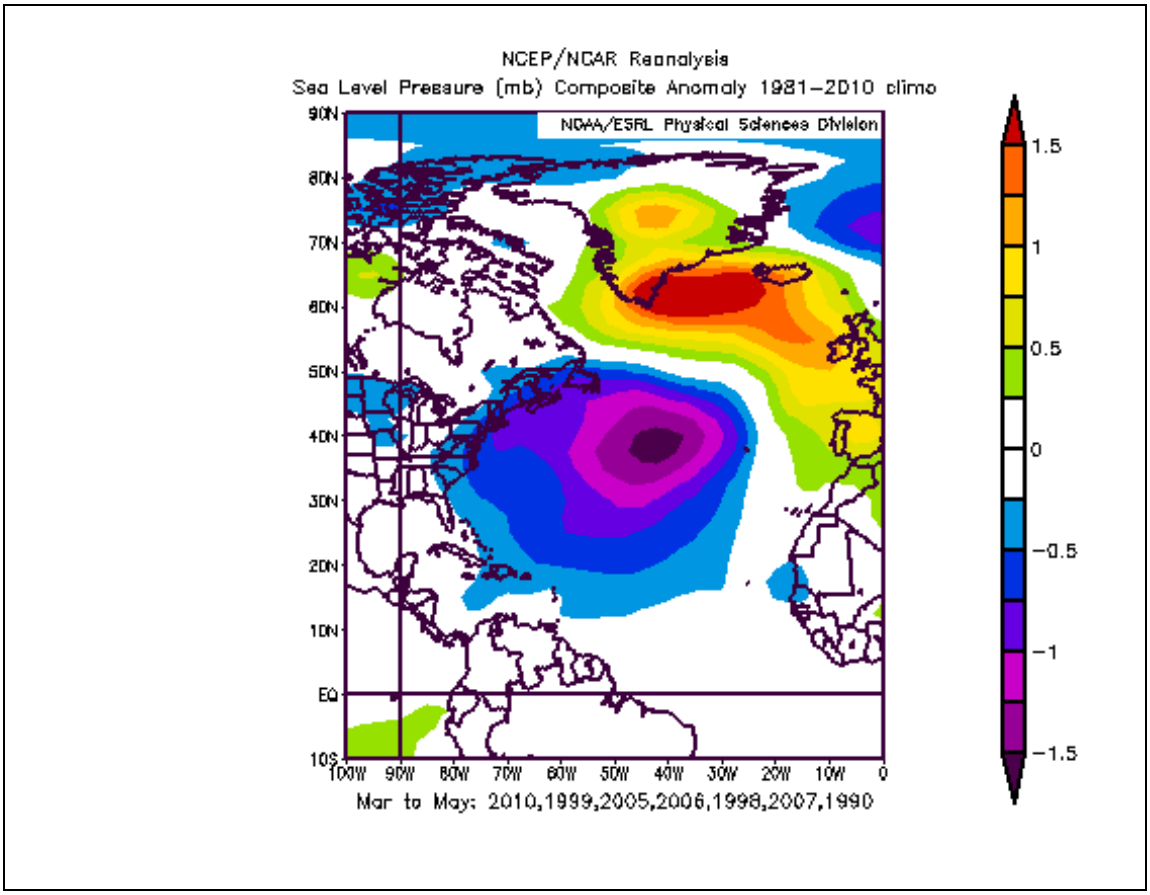

Figure 4.27 Composite map of sea level pressure anomalies for March-May for the seven years with the lowest Hudson Bay sea ice area. Image provided by the NOAA/ESRL Physical Sciences Division, Boulder Colorado from their Web site at http://www.esrl.noaa.gov/psd/ (Kalnay et al., 1996).

4.7 Comparison with existing operational models

In order to understand how models that include cryospheric information compare to those that do not, the CM-CRYO models skill measures of R^2 and MSSS will now be compared to the current operational models of CSU and TSR for the TCPs TC, H, MajH, and ACE. Figure 4.28 shows the R^2 values at the four issuance dates for the CSU and CM-CRYO models. Since the modeling groups issue spring hindcasts in different months, CSU's April forecast will be compared to our March hindcast and CSU's August forecast will be compared to our September

hindcast. The December and June hindcast issuance dates are the same between CSU and our models. Figure 4.28 reveals that the CSU models outperform our models in every TCP and at every hindcast issuance besides the June hindcast of MajHs. The differences in R^2 are largest at longer lead times, attenuated at the June hindcasts and again larger at the September hindcasts.

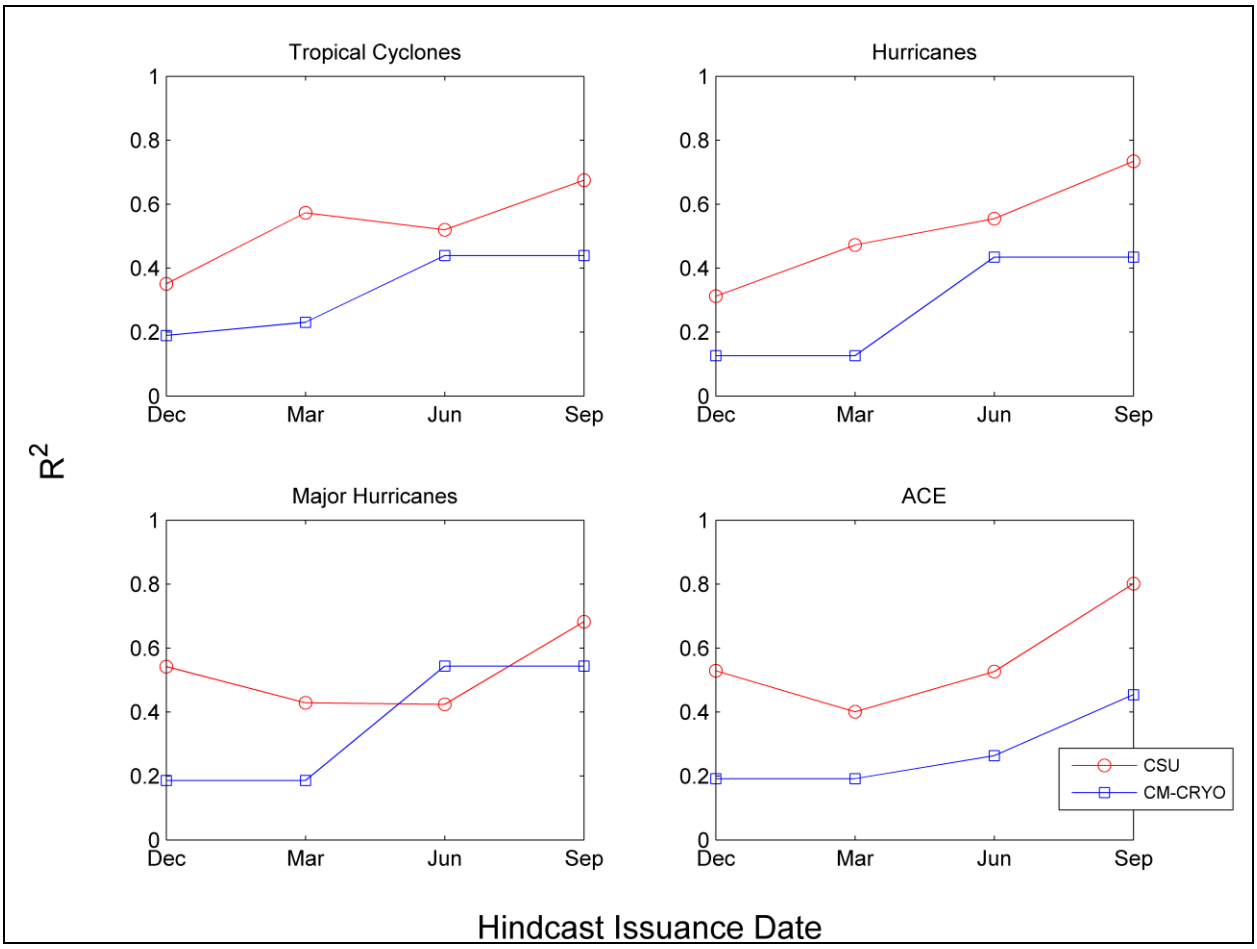

Figure 4.28 Comparison of R^2 for forecasts of tropical cyclone, hurricanes, major hurricanes, and accumulated cyclone energy between the statistical models of Colorado State University (CSU) and the CM-CRYO models.

Figure 4.29 shows the MSSS for the hindcasts of TC, H, MajH, and ACE for the statistical models of CSU, TSR, and the CM-CRYO models. As in Figure 4.28, the other two model groups tend to have better MSSS values then the CM-CRYO models with CSU often having the highest MSSS values. The CM-CRYO models and the TSR models both slightly

outperformed CSU at the June hindcast of MajHs. Large variations in MSSS are seen in the ACE hindcasts while the smallest variations occurring at the TC hindcasts at the longer lead times of December and March. Model agreement tends to be greatest at the shorter lead times of June and September.

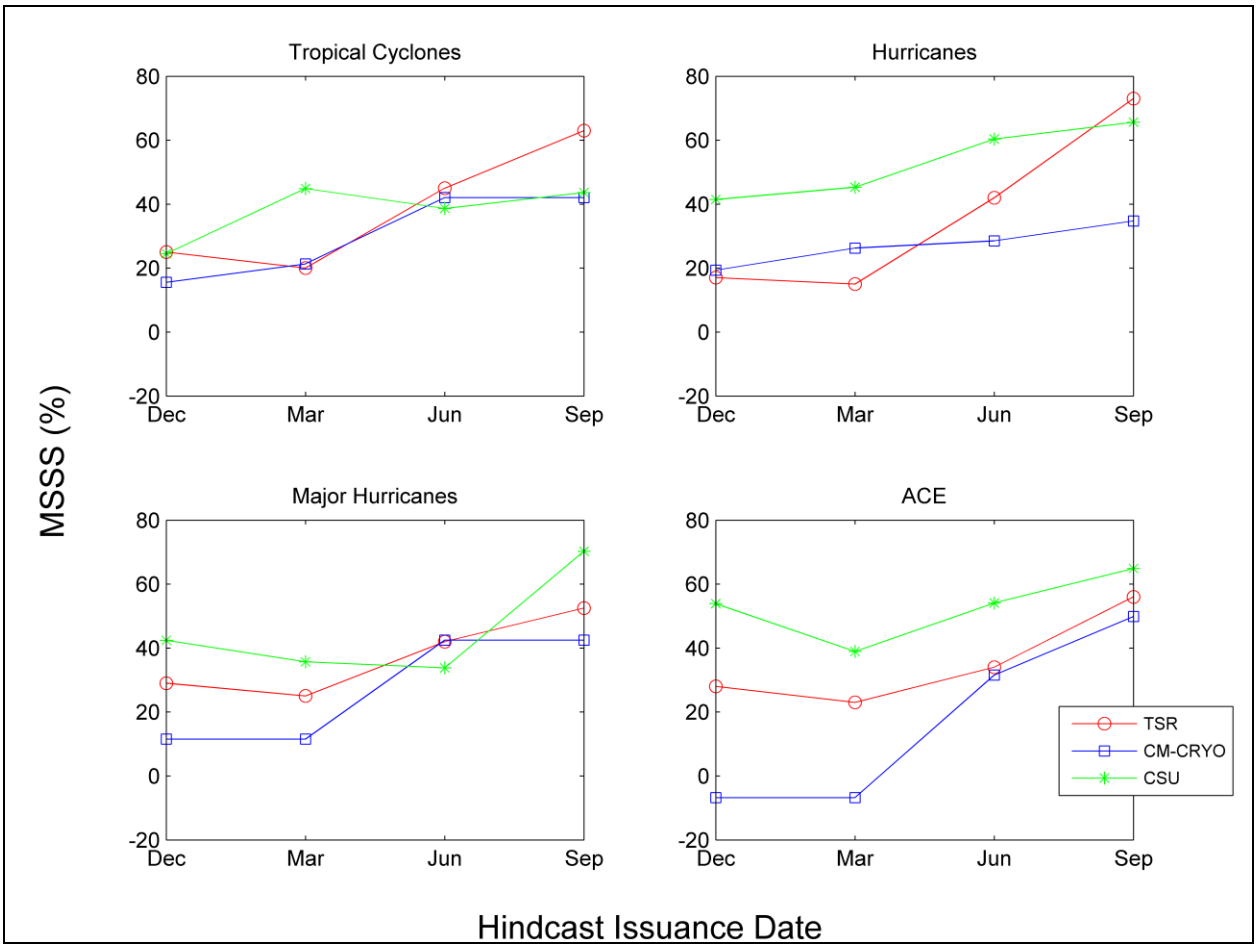

Figure 4.29 Comparison of the mean square skill score for forecasts of tropical cyclone, hurricanes, major hurricanes, and accumulated cyclone energy between the statistical models of Colorado State University, Tropical Storm Risk, and this study.

Both comparison figures (Figure 4.28 and 4.29) show that the largest hindcast errors are present at the longest lead times of December and March and decrease as the start of the TC season approaches in June. Though the CSU and TSR models do outperform the CM-CRYO models in most cases it is important to keep in mind the key predictors used between the models.

To highlight these differences in predictors between the modeling groups, the June hindcasts of MajHs and the December hindcasts of TCs will be examined.

Table 4.4 Forecast predictors and skill for tropical cyclones (TC) and major hurricanes (MajH) between the 3 modeling groups. Acronyms are: CM-CRYO (cryospheric and climate mode models), CSU (Colorado State University), ENSO (El Niño-Southern Oscillation), MDR (main development region), MSSS (mean square skill score), SIA (sea ice area), SIE (sea ice extent), SLP (sea level pressure), SST (sea surface pressure), TSR (Tropical Storm Risk), and U (zonal).

Modeling Group	**December Predictors for TC**	**June Predictors for MajH**
CSU Dec. MSSS:24% Jun. MSSS:33%	1) Oct-Nov. SST in N. Atlantic 2) Nov. 500mb heights in N. Atlantic 3) Nov. SLP in NE Pacific	1) April-May SST E. Atlantic 2) April-May 200mb U wind tropical Pacific 3) Sep. ENSO forecast 4) May SLP in MDR
TSR Dec. MSSS:25% Jun. MSSS:42%	1) July-Sep. 925mb height forecast over Caribbean and tropical Atlantic 2) Aug-Sep. SST forecast for the MDR 3) Aug-Sep. ENSO forecast	1) July-Sep. 925mb height forecast over Caribbean 2) Aug-Sep. SST forecast for the MDR 3) Aug-Sep. ENSO forecast
CM-CRYO Dec. MSSS:19% Jun. MSSS:53%	1) Fall Baffin Bay SIA 2) Fall Baffin Bay SIE	1) Spring Hudson Bay SIA 2) Fall Canadian Archipelago SIA

Table 4.4 compares the December TC and June MajH hindcasts between the three modeling groups. Table 4.4 reveals for the December hindcast the MSSS values between the three groups are quite similar at 24%, 25%, and 19% for CSU, TSR, and CM-CRYO, respectively, even though the predictors used for the December forecasts are quite different. CSU uses SST, SLP, and 500mb geopotential height data as predictors (Klotzbach and Gray, 2010) while TSR uses 925mb geopotential height, SST, and ENSO forecasts (Saunders and Lea, 2011). Both CSU and TSR use a variety of predictors to construct their models. TSR even uses an 18

ensemble member statistical model for ENSO forecasts (Lloyd-Hughes et al., 2004) while the CM-CRYO model only uses two predictors that are both from similar geographic regions, yet the modeling groups all have similar MSSS values. For the June MajH hindcast the CM-CRYO model uses only two predictors (Spring Hudson Bay SIA and Fall Canadian Archipelago SIA) but actually outperforms the other modeling groups with a MSSS of 53% while the TSR had 42% and CSU had 33%. Both CSU and TSR utilized ENSO forecasts in their models and a variety of globe-scale predictors (Klotzbach and Gray, 2012b; Saunders and Lea, 2012), but they were unable to outperform the simple two-predictor model used in this study. Though the CSU and TSR models did show increased skill over the CM-CRYO models for most TCPs and lead times, the CM-CRYO model was comparable to these other models at the December and June hindcasts of TCs and the September ACE hindcast, while being superior at the June MajH hindcast. These results confirm that a forecasting scheme using easy to measure predictors, such as SI, can be comparable those using complex predictors, such as ENSO forecasts.

CHAPTER 5

CONCLUSION

In this study three model groups – CM models, CRYO models, and CM-CRYO models – were used in order to investigate the effects of including SIA, SIE, and SCE in the statistical forecasting of 13 TCPs. Model groups were based on the predictors available to them during model construction. Models were constructed using multiple OLS regression with a jackknife procedure for model validation. A stepwise selection procedure was carried out for each of the models to identify the most influential predictors for the regression equations. These predictors were seasonal averages of SIA and SIE for ten geographic regions, SCE for three regions, and five CMs. The study period 1980-2010 was chosen for this study because of the temporal resolution of high quality SIA and SIE data from satellites. The official Atlantic TC season runs from 1 June to 31 November, so hindcasts of the 13 TCPs were created in December, March, and June leading up to the TC season and a September hindcast for the peak of the season. This led to four hindcasts being created for each of the 13 TCPs for each of the three model groups resulting in 156 models. Model evaluation was based on R^2 and MSSS to quantify the skill of the hindcasts in predicting the observed TCPs for the 31 year study period. These skill measures allowed for the comparison of model performance between not only the three model groups but also between the current operational models of CSU and TSR. In addition to the model comparisons, the top eight most frequently selected predictors of the best performing model group, CM-CRYO, were used in correlation and composite analysis in order to determine how these "key" predictors may be associated with the environmental factors known to influence TC activity. These environmental factors are anomalies in SST, SLP, and wind vectors/wind shear

throughout the Atlantic's MDR between the peak TC months of July-September, when 90% of annual TC activity is experienced.

A review of the proposed research questions and the resulting conclusions will now be presented followed by a further summary of the key findings. The first research question posed was, "Which components of the cryosphere have the strongest associations with North Atlantic TC activity?" This question is aimed at determining if SIA, SIE, or SCE is the most strongly associated with the 13 TCPs and therefore allowing for a cryosphere-TC relationship to be defined. It turns out that SIA has most significant relationships with the 13 TCPs than either SC, SIE, or the CMs do. Of the top predictors, Spring Baffin Bay SIA is significantly correlated with nine of the 13 TCPs (TC, TS, MinH, MajH, Pwind, LMD, MinDOY, MaxDOY, and TSL) while Spring Hudson Bay SIA is significantly correlated with seven TCPs (TC, TS, MajH, ACE, MinDOY, MaxDOY, and TSL). It is now possible to hypothesize that SIA is a more informative measure of the cryosphere's interaction with atmospheric circulation then SIE or SCE due to the finding of the correlations table (Table 4.2) and plots (Figures 4.8-4.11), and the composite analysis (Figure 4.12-4.24).

The second research question posed was, "What geographic areas within the cryosphere are the most influential to the statistical forecast models? How do these regions relate to the CMs?" This two part question is an extension of Question 1 and is aimed at identifying the geographic regions of SIA that are most significantly related to the 13 TCPs as well as determining if these geographic regions are similar to the known areas of influence of CMs. Answers to these questions are suggest by the fact that the top four cryosphere predictors are located within Baffin Bay and Hudson Bay or the Bering Sea, which are near the AO, NAO and NPO, and/or close to the North Atlantic. Many of the most significant cryospheric predictors are

closely related to CMs that have well documented associations with TC variability, which helps explain why the CM-CRYO models represent the best performing model group.

The third research question posed was, "What is the physical mechanism governing the cryosphere-TC relationship?" The aim of this question is to determine how the most significant predictor (i.e., SIA) influences TC variability The physical mechanism governing each of the 13 TCPs remains unresolved but three possible mechanisms have been presented regarding overall TC activity: 1) WES feedback, 2) atmospheric teleconnection wave train, and 3) Baffin Bay and Hudson Bay SIA as an indicator of current and future states of CMs. All of these proposed mechanisms are capable of influencing tropical atmospheric circulation and thus the environmental factors governing tropical cyclogenesis. The WES feedback is not a likely mechanism because of the long time period necessary to influence tropical atmospheric circulation after the initial change in SI. The atmospheric wave train mechanism proposed by Ke (2007) operates at the timescales used in this study and since the correlation analysis findings within Ke (2007) are so similar to those of this study, this mechanism is a likely candidate, though further investigation into the NAO's influence on tropical atmospheric circulation is required to support this mechanism. SIA as an indicator of current and future states of CMs is a completely new mechanism presented in this study so further investigation into how SIA stores CM information is required.

The fourth research question posed was, "How does a forecasting scheme incorporating cryospheric information compare to current operational forecasting schemes?" The aim of this question is to determine whether incorporating cryospheric data into a forecasting scheme represents a fruitful future research area. The CM-CRYO models comparably performed (within 6%) the TSR and CSU June hindcasts of TCs, and was 11% points better than the top

performing model for June hindcasts of MajHs. In general, model performance featured large deviations from the TSR and CSU models during the December and March hindcasts and smaller deviations during the June and September hindcasts. Though the CM-CRYO model in most cases was outperformed by the current models, this simple model does show promise in forecasting of MajHs and TCs. By further refining the CM-CRYO and including an ENSO forecast, like the current (i.e., CSU and TSR) models, the CM-CRYO model could exceed the skill level of current models for certain TCPs and lead times. Additionally, with future SI reductions expected (Stroeve et al., 2012) incorporating cryospheric information into a forecasting scheme could provide valuable insight into the unresolved question of how TCs will be effected in a warming world.

Key findings from this study can be summarized as:

1. When comparing the three model groups of CM, CRYO, and CM-CRYO the top performing group was the CM-CRYO followed by the CRYO and lastly CM. On average the MSSS values for the 13 TCPs of the CRYO and CM groups were 19% and 28% lower than those of the CM-CRYO group, respectively.
2. Of the top eight most frequently selected predictors of the CM-CRYO, Spring Baffin Bay and Hudson Bay SIA had the most significant relationships with the environmental conditions known to influence TC activity based on the correlation and composite analysis. These predictors have strong ($r > 0.5$) correlations with SST, strong ($r > -0.5$) inverse correlations with SLP, and an inverse relationship between 1000 mb wind vector [proxy for wind shear] anomalies throughout the Atlantic's MDR.

3. Composite analysis revealed that during the seven highest and lowest SIA years in 1980-2010 small seasonal variations (<± 20% of climatology) in SIA were associated with large changes (>±40% of climatology) in the TCPs. During years of high (low) Spring Hudson Bay SIA there were decreases (increases) of 20% (45%) in MinHs and 46% (42%) in the PDI, while during high (low) Spring Baffin Bay SIA years decreased (increases) of 57% (46%) in MajHs and 56% (67%) in the PDI were experienced. A total of seven TCPs (TC, TS, H, MinH, MajH, ACE, and PDI) had statistically significant differences in their means between high and low SIA years.
5. The CM-CRYO model group's June hindcast of MajHs outperforms the June hindcasts of TSR and CSU by 11 and 20 percentage points, respectively, based on MSSS values when using only two SIA predictors while TSR and CSU use three and four predictors from a variety of atmospheric observations and ENSO forecasts, respectively.

The main goal of this study was to support the hypothesis that the cryosphere has some association with Atlantic seasonal TC activity, and based on the findings presented, this study provides a strong argument for this hypothesis. This allows a new forecasting scheme to be created, and lays out a foundation for future studies investigated the interactions between the cryosphere and TCs.

REFERENCES

ACIA (Arctic Climate Impact Assessment). 2005. C. Symon, L. Arris, and B. Heal (eds.) Cambridge University Press, Cambridge, United Kingdom and New York, NY, USA.

Bamzai, A. S. 2003. Relationship between snow cover variability and arctic oscillation index on a hierarchy of time scales. *International Journal of Climatology* 23, 131-142.

Bader, J , M. D. S., Mesquita, K. I. Hodges, N. Keelnyside, S. Osterhus, and M. Miles. 2011. A review on Northern Hemisphere sea-ice, storminess and North Atlantic Oscillation: Observations and projected changes. *Atmospheric Research* 101, 809-834

Barnston, A. G. and R. E. Livezey. 1987. Classification, seasonality and persistence of low-frequency atmospheric circulation patterns. *Monthly Weather Review* 115, 1083-1126.

Bartolini, E., P. Claps, and P. D'Odorico. 2010. Connecting European snow cover variability with large scale atmospheric patterns. *Advances in Geosciences* 26, 93-97.

Bekryaev, R. V., I. V. Polyakov, and V. A. Alexeev. 2010. Role of polar amplification in long-term surface air temperature variations and modern Arctic warming. *Journal of Climate* 23, 3888-3906.

Bell, and Coauthers, 2000. Climate assessment for 1999. *Bulletin of the American Meteorological Society* 81, 1-50.

Bell, G. D. and M. Chelliah, 2006. Leading tropical modes associated with interannual and multi-decadal fluctuations in North Atlantic hurricane activity. *Journal of Climate* 19, 590-612.

Bojariu, R. and L. Gimeno, 2003. The role of snow cover fluctuations on multiannual NAO persistence. *Geophysical Research Letters* 30, 1156-1160.

Budikova, D., 2009. Role of Arctic sea ice in global atmospheric circulation: a review. *Global and Planetary Change* 68, 149-163.

Camargo, S. J., A. G. Barnston, P. J. Klotzbach, and C. W. Landsea. 2007. Seasonal tropical cyclone forecasts. *World Meteorological Organization Bulletin* 56, 297-309.

Camargo, S. J. and S. E. Zebiak. 2002. Improving the detection and tracking of tropical storms in atmospheric general circulation models. *Weather and Forecasting* 17, 1152-1162.

Chiang, J. C. H. and C. M. Bitz. 2005. Influence of high latitude ice cover on the marine intertropical convergence zone. *Climate Dynamics* 25, 477-496.

Choi, K.S., J. Y. Moon, D. W. Kim, and P. S. Chu, 2010. Seasonal predictions of tropical cyclone genesis frequency over the western North Pacific using teleconnections. *Theoretical and Applied Climatology* 100, 191-206.

Cohen J. and D. Entekhabi. 2001: The influence of snow cover on northern hemisphere climate variability. *Atmosphere-Ocean* 39, 35-53.

Deser, C., J. E. Walsh, and M. S. Timlin. 2000. Arctic sea ice variability in the context of recent atmospheric circulation trends. *Journal of Climate* 13, 617-633.

Dery, S. J. and R. D. Brown. 2007. Recent northern hemisphere snow cover extent trends and implications for the snow-albedo feedback. *Letters of Geophysical Research* 34, L22504. DOI:10.1029/2007GL031474.

Elsner, J. B. and C. P. Schmertmann. 1993. Improving extended-range seasonal predictions of intense Atlantic hurricane activity. *Weather and Forecasting* 8, 345-351.

Elsner, J. B. and C. P. Schmertmann. 1994. Assessing forecast skill through cross validation. *Weather and Forecasting* 9, 619-624.

Elsner, J. B., K. B. Liu, and B. Kocher. 2000. Spatial variations in major U.S. hurricane activity: statistics and a physical mechanism. *Journal of Climate* 13, 2293-2305.

Elsner, J. B. and T. Jagger. 2004. A hierarchical Bayesian approach to seasonal hurricane modeling. *Journal of Climate* 17, 2813-2827.

Elsner, J. B. and T. Jagger. 2006. Prediction models for annual U.S. hurricane counts. *Journal of Climate* 19, 2935-2952.

Emanuel, K. 2005. Increasing destructiveness of tropical cyclones over the past 30 years. *Nature* 436, 686-688.

ESRL (Earth System Research Laboratory). 2013. Physical Sciences Division – PSD Interactive Plotting and Analysis Pages. Webpage. [http://www.esrl.noaa.gov/psd/cgi-bin/data/getpage.pl].

ESRL (Earth System Research Laboratory). 2012. Climate Indices: Monthly Atmsopheric and Oceanic Timeseries . Webpage. [http://www.esrl.noaa.gov/psd/data/climateindices/list/]

Ke, k. 2007. North Pacific sea ice cover, a predictor for the Western North Pacific typhoon frequency. *Science in China Series D: Earth Science* 50, 1251-1257.

Gray, W. M. 1968. Global view of the origin of tropical disturbances and storms. *Monthly Weather Review* 96, 669–700.

Gray, W. M. 1979. Hurricanes: Their formation, structure and likely role in the tropical circulation" *Meteorology Over Tropical Oceans*. D. B. Shaw (Ed.), Roy. Meteor. Soc., James Glaisher House, Grenville Place, Bracknell, Berkshire, RG12 1BX, pp.155-218

Gray,W. M. 1984a. Atlantic seasonal hurricane frequency. Part I: El Niño and 30mb quasi-biennial oscillation influences. *Monthly Weather Review* 112, 1649-1668.

Gray, W. M., 1984b. Atlantic seasonal hurricane frequency. Part II: Forecasting its variability. *Monthly Weather Review* 112, 1669-1683.

Gray, W. M., C. W. Landsea, P. W. Mielke Jr., and K. J. Berry. 1992. Predicting Atlantic seasonal hurricane activity 6-11 months in advance. *Weather and Forecasting* 7, 440-455.

Gray, W. M. C. W. Landsea, P. W. Mielke Jr., and K. J. Berry. 1993. Predicting Atlantic basin seasonal tropical cyclone activity by 1 August. *Weather and Forecasting* 8, 73-86.

Gray, W. M., C. W. Landsea, P. W. Mielke Jr., and K. J. Berry. 1994. Predicting Atlantic basin seasonal tropical cyclone activity by 1 June. *Weather and Forecasting* 9, 103-115.

Gray, W., C. W. Landsea, P.W. Mielke Jr., and K. J. Berry. 2000. Extended range forecast of Atlantic seasonal hurricane activity and US landfall strike probability for 2001. Department of Atmospheric Science Report, Colorado State University, Fort Collins, CO, 22pp

Goldenberg, S. B., C. W. Landsea, A. M. Mestas-Nuñez, and W. M. Gray. 2001. The recent increase in Atlantic hurricane activity: causes and implications. *Science*, 293, 474-479.

Goldenberg, S. B. and L. J. Shapiro. 1996. Physical mechanisms for the association for El Niño and West African rainfall with Atlantic major hurricane activity. *Journal of Climate* 9: 1169-1187.

Gong, C., D. Entekhabi, and J. Cohen. 2003. Orographic constraints on a modeled Siberian snow-tropospheric-stratospheric teleconnection pathway. *Journal of Climate* 17, 1176-1188.

GSL (Rutgers University Global Snow Lab). 2013. Monthly Area Extent Dataset. Webpage. [http://climate.rutgers.edu/snowcover/table_area.php?ui_set=1&ui_sort=0]

Holland, M. M. and C. M. Bitz. 2003. Polar amplification of climate change in coupled models. *Climate Dynamics* 21, 221-232. DOI: 10.1007/s00382-003-0332-6.

Holland, G. J. 1993. "Ready Reckoner" – Chapter 9, Global Guide to Tropical Cyclone Forecasting. WMO/TC-No. 560, Report No. TCP-31, World Meteorological Organization, Geneva, Switzerland.

Hughen, K.A., J. R. Southon, S. J. Lehman, and J. T. Overpeck. 2000. Synchronous radiocarbon and climate shifts during the last deglaciation. *Science* 290, 1951-1954.

Hurrell, J. W. and H. Van Loon. 1997. Decadal variations in climate associated with the North Atlantic Oscillation. *Climate Change* 36, 301-326.

IPCC (Intergovernmental Panel on Climate Change). 2007. Contribution of Working Group I to the Fourth Assessment Report. Solomon, S., D. Qin, M. Manning, Z. Chen, M. Marquis, K.B. Averyt, M. Tignor and H.L. Miller (eds.) Cambridge University Press, Cambridge, United Kingdom and New York, NY, USA.

IPCC (Intergovernmental Panel on Climate Change). 2007. Lemke, P. J. and coauthors, Observations: Changes to snow, ice, and frozen ground. In Contribution of Working Group I to the Fourth Assessment Report. Solomon, S., D. Qin, M. Manning, Z. Chen, M. Marquis, K.B. Averyt, M. Tignor and H.L. Miller (eds.) Cambridge University Press, Cambridge, United Kingdom and New York, NY, USA.

Jarvinen, B. R., C. J. Neumann, and M. A. S. Davis. 1984. A tropical cyclone data tape for the North Atlantic Basin., 1886-1983: Contents , limitations, and uses. *NOAA Technical Memorandum NWS NHC 22*, Coral Gables, FL, 21 pp.

Johannessen, O. M., L. Bengtsson, M. W. Miles, S. I. Kuzmina, V. A. Semenov, G. V. Alekseev, A. P. Nagurnyi, V. F. Zakharov, L. P. Bobylev, L. H. Pettersson, K. Hasselmann, and H. P. Cattle. 2004. Arctic climate change: observed and modelled temperature and sea-ice variability. *Tellus A* 56, 328–341. DOI: 10.1111/j.1600-0870.2004.00060.x

Kalnay, E. and Coauthors, 1996: The NCEP/NCAR Reanalysis 40-year Project. *Bulletin of the American Meteorological Society* 77, 437-471.

Ke, F. 2007. North Pacific sea ice cover, a predictor for the Western North Pacific typhoon frequency? *Science in China Series D: Earth Sciences* 50, 1251-1257.

Kistler, R., and Coauthers, 2001. The NCEP-NCAR 50-year reanalysis: Monthly means CD-ROM and documentation. *Bulletin of the American Meteorological Society* 82, 247-267.

Klotzbach, P. J, and W. M. Gray. 2004. Updated 6-11 month prediction of Atlantic basin seasonal hurricane activity. *Weather and Forecasting* 9, 917-933.

Klotzbach, P. J. 2007. Recent developments in statistical prediction of the seasonal Atlantic basin tropical cyclone activity. *Tellus* 59A, 511-518.

Klotzbach, P. J. 2008. Refinements to Atlantic basin seasonal hurricane prediction from 1 December. *Journal of Geophysical Research* 113. DOI: 10.1029/2008JD010047

Klotzbach and Coauthers. 2011. Seasonal forecasting of tropical cyclones. Lamont-Doherty Earth Observatory Webpage. Accessed: 12/1/12. [http://www.ldeo.columbia.edu/~suzana/papers/Global_Guide_Seasonal_Forecast_Chapter.pdf].

Klotzbach, P. J. and W. M. Gray. 2011. Qualitative discussion of Atlantic basin seasonal hurricane activity for 2012. Department of Atmospheric Science Report, Colorado State University, Fort Collins, CO, 27pp.

Klotzbach, P. J. and W. M. Gray. 2012a. Extended range forecast of Atlantic seasonal hurricane activity and landfall strike probability for 2012 – 4 April Forecast. Department of Atmospheric Science Report, Colorado State University, Fort Collins, CO, 43pp.

Klotzbach, P. J. and W. M. Gray. 2012b. Extended range forecast of Atlantic seasonal hurricane activity and landfall strike probability for 2012 – 1 June Forecast. Department of Atmospheric Science Report, Colorado State University, Fort Collins, CO, 42pp.

Klotzbach, P. J. and W. M. Gray. 2012c. Extended range forecast of Atlantic seasonal hurricane activity and landfall strike probability for 2012 – 3 August Forecast. Department of Atmospheric Science Report, Colorado State University, Fort Collins, CO, 40pp.

Knaff, J. A. 1997. Implications of summertime sea level pressure anomalies. *Journal of Climate* 10, 789-804.

Knaff, J. A. 1998. Predicting summertime Caribbean sea level pressure. *Weather and Forecasting* 13, 740-752.

Kossin, J. P. and D. J. Vimont. 2007. A more general framework for understanding Atlatnci hurricane variability and trends. *Bulletin of the American Meteorological Society* 88, 1767-1781.

Kushnir, Y. 1994. Interdecadal variations in North Atlantic sea surface temperature and associated atmospheric conditions. *Journal of Climate* 7, 141-157.

LaRow, T. E., Y-K. Lim, D. W. Shin, E. P. Chassignet, and S. Cocke. 2008. Atlantic basin seasonal hurricane simulations. *Journal of Climate* 21, 3191-3206.

Landsea, C. W., G. D. Bell, W. M. Gray, and S. B. Goldenberg. 1998. The extremely active 1995 Atlantic hurricane season: environmental conditions and verification of seasonal forecasts. *Monthly Weather Review* 126, 1174-1193.

Larkin, N. K. and D. E. Harrison. 2002. ENSO warm (El Niño) and cold (La Niña) event life cycles: Ocean surface anomaly patterns, their symmetries, asymmetries, and implications. *Journal of Climate* 15, 1118-1140.

Larson, J, Y. Zhou, R. W. Higgins. 2005. Characteristics of landfalling tropical cyclones in the United States and Mexico: climatology and interannual variability. *Journal of Climate* 18, 1247-1262.

Lea, A. S. and M. A. Saunders. 2004. Seasonal predictability of accumulated cyclone energy in the north Atlantic. Proceedings of the 26th conference of hurricanes and tropical meteorology, Miami, USA, May 3-7, pp. 419-420.

Lea, A. S. and M. A. Saunders, 2011. August forecast update for Atlantic hurricane activity in 2012 – issued 6th August 2012. Department of Space and Climate Physics, University College London, UK, 5pp.

Liebmann, B. and C. A. Smith. 1996: Description of a Complete (Interpolated) Outgoing Longwave Radiation Dataset. *Bulletin of the American Meteorological Society* 77, 1275-1277.

L'Heureux, M. L., A. Kumar, G. D. Bell, M. S. Halpert, and R. W. Higgins. 2008. Role of the Pacific-North American (PNA) pattern in the 2007 Arctic sea ice decline. *Geophysical Research Letters* 35, L20701. DOI:10.1029/2008GL035205.

Lloyd-Hughes, B., M. A. Saunders, and P. Rockett. 2004. A consolodiated CLIPER model for improved August-September ENSO prediction skill. *Journal of Climate* 19, 1089-1105.

Malkus, J. S. and H. riehl. 1960. On the dynamics and energy transformation in steady-state hurricanes. *Tellus* 12, 1-20.

Marshall, J. and Coauthers. 2001. North Atlantic climate variability: Phenomena, impacts, and mechanisms. *International Journal of Climatology* 21, 1863-1898.

Mysak, L. A., R. G. Ingram, J. Wang, and A. van der Baaren. 1996. The anomalous sea-ice extent in Hudson bay, Baffin bay and the Labrador sea during three simultaneous NAO and ENSO episodes. *Atmosphere-Ocean* 34, 313-343.

Neumann, C.J., B.R. Jarvinen, C.J. McAdie, and J.D. Elms.1993. Tropical Cyclones of the North Atlantic Ocean, 1871-1992, Prepared by the National Climatic Data Center, Asheville, NC, in cooperation with the NHC, Coral Gables, FL, 193pp

Nicholls, N. 1979. A possible method for predicting season tropical cyclone activity in the Australian region. *Monthly Weather Review*107, 1221:1224.

NOAA (National Oceanic and Atmospheric Administration). 2012a. Tropical Cyclone Climatology webpage of the National Hurricane Center website. Last modified: 6/18/2012. Accessed: 12/28/12.[http://www.nhc.noaa.gov/climo/].

NOAA (National Oceanic and Atmospheric Administration). 2012b. NOAA 2012 Atlantic Hurricane Season Outlook Update: Issued 9 August 2012. From the Climate Prediction Center website. Last Modified: 8/9/12. Accessed: 12/28/12. [http://www.cpc.ncep.noaa.gov/products/outlooks/hurricane.shtml].

NOAA (National Oceanic and Atmospheric Administration). 2012c. Climate Watch Magazine: Record low spring snow cover in Northern Hemisphere 2012. Released: December 5, 2012. Accessed: 1/7/13. [http://www.climatewatch.noaa.gov/image/2012/record-low-spring-snow-cover-in-northern-hemisphere-2012].

NSIDC (National Snow and Ice Data Center). 2012a. Monthly Archives: Arctic sea ice maximum marks beginning of melt season. NSIDC webpage. Released: March 26, 2012. Accessed: 1/7/13. [http://nsidc.org/arcticseaicenews/2012/03/].

NSIDC (National Snow and Ice Data Center). 2012b. Monthly Archives: Arctic sea ice extent settle at record seasonal minimum. NSIDC webpage. Released: September 19, 2012. Accessed: 1/7/13. [http://nsidc.org/arcticseaicenews/2012/09/].

NSIDC (National Snow and Ice Data Center). 2013a. Frequently asked questions about Arctic sea ice. NSIDC webpage. Accessed 2/7/13. [http://nsidc.org/arcticseaicenews/faq/#area_extent].

NSIDC (National Snow and Ice Data Center). 2013b. Sea ice trends & climatologies from SMMR & SSM/I-SSMIS. Metadata webpage. Accessed 2/24/13. [http://nsidc.org/data/smmr_ssmi_ancillary/area_extent.html].

Overland, J. E. and M. Wang. 2010. Large-scale atmospheric circulation changes are associated with the recent loss of Arctic sea ice. *Tellus* 62A,1-9.

Pielke, R. A. Jr., J. Gratz, C. S. Landsea, D. Collins, M. A. Saunders, and R. Musulin. 2008. Normalized hurricane damage in the United States: 1900-2005. *Natural Hazards Review* 9, 29-42. DOI: 10.1061/(ASCE)1527-6988(2008)9:1(29)

Rigor, I. G., J. M. Wallace, R. L. Colony. 2002. Response of sea ice to the arctic oscillation. *Journal of Climate* 15, 2648–2663

Robinson, D. 2012. Northern hemisphere continental snow cover extent 2011 Update. Global Snow Lab, Rutgers University, New Jersey, 3 pp.

Robock, Alan. 1980. The seasonal cycle of snow cover, sea ice and surface albedo. *Monthly Weather Review* 108, 267–285.

Rogers, J. C. 1981. The North Pacific Oscillation. *International Journal of Climatology* 1, 39-57.

Saunders, M. A. and A. S. Lea. 2011. Extended range forecast for Atlantic hurricane activity in 2012 – 7th June, 2011 Forecast . Department of Space and Climate Physics, University College London, United Kingdom, 3pp.

Saunders, M. A. and A. S. Lea. 2012. Extended range forecast for Atlantic hurricane activity in 2012 – 6th June, 2012 Forecast. Department of Space and Climate Physics, University College London, United Kingdom, 3pp.

Saunders, M. A., and A. S. Lea. 2005. Seasonal prediction of hurricane activity reaching the coast of the United States. *Nature* 434, 1005-1008.

Screen, J. A. and Ian Sommonds. 2010. The Central Role of Diminishing Sea Ice in Recent Arctic Temperature Amplification. *Nature* 464, 1334-1337. DOI, 10.1038/nature0905

Seager, R., Y. Kushnir, J. Nakamura, M. Ting, and N. Naik. 2010. Northern hemisphere winter snow anomalies: ENSO, NAO and the winter of 2009/10. *Geophysical Research Letters* 37, L14703. DOI:10.1029/2010GL043830

Shapiro, L. J. 1982. Hurricane climatic fluctuations. Part II: relation to large-scale circulation. *Monthly Weather Review* 110, 1014-1023.

Stroeve, J. C., M. C. Serreze, M. M. Holland, J. E. Kay, J. Malanik, and A. P. Barrett. 2012. The Arctic's rapidly shrinking sea ice cover: a research synthesis, *Climatic Change* 110, 1005-1027.

Tachibana, Y, M. Honda, and K. Takeuchi. 1996. The abrupt decrease of the sea ice over the southern part of the Sea of Okhotsk in 1989 and its relation to the recent weakening of the Aleutian low. *Journal of the Meteorological Society of Japan*, Vo. 74: 579-584.

Thompson, D. W. J., and J. M. Wallace. 1998. The Arctic oscillation signature in the wintertime geopotential height and temperature fields. *Geophysical Research Letters* 25, 1297-1300.

Wallace, J. M. 2000. North atlantic oscillation/annular mode: Two paraidgms – one phenomenon. *Quarterly Journal of the Royal Meteorological Society* 126, 791-805.

Walland, D. J., and I. Simmonds. 1996. Modeled atmospheric response to changes in Northern Hemisphere snow extent. *Climate Dynamics* 13, 25-34.

Wang, J. L. A. Mysak, and R. G. Ingram. 1994. Interannual variability of sea-ice cover in the Hudson Bay, Baffin Bay and the Labrador Sea. *Atmosphere-Ocean* 32, 421-447.

WMO (World Meteorological Organization). 2002. Standardized verification system (SVS) for long-range forecasts (LRF). New Attachment II-9 to the Manual on the GDPS (WMO-No. 485), Vol. 1 Geneva, Switzerland.

Xie, L, T. Yan, L. J. Pietrafesa, J. M. Morrison, and T. Karl. 2005. Climatology and interannual variability of North Atlantic hurricane tracks. *Journal of Climate* 18, 5370-5381.

Xie, L., M. Lennon, and M. Fuentes. 2012. Summary of 2012 Forecast Results. Department of Marine, Earth, and Atmospheric Sciences and Department of Statistics, North Carolina State University, USA

Xie, S. P. 1999. A dynamic ocean-atmosphere model of the tropica Atlantic decadal variability. *Journal of Climate* 12, 64-70.

Yan, T., L. J. Pietrafesa, G. D. Bell, and D. A. Dickey. 2012. On the inverse relationship between North American snow extent and North Atlantic hurricane activity, *International Journal of Climatology*. DOI:10.1002/joc.3485

APPENDICES

APPENDIX A – HINDCASTS

1980-2010 hindcasts for tropical storms (TS) between the 3 model groups

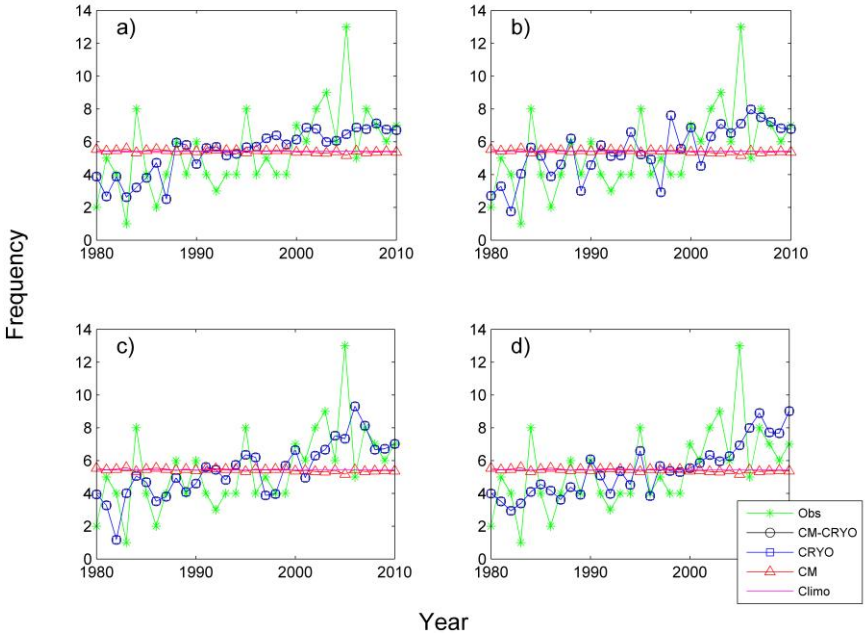

1980-2010 hindcasts for hurricanes between the 3 model groups

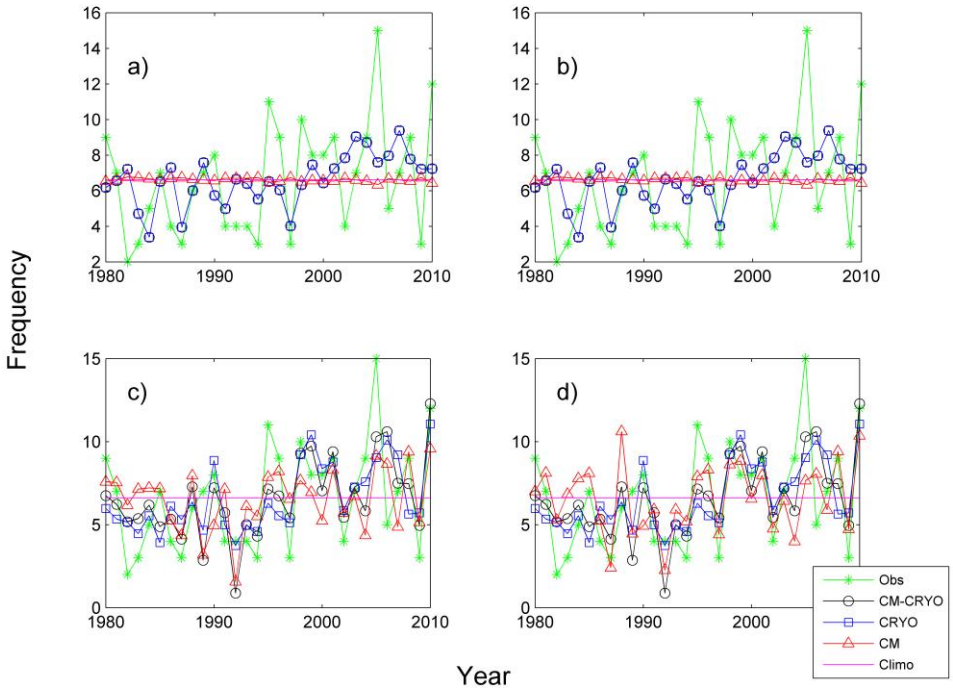

APPENDIX A – HINDCASTS

1980-2010 hindcasts for minor hurricanes (Minor) between the 3 model groups

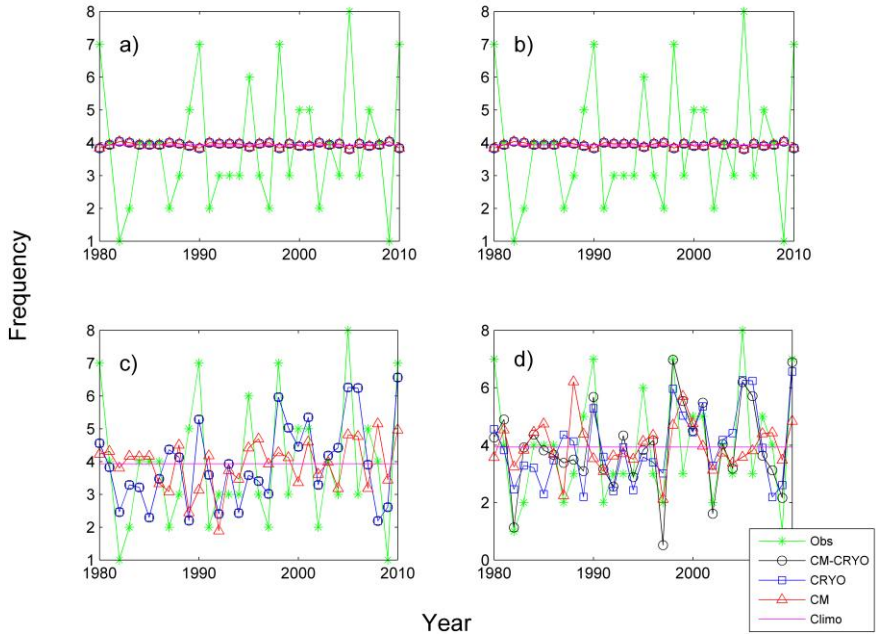

1980-2010 hindcasts for accumulative cyclone energy (ACE) between the 3 model groups

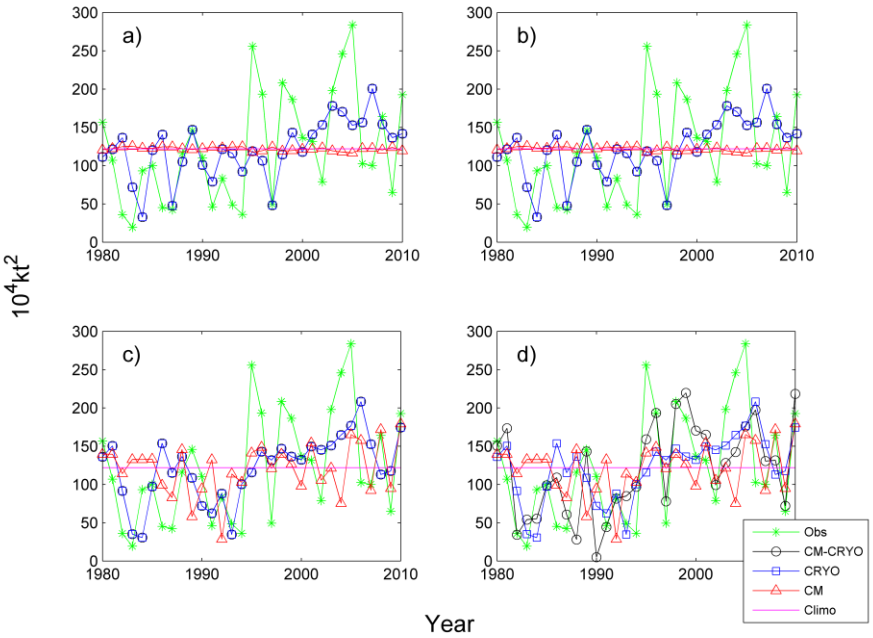

APPENDIX A – HINDCASTS

1980-2010 hindcasts for power dissipation index (PDI) between the 3 model groups

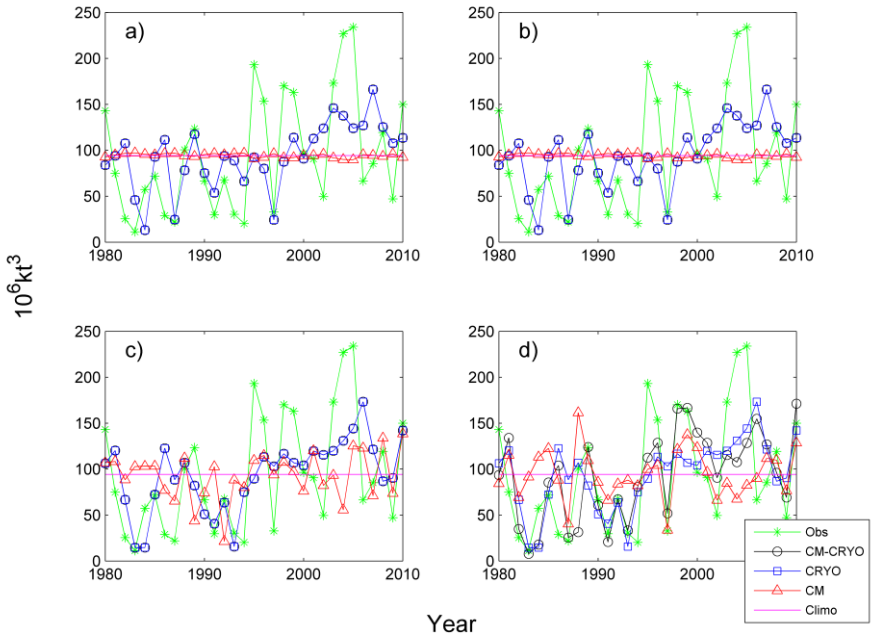

1980-2010 hindcasts for annual mean peak wind (Peak Wind) between the 3 model groups

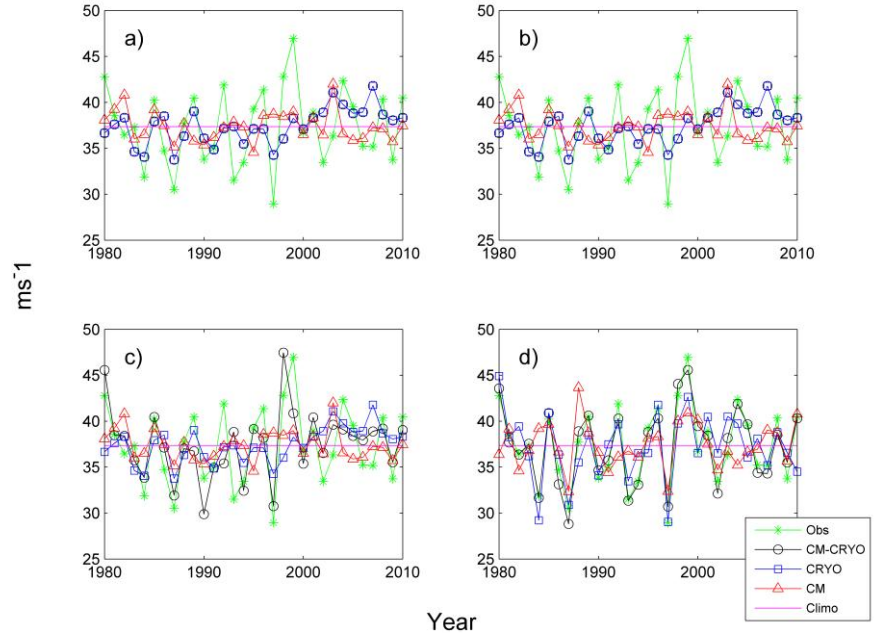

APPENDIX A – HINDCASTS

1980-2010 hindcasts for US landfalling tropical cyclones between the 3 model groups

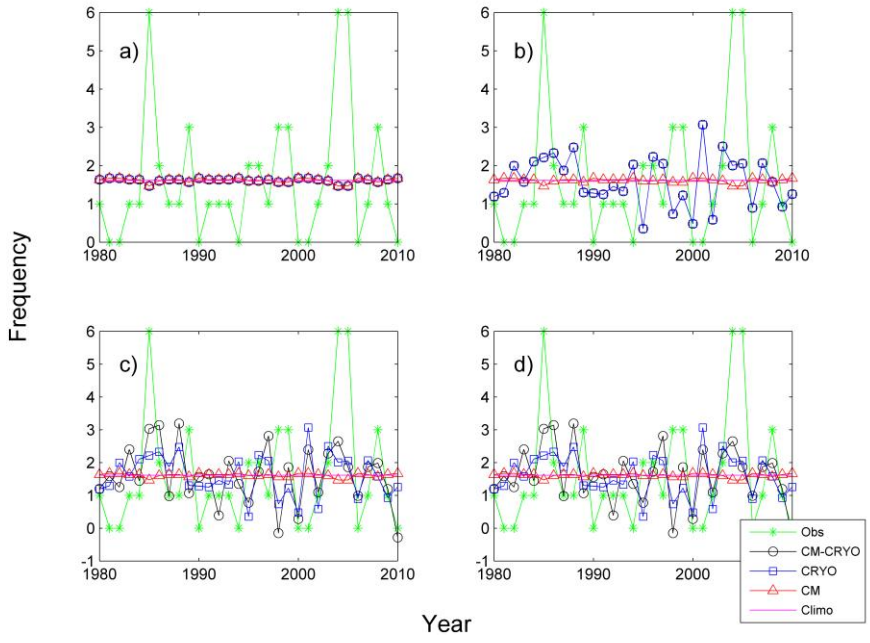

1980-2010 hindcasts for lifetime mean duration (LMD) between the 3 model groups

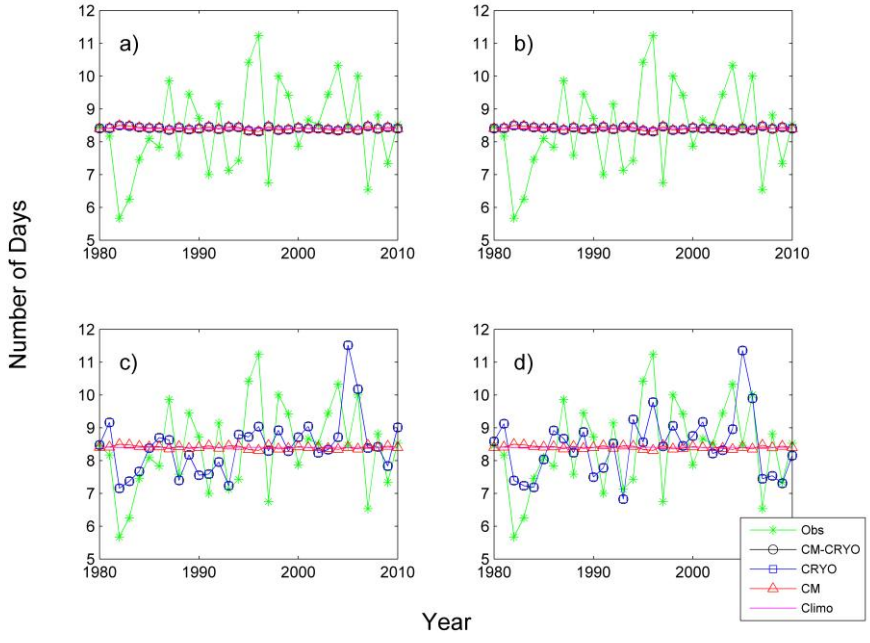

APPENDIX A – HINDCASTS

1980-2010 hindcasts for latest tropical cyclogenesis day-of-year (MaxDOY) between the 3 model groups

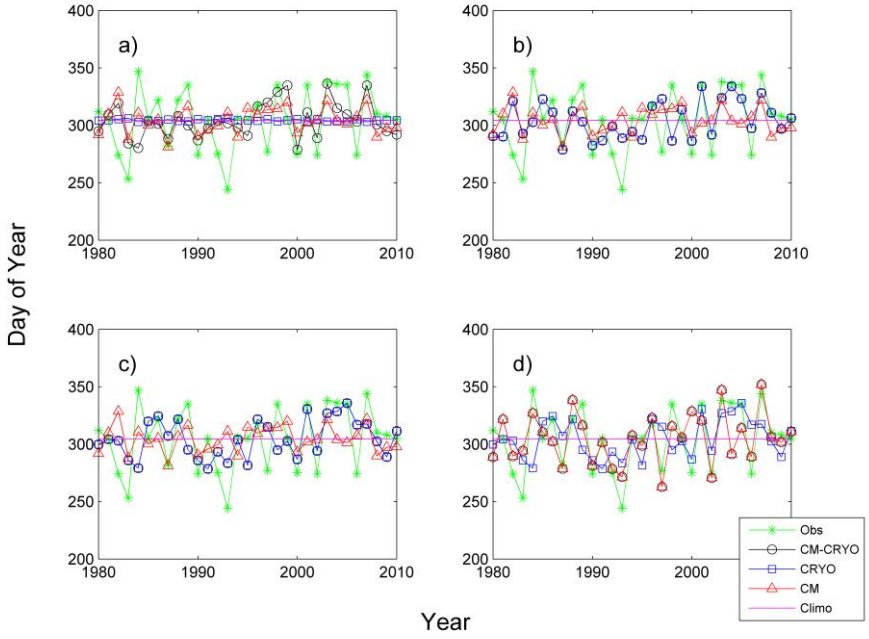

1980-2010 hindcasts for earliest tropical cyclogenesis day-of-year (MinDOY) between the 3 model groups

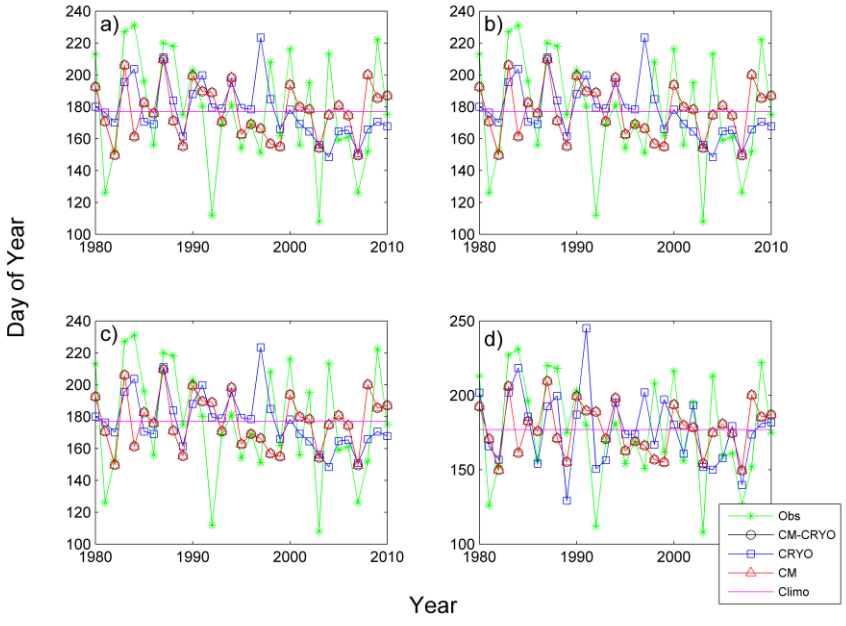

APPENDIX A – HINDCASTS

1980-2010 hindcasts total season length (TSL) measured in days between the 3 model groups

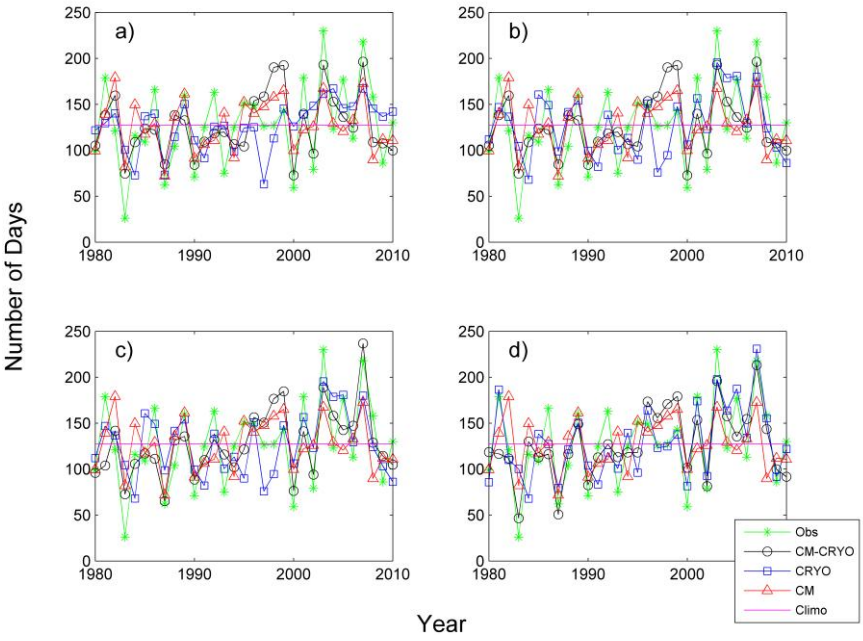

APPENDIX B – CORRELATION ANALYSIS – SPRING AO

Correlation plot between July-September 500 mb geopotential height and the Spring Arctic Oscillation for 1980-2010. Image provided by the NOAA/ESRL Physical Sciences Division, Boulder Colorado from their Web site at http://www.esrl.noaa.gov/psd/ (Kalnay et al., 1996).

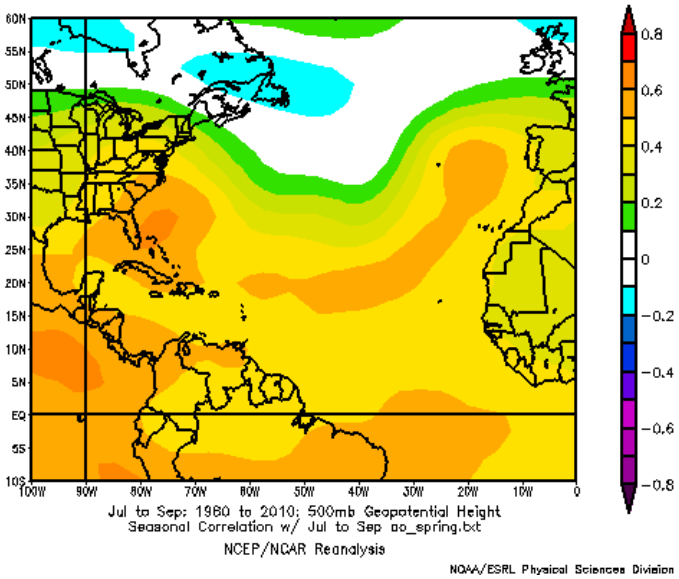

Correlation plot between July-September sea level pressure (SLP) and the Spring Arctic Oscillation for 1980-2010. Image provided by the NOAA/ESRL Physical Sciences Division, Boulder Colorado from their Web site at http://www.esrl.noaa.gov/psd/ (Kalnay et al., 1996).

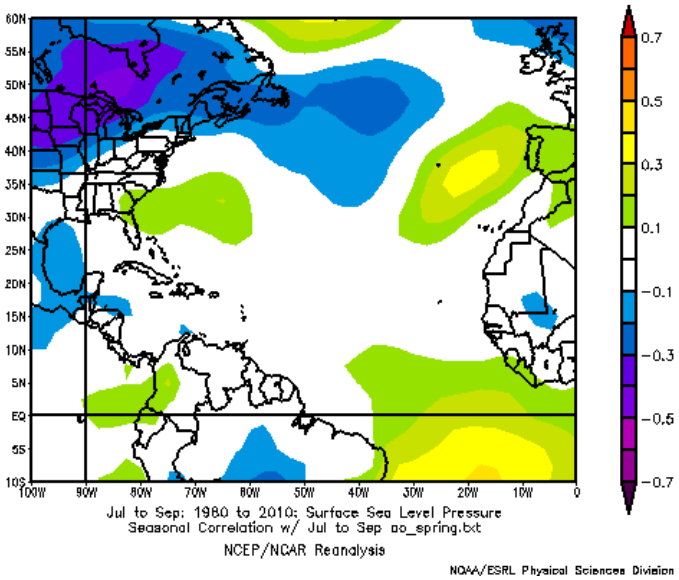

APPENDIX B – CORRELATION ANALYSIS – SPRING AO

Correlation plot between July-September sea surface temperature (SST) and the Spring Arctic Oscillation for 1980-2010. Image provided by the NOAA/ESRL Physical Sciences Division, Boulder Colorado from their Web site at http://www.esrl.noaa.gov/psd/ (Kalnay et al., 1996).

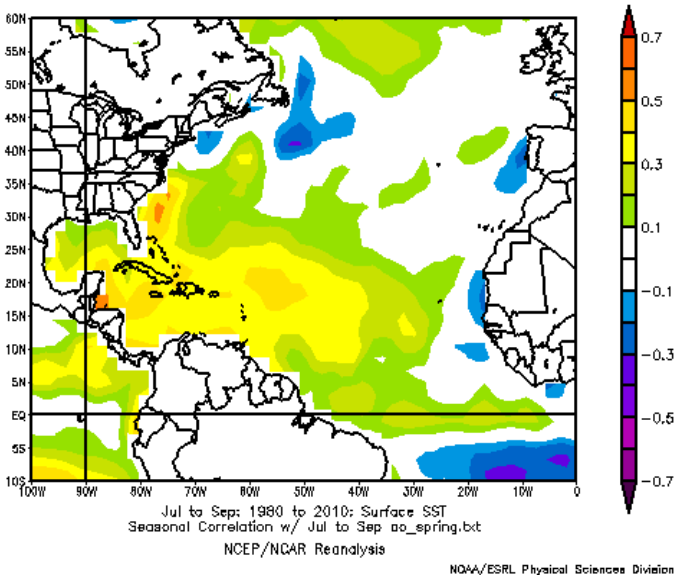

Correlation plot between July-September outgoing longwave radiation (OLR) at the tropopause and the Spring Arctic Oscillation for 1980-2010. Image provided by the NOAA/ESRL Physical Sciences Division, Boulder Colorado from their Web site at http://www.esrl.noaa.gov/psd/ (Liebmann and Smith, 1996).

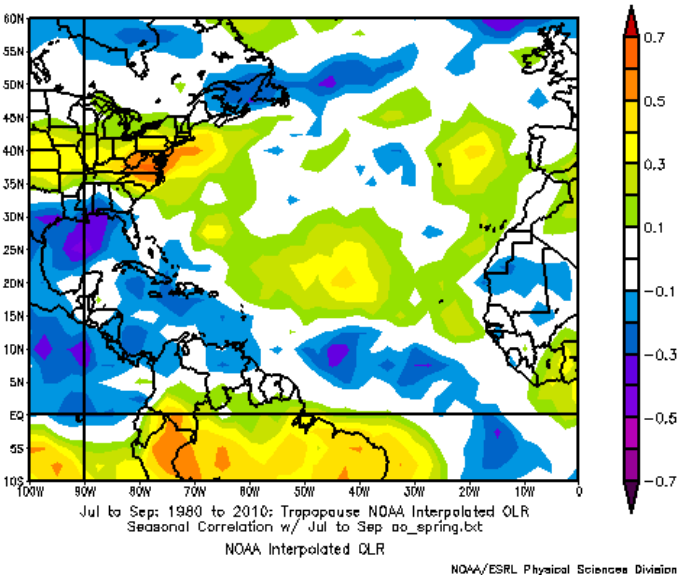

APPENDIX B – CORRELATION ANALYSIS – FALL BAFFIN BAY SIE

Correlation plot between July-September 500 mb geopotential height and Fall Baffin Bay SIE for 1980-2010. Image provided by the NOAA/ESRL Physical Sciences Division, Boulder Colorado from their Web site at http://www.esrl.noaa.gov/psd/ (Kalnay et al., 1996).

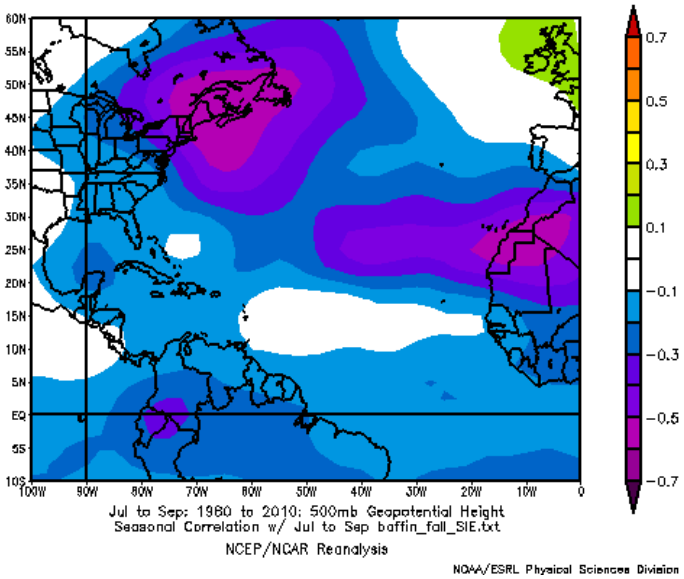

Correlation plot between July-September sea level pressure (SLP) and Fall Baffin Bay SIE for 1980-2010. Image provided by the NOAA/ESRL Physical Sciences Division, Boulder Colorado from their Web site at http://www.esrl.noaa.gov/psd/ (Kalnay et al., 1996).

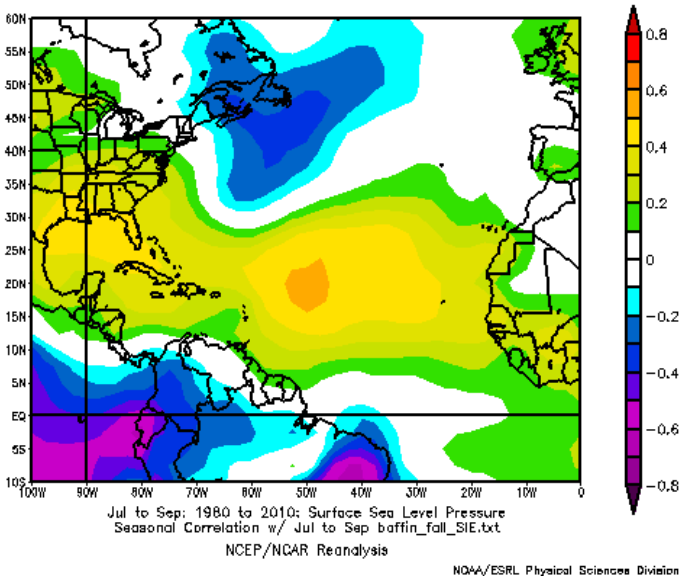

APPENDIX B – CORRELATION ANALYSIS – FALL BAFFIN BAY SIE

Correlation plot between July-September sea level pressure (SLP) and Fall Baffin Bay SIE for 1980-2010. Image provided by the NOAA/ESRL Physical Sciences Division, Boulder Colorado from their Web site at http://www.esrl.noaa.gov/psd/ (Kalnay et al., 1996).

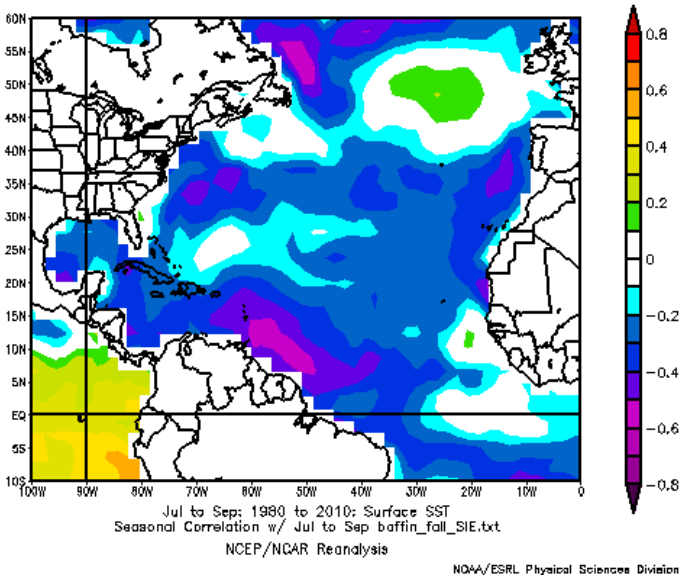

Correlation plot between July-September outgoing longwave radiation (OLR) at the tropopause and Fall Baffin Bay SIE for 1980-2010. Image provided by the NOAA/ESRL Physical Sciences Division, Boulder Colorado from their Web site at http://www.esrl.noaa.gov/psd/ (Liebmann and Smith, 1996).

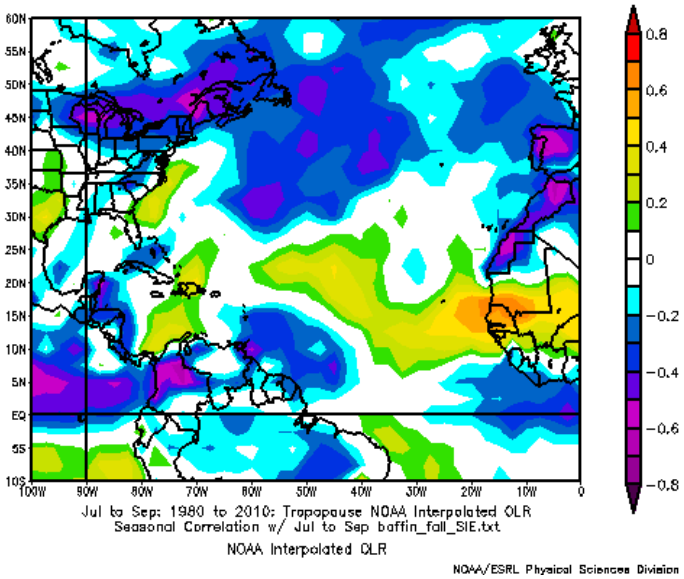

APPENDIX B – CORRELATION ANALYSIS – SPRING BAFFIN BAY SIA

Correlation plot between July-September 500 mb geopotential height and Spring Baffin Bay SIA for 1980-2010. Image provided by the NOAA/ESRL Physical Sciences Division, Boulder Colorado from their Web site at http://www.esrl.noaa.gov/psd/ (Kalnay et al., 1996).

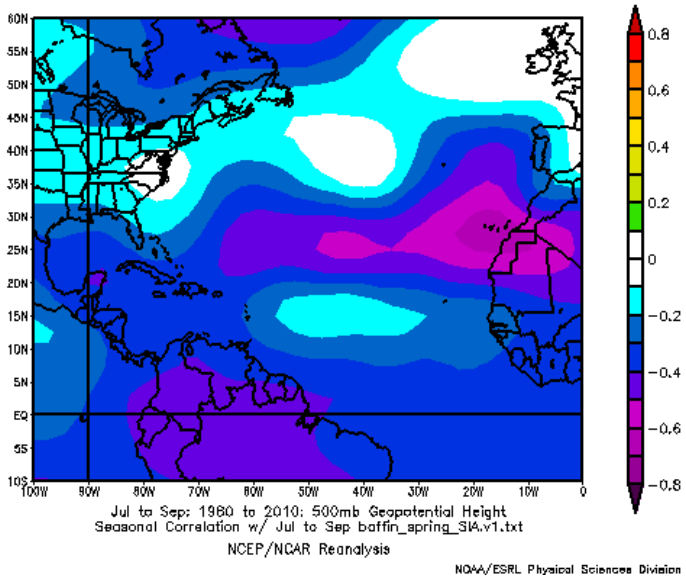

Correlation plot between July-September outgoing longwave radiation (OLR) at the tropopause and Spring Baffin Bay SIA for 1980-2010. Image provided by the NOAA/ESRL Physical Sciences Division, Boulder Colorado from their Web site at http://www.esrl.noaa.gov/psd/ (Liebmann and Smith, 1996).

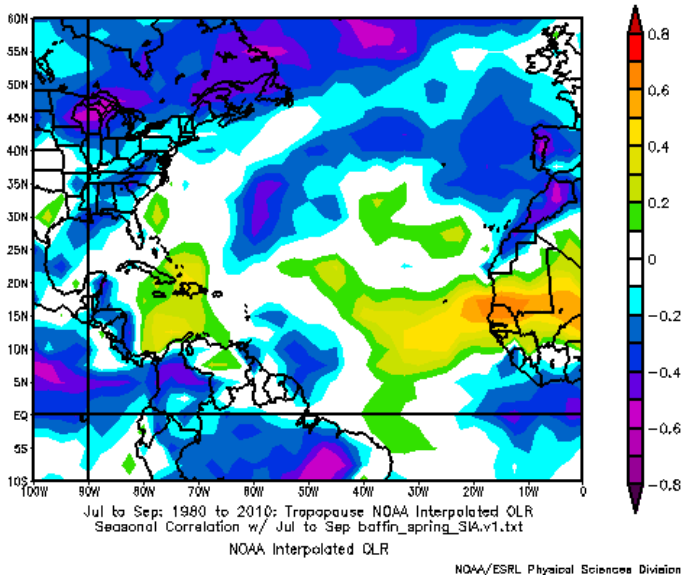

APPENDIX B – CORRELATION ANALYSIS – FALL BERING SEA SIA

Correlation plot between July-September 500 mb geopotential height and Fall Bering Sea SIA for 1980-2010. Image provided by the NOAA/ESRL Physical Sciences Division, Boulder Colorado from their Web site at http://www.esrl.noaa.gov/psd/ (Kalnay et al., 1996).

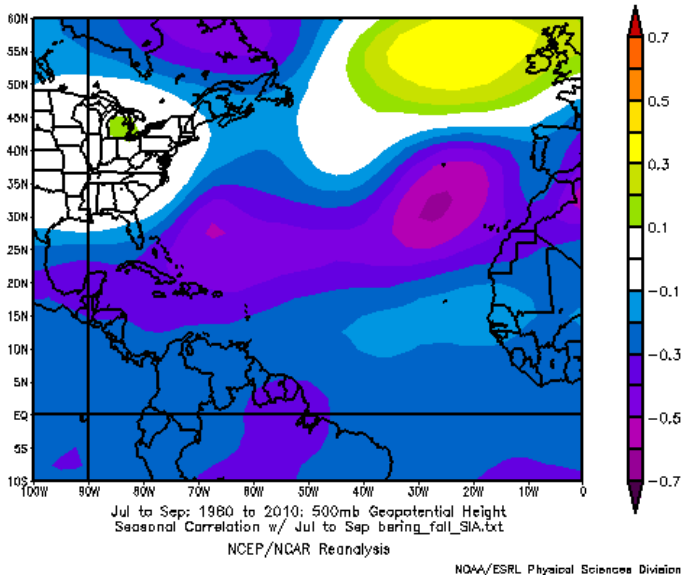

Correlation plot between July-September sea level pressure (SLP) and Fall Bering Sea SIA for 1980-2010. Image provided by the NOAA/ESRL Physical Sciences Division, Boulder Colorado from their Web site at http://www.esrl.noaa.gov/psd/ (Kalnay et al., 1996).

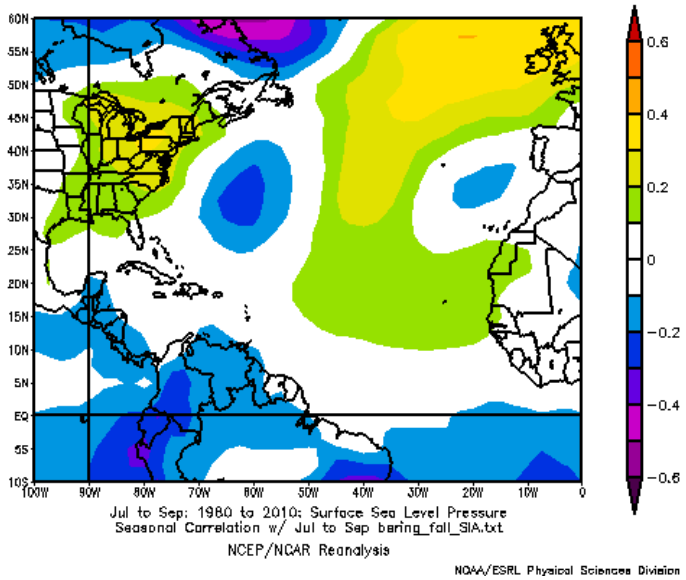

APPENDIX B – CORRELATION ANALYSIS – FALL BERING SEA SIA

Correlation plot between July-September sea surface temperature (SST) and Fall Bering Sea SIA for 1980-2010. Image provided by the NOAA/ESRL Physical Sciences Division, Boulder Colorado from their Web site at http://www.esrl.noaa.gov/psd/ (Kalnay et al., 1996).

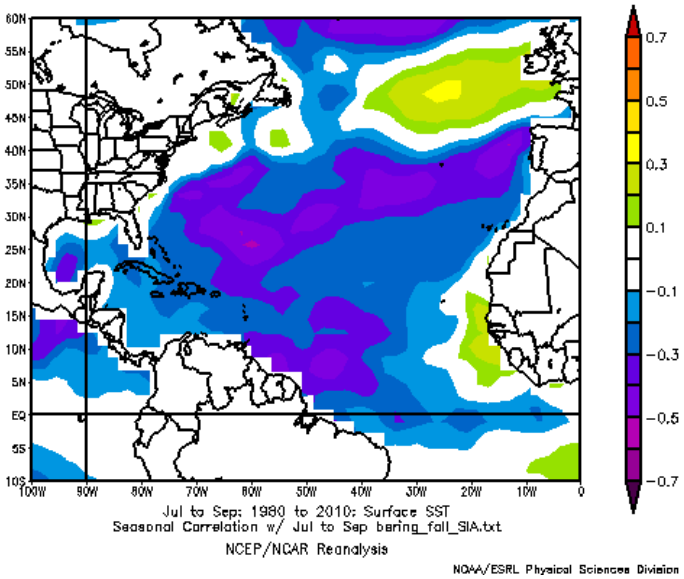

Correlation plot between July-September outgoing longwave radiation (OLR) at the tropopause and Fall Bering Sea SIA for 1980-2010. Image provided by the NOAA/ESRL Physical Sciences Division, Boulder Colorado from their Web site at http://www.esrl.noaa.gov/psd/ (Liebmann and Smith, 1996).

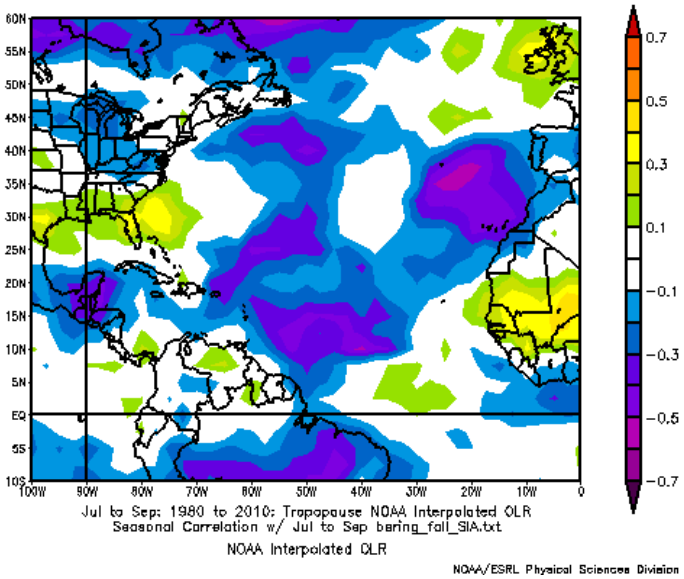

APPENDIX B – CORRELATION ANALYSIS – SUMMER ENSO

Correlation plot between July-September 500 mb geopotential height and Summer ENSO for 1980-2010. Image provided by the NOAA/ESRL Physical Sciences Division, Boulder Colorado from their Web site at http://www.esrl.noaa.gov/psd/ (Kalnay et al., 1996).

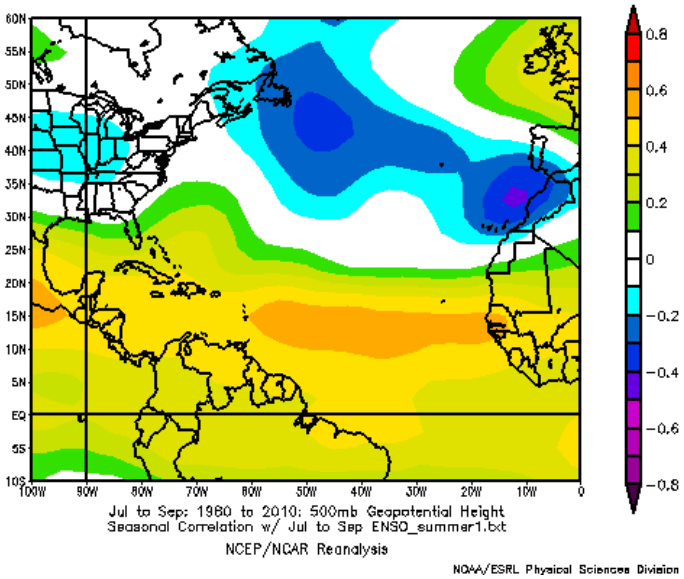

Correlation plot between July-September sea level pressure (SLP) and Summer ENSO for 1980-2010. Image provided by the NOAA/ESRL Physical Sciences Division, Boulder Colorado from their Web site at http://www.esrl.noaa.gov/psd/ (Kalnay et al., 1996).

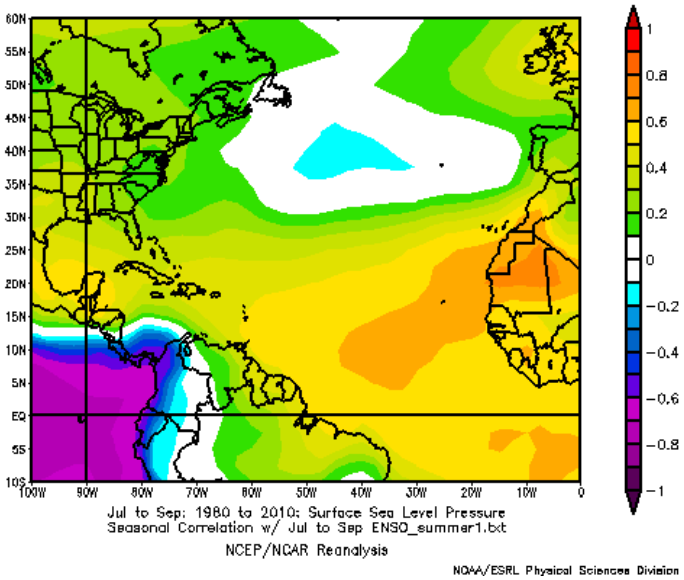

APPENDIX B – CORRELATION ANALYSIS – SUMMER ENSO

Correlation plot between July-September sea surface temperature (SST) and Summer ENSO for 1980-2010. Image provided by the NOAA/ESRL Physical Sciences Division, Boulder Colorado from their Web site at http://www.esrl.noaa.gov/psd/ (Kalnay et al., 1996).

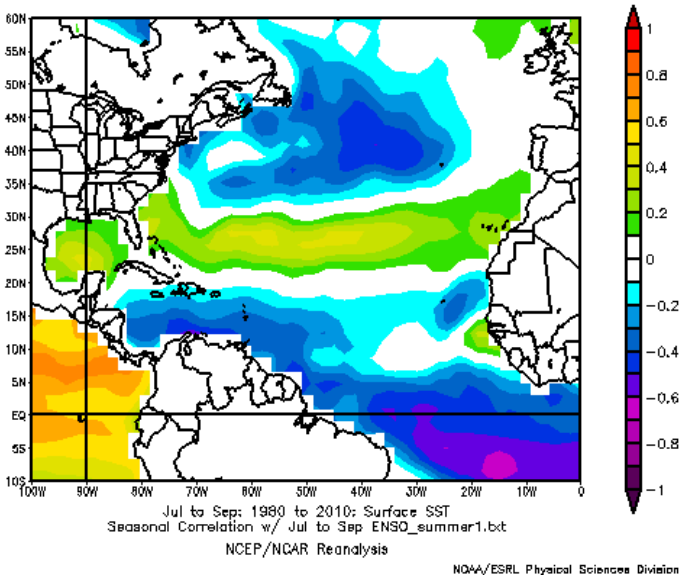

Correlation plot between July-September outgoing longwave radiation (OLR) at the tropopause and Summer ENSO for 1980-2010. Image provided by the NOAA/ESRL Physical Sciences Division, Boulder Colorado from their Web site at http://www.esrl.noaa.gov/psd/ (Liebmann and Smith, 1996).

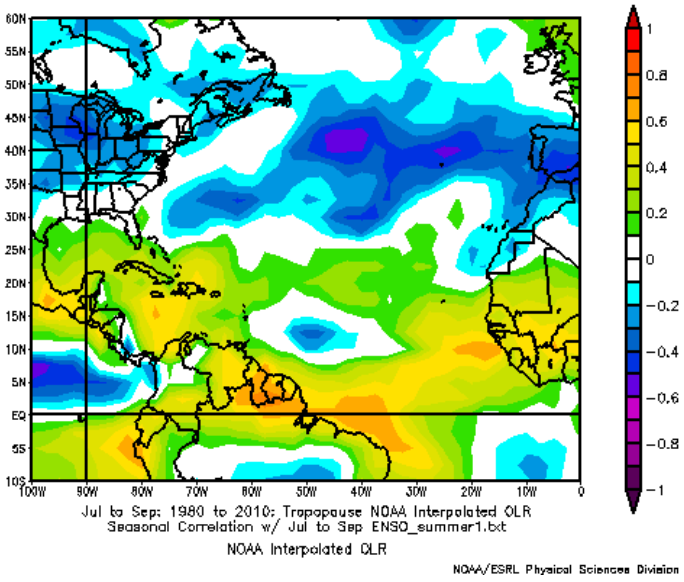

APPENDIX B – CORRELATION ANALYSIS – SPRING HUDSON BAY SIA

Correlation plot between July-September 500 mb geopotential height and Spring Hudson Bay SIA for 1980-2010. Image provided by the NOAA/ESRL Physical Sciences Division, Boulder Colorado from their Web site at http://www.esrl.noaa.gov/psd/ (Kalnay et al., 1996).

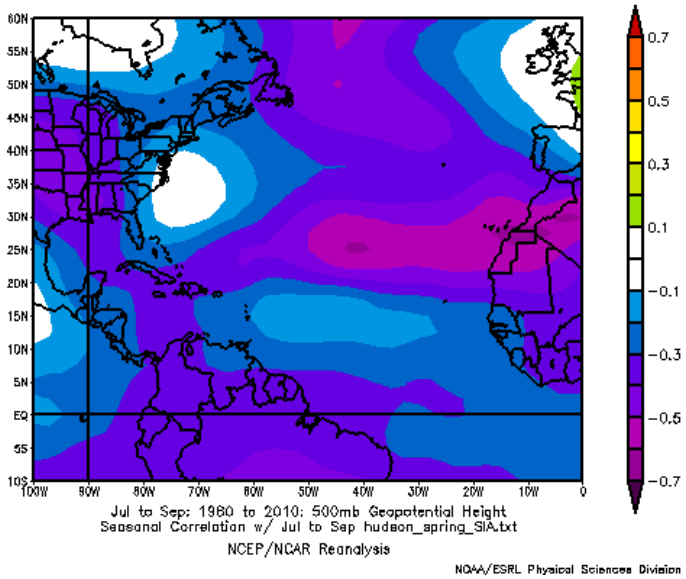

Correlation plot between July-September outgoing longwave radiation (OLR) at the tropopause and Spring Hudson Bay SIA for 1980-2010. Image provided by the NOAA/ESRL Physical Sciences Division, Boulder Colorado from their Web site at http://www.esrl.noaa.gov/psd/ (Liebmann and Smith, 1996).

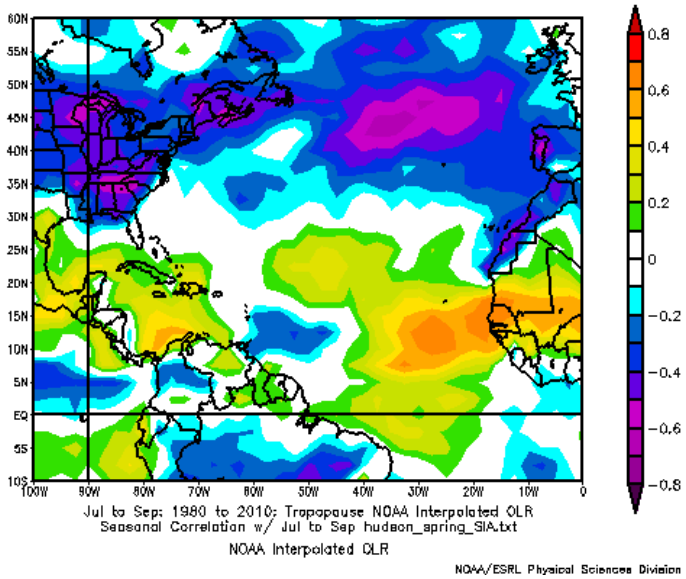

APPENDIX B – CORRELATION ANALYSIS – FALL NAO

Correlation plot between July-September 500 mb geopotential height and the Fall NAO for 1980-2010. Image provided by the NOAA/ESRL Physical Sciences Division, Boulder Colorado from their Web site at http://www.esrl.noaa.gov/psd/ (Kalnay et al., 1996).

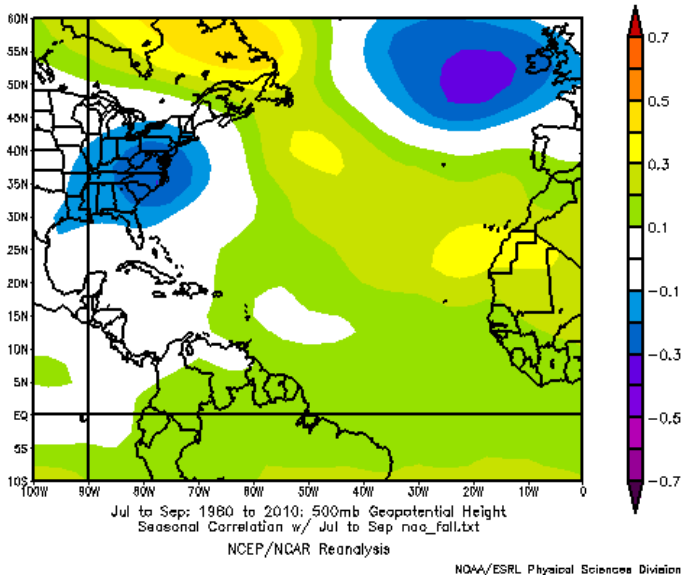

Correlation plot between July-September sea level pressure (SLP) and the Fall NAO for 1980-2010. Image provided by the NOAA/ESRL Physical Sciences Division, Boulder Colorado from their Web site at http://www.esrl.noaa.gov/psd/ (Kalnay et al., 1996).

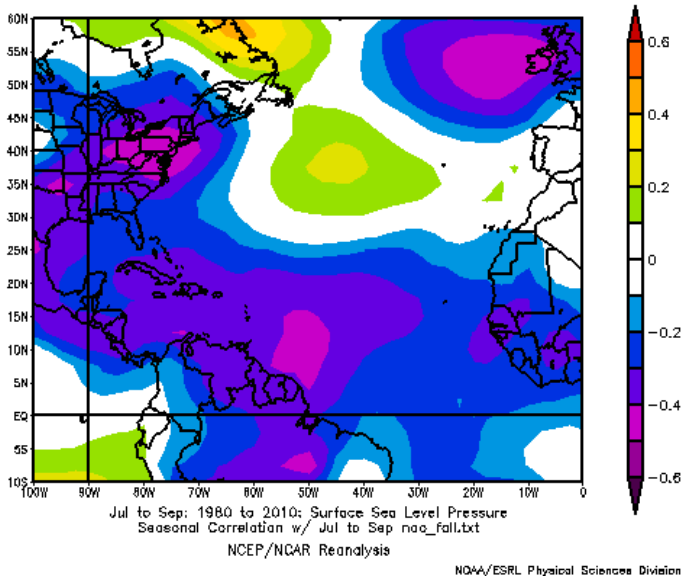

APPENDIX B – CORRELATION ANALYSIS – FALL NAO

Correlation plot between July-September sea surface temperature (SST) and the Fall NAO for 1980-2010. Image provided by the NOAA/ESRL Physical Sciences Division, Boulder Colorado from their Web site at http://www.esrl.noaa.gov/psd/ (Kalnay et al., 1996).

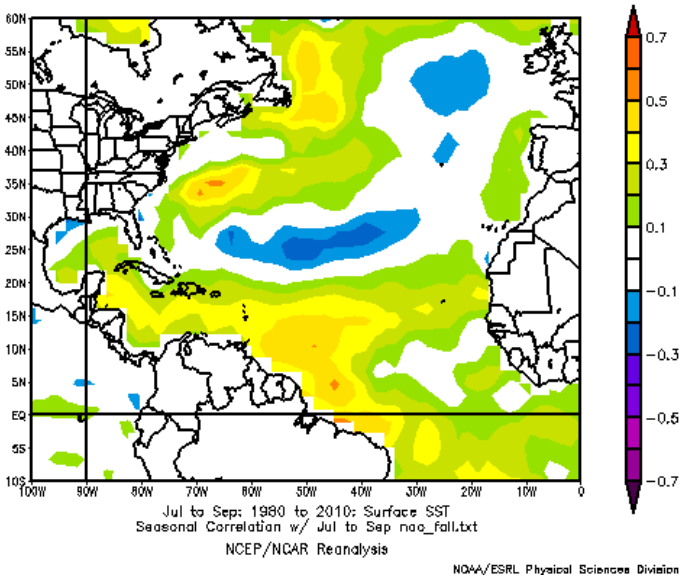

Correlation plot between July-September outgoing longwave radiation (OLR) at the tropopause and the Fall NAO for 1980-2010. Image provided by the NOAA/ESRL Physical Sciences Division, Boulder Colorado from their Web site at http://www.esrl.noaa.gov/psd/ (Liebmann and Smith, 1996).

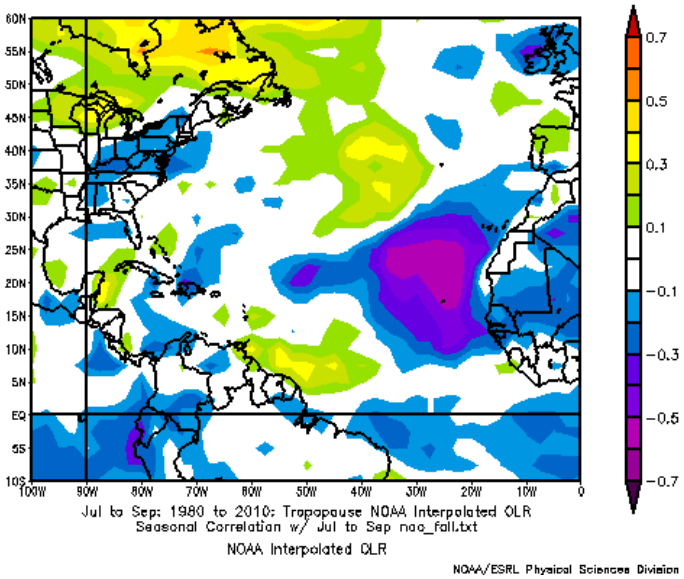

APPENDIX B – CORRELATION ANALYSIS – SPRING NAO

Correlation plot between July-September 500 mb geopotential height and the Spring NAO for 1980-2010. Image provided by the NOAA/ESRL Physical Sciences Division, Boulder Colorado from their Web site at http://www.esrl.noaa.gov/psd/ (Kalnay et al., 1996).

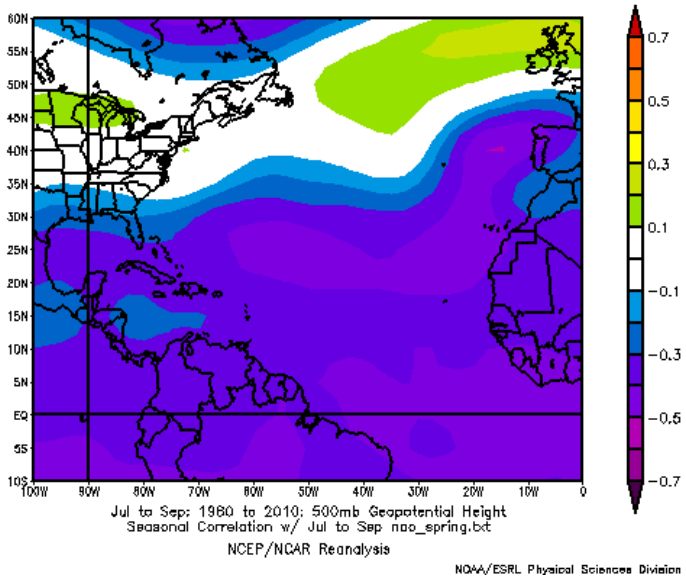

Correlation plot between July-September sea level pressure (SLP) and the Spring NAO for 1980-2010. Image provided by the NOAA/ESRL Physical Sciences Division, Boulder Colorado from their Web site at http://www.esrl.noaa.gov/psd/ (Kalnay et al., 1996).

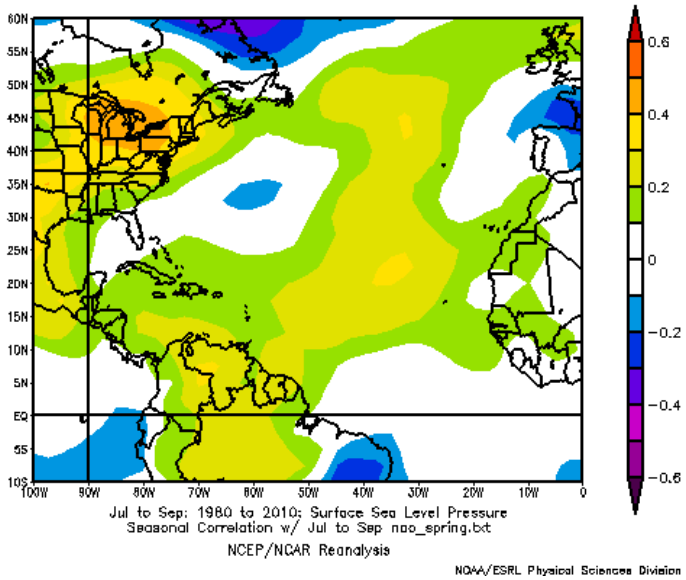

APPENDIX B – CORRELATION ANALYSIS – SPRING NAO

Correlation plot between July-September sea surface temperature (SST) and the Spring NAO for 1980-2010. Image provided by the NOAA/ESRL Physical Sciences Division, Boulder Colorado from their Web site at http://www.esrl.noaa.gov/psd/ (Kalnay et al., 1996).

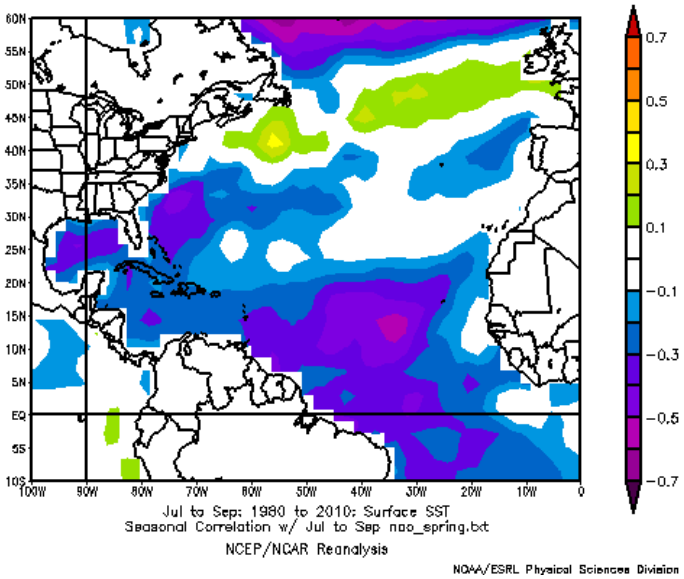

Correlation plot between July-September outgoing longwave radiation (OLR) at the tropopause and the Spring NAO for 1980-2010. Image provided by the NOAA/ESRL Physical Sciences Division, Boulder Colorado from their Web site at http://www.esrl.noaa.gov/psd/ (Liebmann and Smith, 1996).

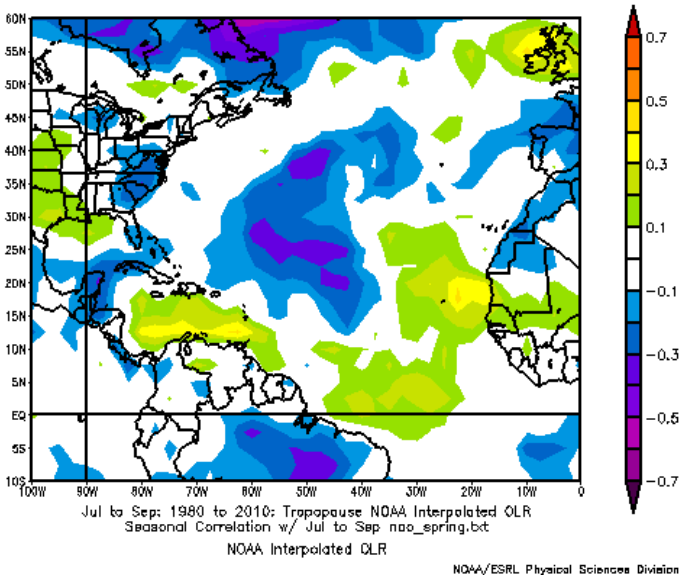

APPENDIX C – COMPOSITE ANALYSIS – TABLES

Composite analysis table highlighting the difference between the 7 highest and lowest Baffin Bay sea ice area years during the spring preceding the tropical cyclone season. Acronyms used are: SIA (sea ice area), ACE (accumulated cyclone energy), and PDI(power dissipation index). All means were tested using a two-tailed paired sample T test and were all found to be significantly different at alpha 0.05.

Parameters	7 Lowest SIA Years	Climatology	7 Highest SIA Years
SIA (km^2)	838,671	981,859	1,169,114
Tropical Cyclones	17	12	9
Tropical Storms	7	5	4
Hurricanes	9	7	4
Minor Hurricanes	5	4	3
Major Hurricanes	4	3	1
ACE (10^4kt^2)	190	122	62
PDI (10^6kt^3)	158	94	41

Composite analysis table highlighting the difference between the 7 highest and lowest Hudson Bay sea ice area years during the spring preceding the tropical cyclone season. Acronyms used are: SIA (sea ice area), ACE (accumulated cyclone energy), and PDI(power dissipation index). All means were tested using a two-tailed paired sample T test and were all found to be significantly different at alpha 0.05.

Parameters	7 Lowest SIA Years	Climatology	7 Highest SIA Years
SIA (km^2)	1049114	1105284	1144343
Tropical Cyclones	16	12	8
Tropical Storms	7	5	3
Hurricanes	9	7	5
Minor Hurricanes	6	4	3
Major Hurricanes	4	3	1
ACE (10^4kt^2)	169	122	68
PDI (10^6kt^3)	134	94	51

APPENDIX C – COMPOSITE ANALYSIS – SPRING AO

Composite map for sea surface pressure (SLP) anomalies during the 7 highest Spring AO years between 1980-2010. Image provided by the NOAA/ESRL Physical Sciences Division, Boulder Colorado from their Web site at http://www.esrl.noaa.gov/psd/ (Kalnay et al., 1996).

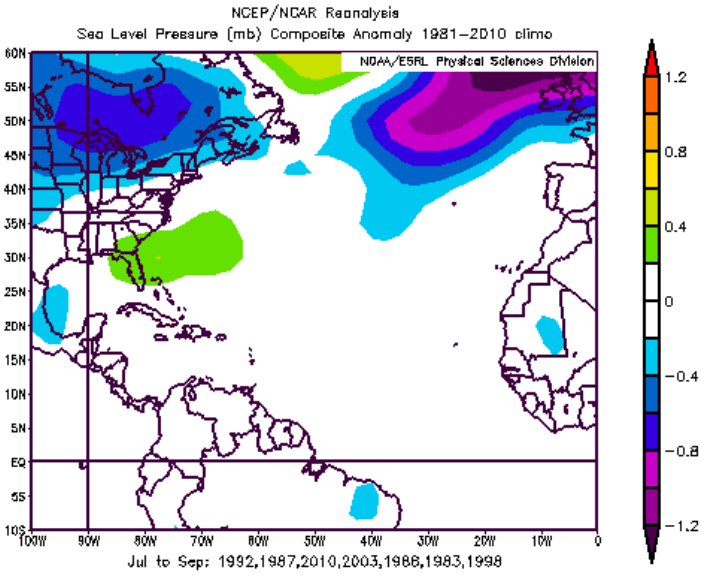

Composite map for sea surface pressure (SLP) anomalies during the 7 lowest Spring AO years between 1980-2010. Image provided by the NOAA/ESRL Physical Sciences Division, Boulder Colorado from their Web site at http://www.esrl.noaa.gov/psd/ (Kalnay et al., 1996).

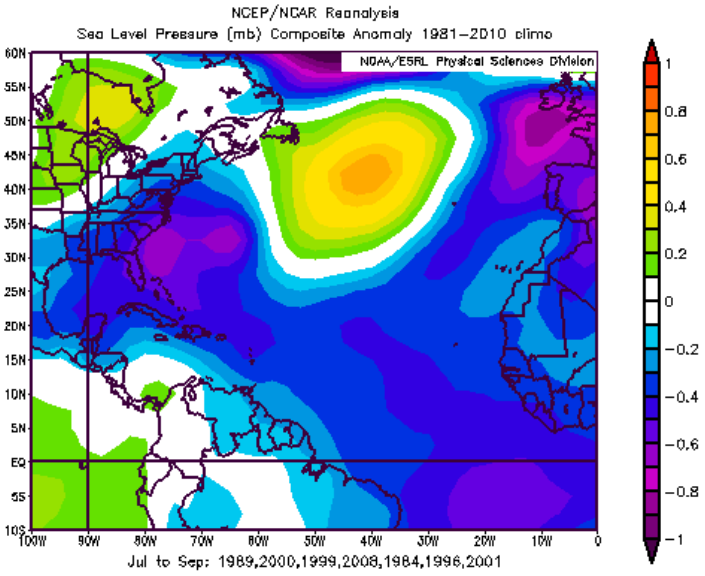

APPENDIX C – COMPOSITE ANALYSIS – SPRING AO

Composite map for sea surface temperature (SST) anomalies during the 7 highest Spring AO years between 1980-2010. Image provided by the NOAA/ESRL Physical Sciences Division, Boulder Colorado from their Web site at http://www.esrl.noaa.gov/psd/ (Kalnay et al., 1996).

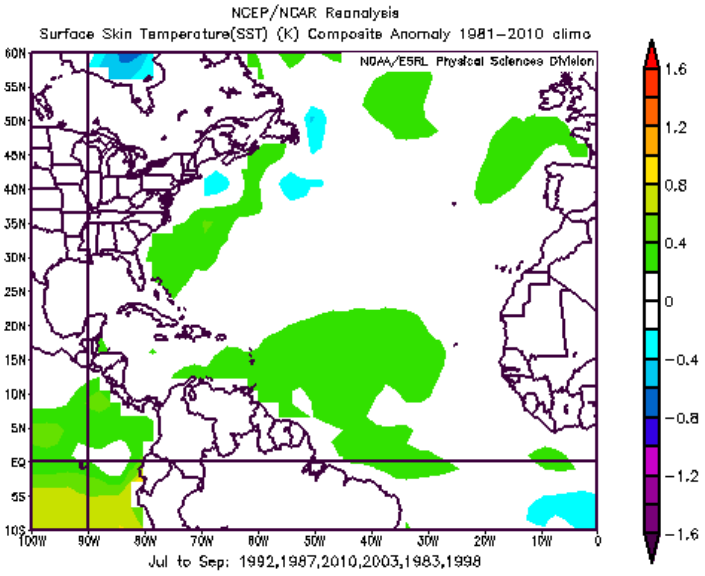

Composite map for sea surface temperature (SST) anomalies during the 7 lowest Spring AO years between 1980-2010. Image provided by the NOAA/ESRL Physical Sciences Division, Boulder Colorado from their Web site at http://www.esrl.noaa.gov/psd/ (Kalnay et al., 1996).

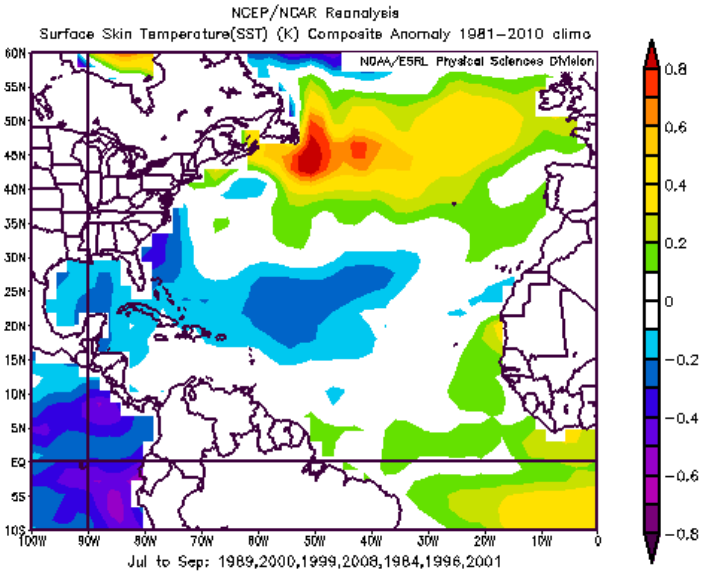

APPENDIX C – COMPOSITE ANALYSIS – SPRING AO

Composite map for 1000 mb vector wind anomalies during the 7 highest Spring AO years between 1980-2010. Image provided by the NOAA/ESRL Physical Sciences Division, Boulder Colorado from their Web site at http://www.esrl.noaa.gov/psd/ (Kalnay et al., 1996).

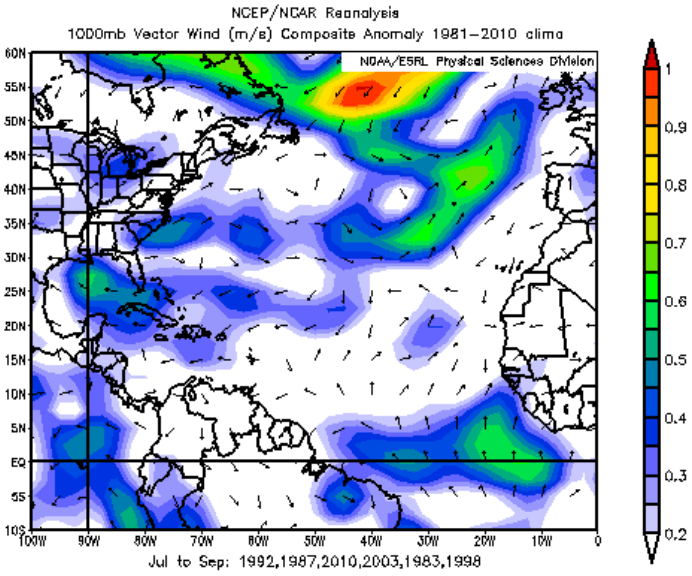

Composite map for 1000 mb vector wind anomalies during the 7 lowest Spring AO years between 1980-2010. Image provided by the NOAA/ESRL Physical Sciences Division, Boulder Colorado from their Web site at http://www.esrl.noaa.gov/psd/ (Kalnay et al., 1996).

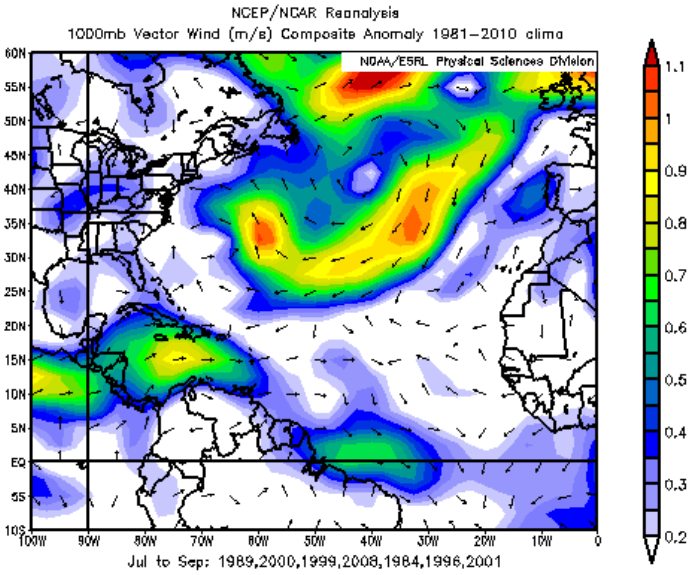

APPENDIX C – COMPOSITE ANALYSIS – FALL BERING SEA SIA

Composite map for sea level pressure (SLP) anomalies during the 7 highest Fall Bering Sea SIE years between 1980-2010. Image provided by the NOAA/ESRL Physical Sciences Division, Boulder Colorado from their Web site at http://www.esrl.noaa.gov/psd/ (Kalnay et al., 1996).

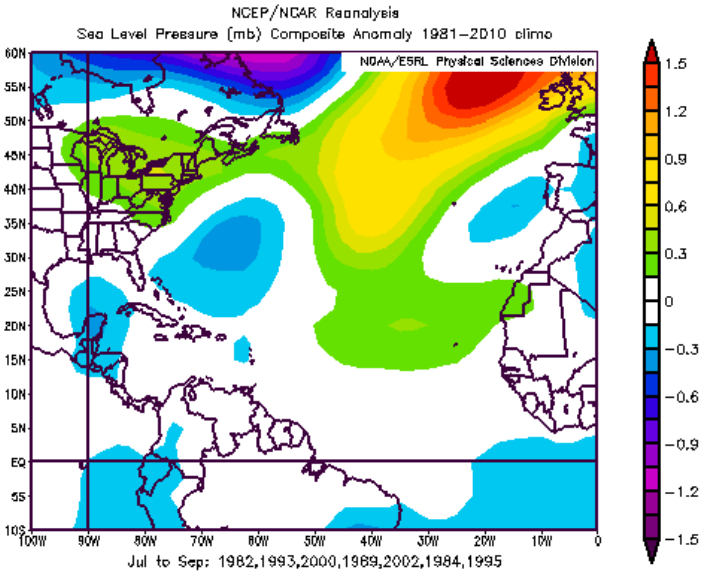

Composite map for sea level pressure (SLP) anomalies during the 7 lowest Fall Bering Sea SIE years between 1980-2010. Image provided by the NOAA/ESRL Physical Sciences Division, Boulder Colorado from their Web site at http://www.esrl.noaa.gov/psd/ (Kalnay et al., 1996).

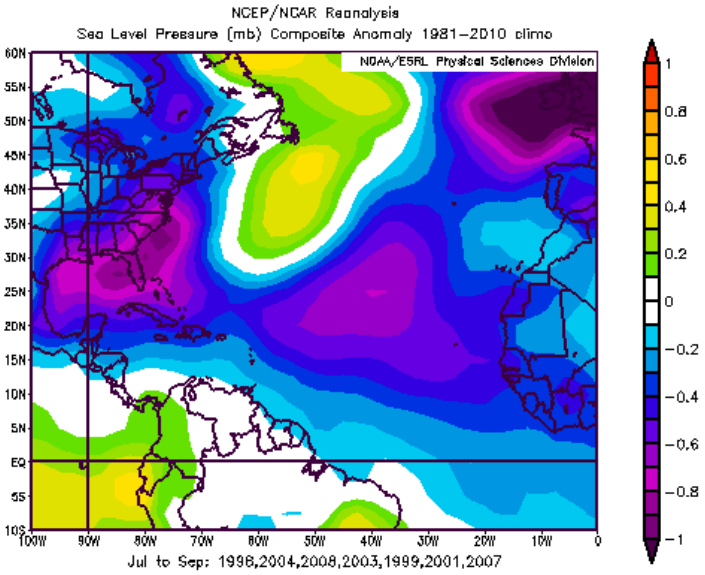

APPENDIX C – COMPOSITE ANALYSIS – FALL BERING SEA SIA

Composite map for sea surface temperature (SST) anomalies during the 7 highest Fall Bering Sea SIE years between 1980-2010. Image provided by the NOAA/ESRL Physical Sciences Division, Boulder Colorado from their Web site at http://www.esrl.noaa.gov/psd/ (Kalnay et al., 1996).

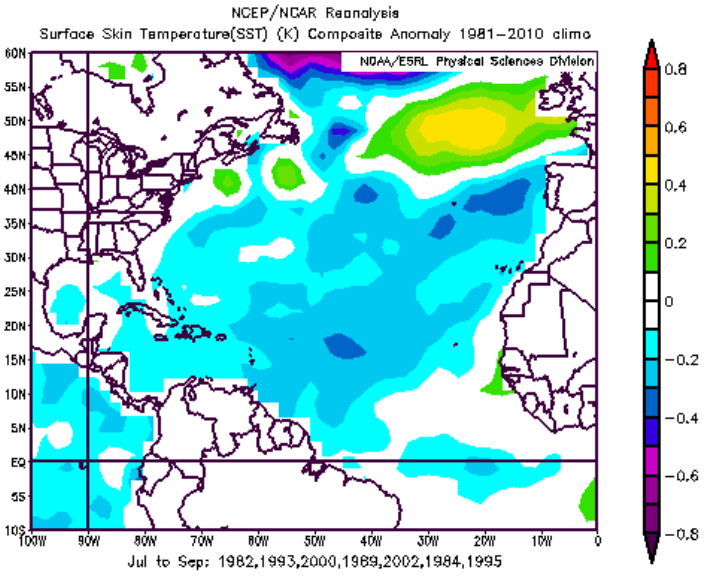

Composite map for sea surface temperature (SST) anomalies during the 7 lowest Fall Bering Sea SIE years between 1980-2010. Image provided by the NOAA/ESRL Physical Sciences Division, Boulder Colorado from their Web site at http://www.esrl.noaa.gov/psd/ (Kalnay et al., 1996).

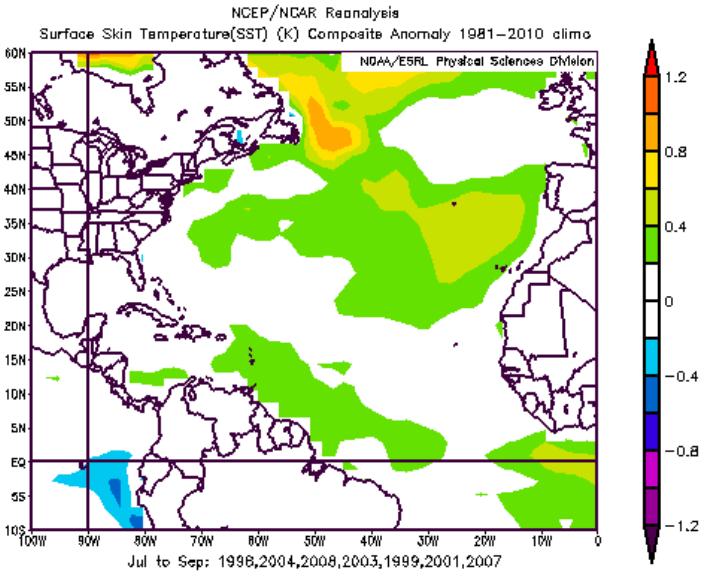

APPENDIX C – COMPOSITE ANALYSIS – FALL BERING SEA SIA

Composite map for 1000 mb vector wind anomalies during the 7 highest Fall Bering Sea SIE years between 1980-2010. Image provided by the NOAA/ESRL Physical Sciences Division, Boulder Colorado from their Web site at http://www.esrl.noaa.gov/psd/ (Kalnay et al., 1996).

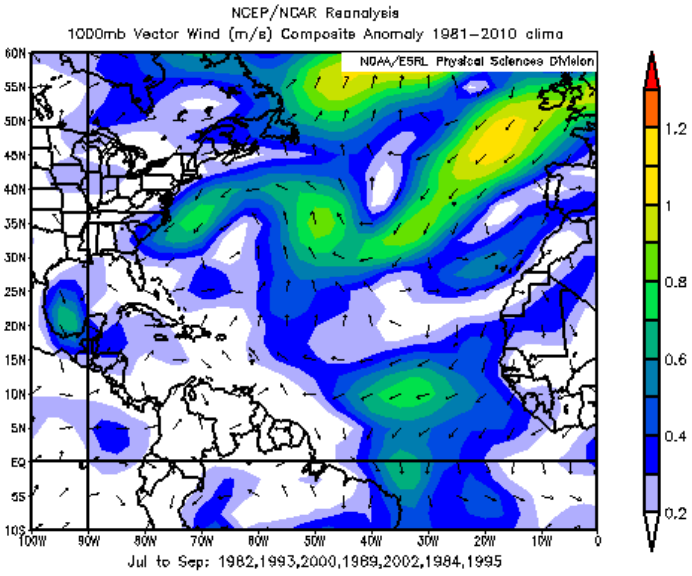

Composite map for 1000 mb vector wind anomalies during the 7 lowest Fall Bering Sea SIE years between 1980-2010. Image provided by the NOAA/ESRL Physical Sciences Division, Boulder Colorado from their Web site at http://www.esrl.noaa.gov/psd/ (Kalnay et al., 1996).

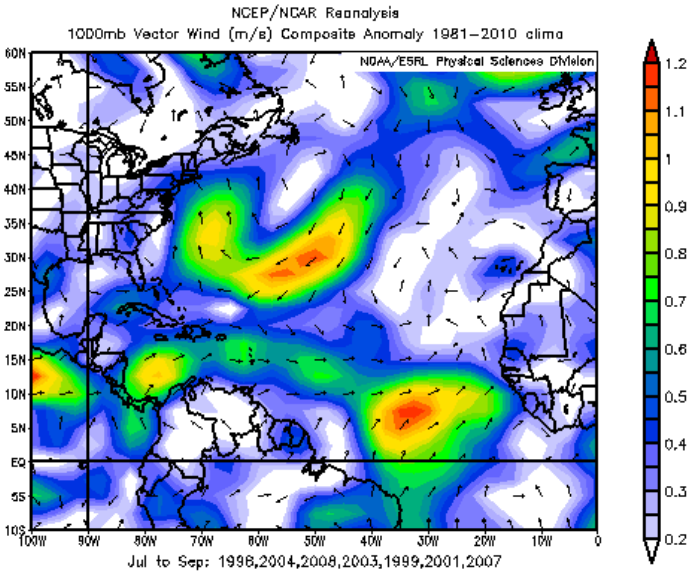

APPENDIX C – COMPOSITE ANALYSIS – FALL BAFFIN BAY SIE

Composite map for sea level pressure (SLP) anomalies during the 7 highest Fall Baffin Bay SIA years between 1980-2010. Image provided by the NOAA/ESRL Physical Sciences Division, Boulder Colorado from their Web site at http://www.esrl.noaa.gov/psd/ (Kalnay et al., 1996).

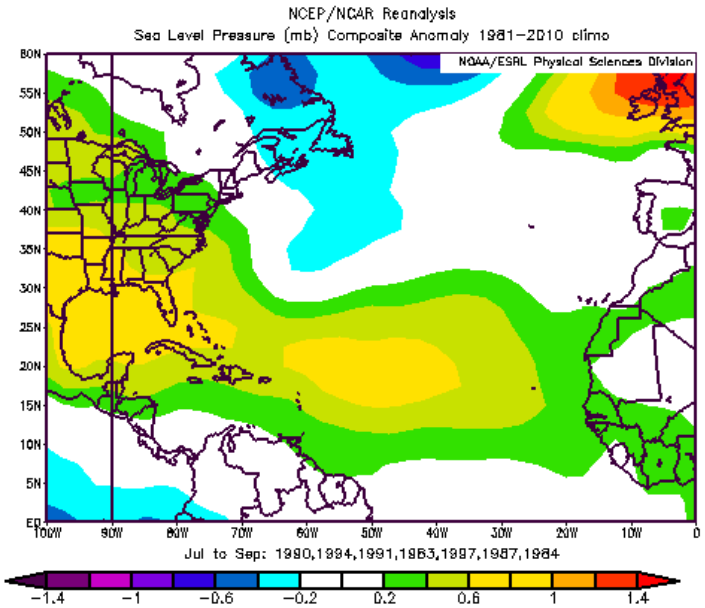

Composite map for sea level pressure (SLP) anomalies during the 7 lowest Fall Baffin Bay SIA years between 1980-2010. Image provided by the NOAA/ESRL Physical Sciences Division, Boulder Colorado from their Web site at http://www.esrl.noaa.gov/psd/ (Kalnay et al., 1996).

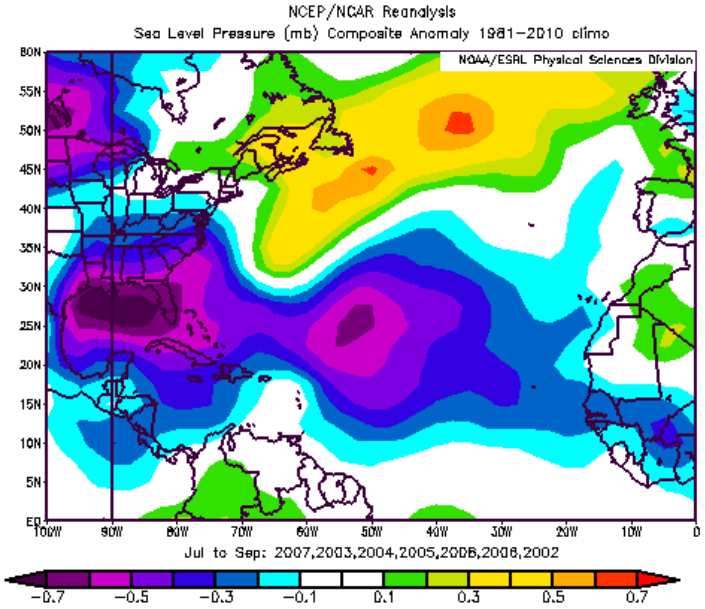

APPENDIX C – COMPOSITE ANALYSIS – FALL BAFFIN BAY SIE

Composite map for sea surface temperature (SST) anomalies during the 7 highest Fall Baffin Bay SIA years between 1980-2010. Image provided by the NOAA/ESRL Physical Sciences Division, Boulder Colorado from their Web site at http://www.esrl.noaa.gov/psd/ (Kalnay et al., 1996).

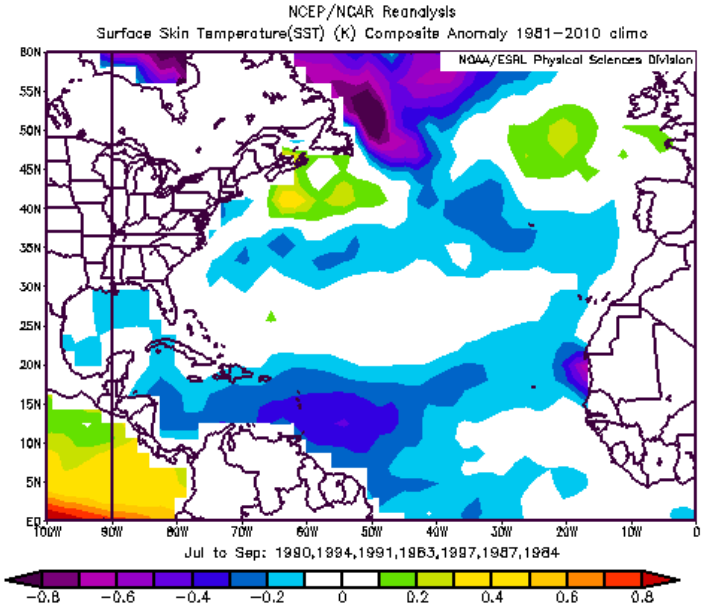

Composite map for sea surface temperature (SST) anomalies during the 7 lowest Fall Baffin Bay SIA years between 1980-2010. Image provided by the NOAA/ESRL Physical Sciences Division, Boulder Colorado from their Web site at http://www.esrl.noaa.gov/psd/ (Kalnay et al., 1996).

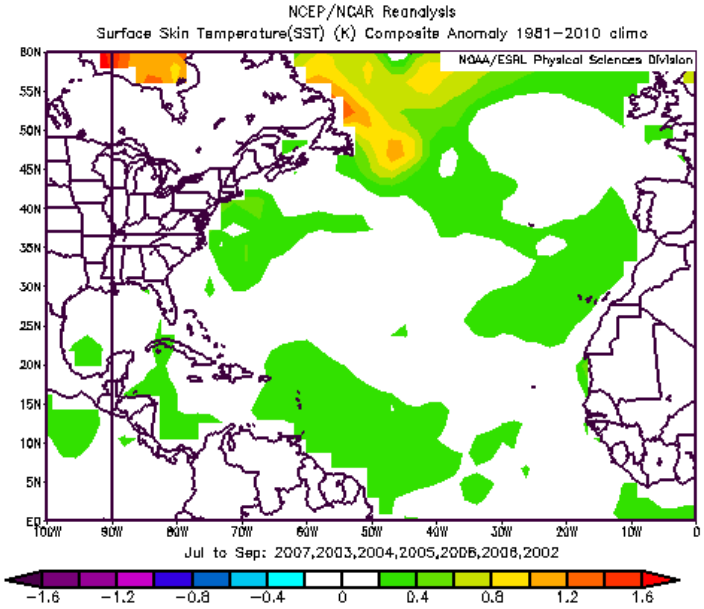

APPENDIX C – COMPOSITE ANALYSIS – FALL BAFFIN BAY SIE

Composite map for 1000 mb vector wind anomalies during the 7 highest Fall Baffin Bay SIA years between 1980-2010. Image provided by the NOAA/ESRL Physical Sciences Division, Boulder Colorado from their Web site at http://www.esrl.noaa.gov/psd/ (Kalnay et al., 1996).

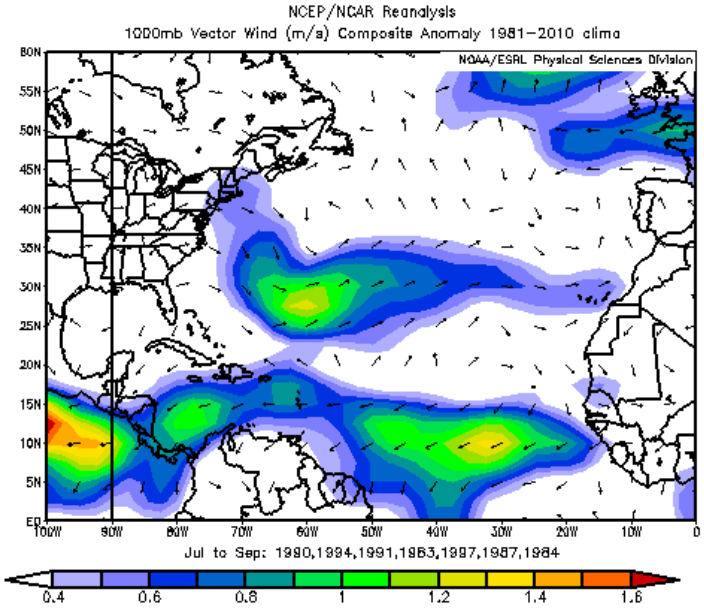

Composite map for 1000 mb vector wind anomalies during the 7 lowest Fall Baffin Bay SIA years between 1980-2010. Image provided by the NOAA/ESRL Physical Sciences Division, Boulder Colorado from their Web site at http://www.esrl.noaa.gov/psd/ (Kalnay et al., 1996).

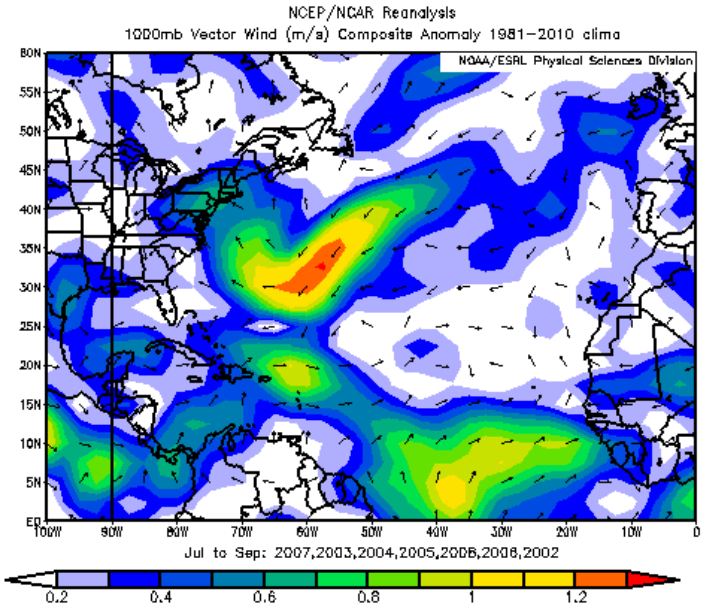

APPENDIX C – COMPOSITE ANALYSIS – SUMMER ENSO

Composite map for sea level pressure (SLP) anomalies during the 7 highest Summer ENSO years between 1980-2010. Image provided by the NOAA/ESRL Physical Sciences Division, Boulder Colorado from their Web site at http://www.esrl.noaa.gov/psd/ (Kalnay et al., 1996).

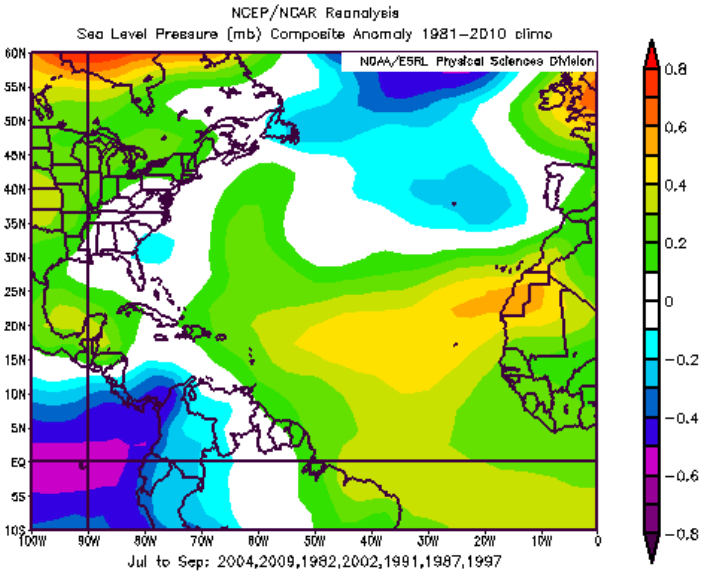

Composite map for sea level pressure (SLP) anomalies during the 7 lowest Summer ENSO years between 1980-2010. Image provided by the NOAA/ESRL Physical Sciences Division, Boulder Colorado from their Web site at http://www.esrl.noaa.gov/psd/ (Kalnay et al., 1996).

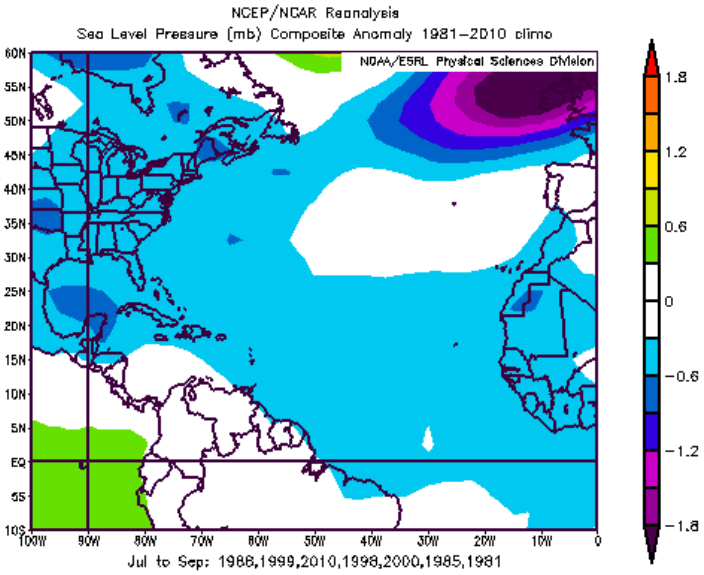

APPENDIX C – COMPOSITE ANALYSIS – SUMMER ENSO

Composite map for sea surface temperature (SST) anomalies during the 7 highest Summer ENSO years between 1980-2010. Image provided by the NOAA/ESRL Physical Sciences Division, Boulder Colorado from their Web site at http://www.esrl.noaa.gov/psd/ (Kalnay et al., 1996).

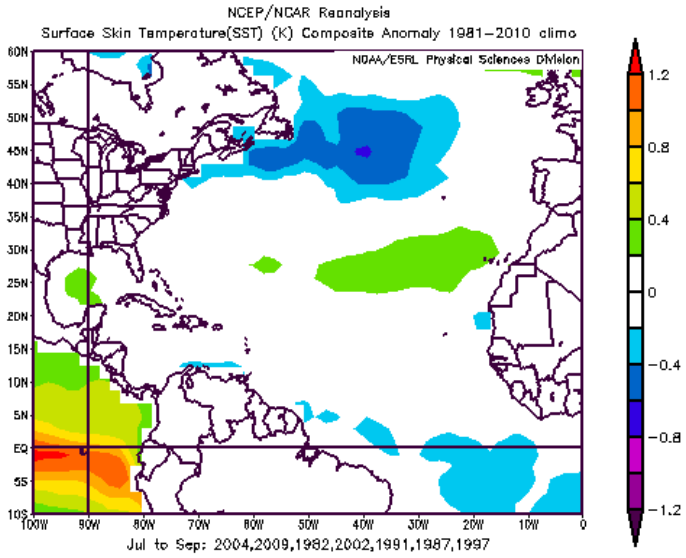

Composite map for sea surface temperature (SST) anomalies during the 7 lowest Summer ENSO years between 1980-2010. Image provided by the NOAA/ESRL Physical Sciences Division, Boulder Colorado from their Web site at http://www.esrl.noaa.gov/psd/ (Kalnay et al., 1996).

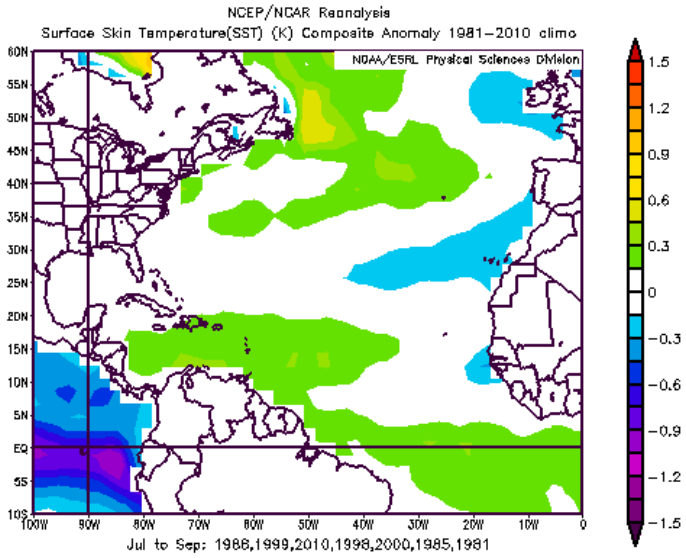

APPENDIX C – COMPOSITE ANALYSIS – SUMMER ENSO

Composite map for 1000 mb vector wind anomalies during the 7 highest Summer ENSO years between 1980-2010. Image provided by the NOAA/ESRL Physical Sciences Division, Boulder Colorado from their Web site at http://www.esrl.noaa.gov/psd/ (Kalnay et al., 1996).

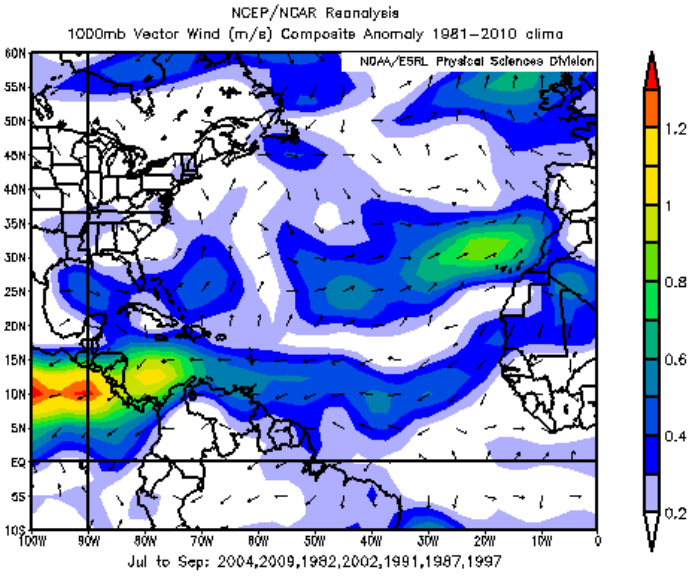

Composite map for 1000 mb vector wind anomalies during the 7 lowest Summer ENSO years between 1980-2010. Image provided by the NOAA/ESRL Physical Sciences Division, Boulder Colorado from their Web site at http://www.esrl.noaa.gov/psd/ (Kalnay et al., 1996).

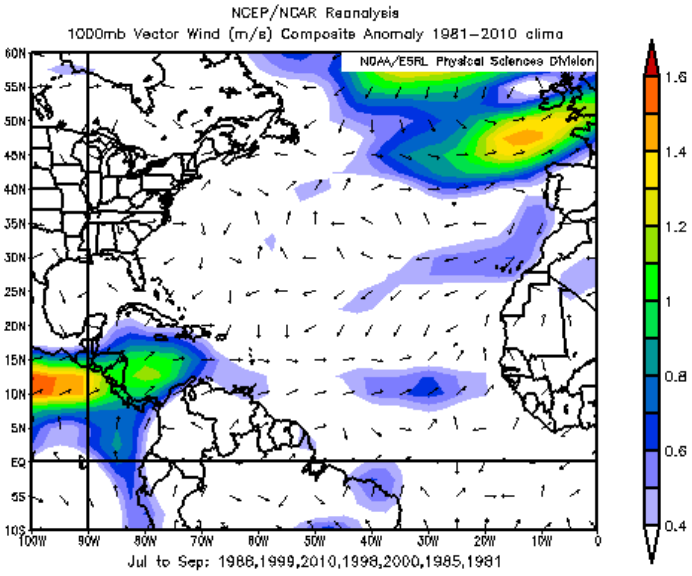

APPENDIX C – COMPOSITE ANALYSIS – FALL NAO

Composite map for sea level pressure (SLP) anomalies during the 7 highest Fall NAO years between 1980-2010. Image provided by the NOAA/ESRL Physical Sciences Division, Boulder Colorado from their Web site at http://www.esrl.noaa.gov/psd/ (Kalnay et al., 1996).

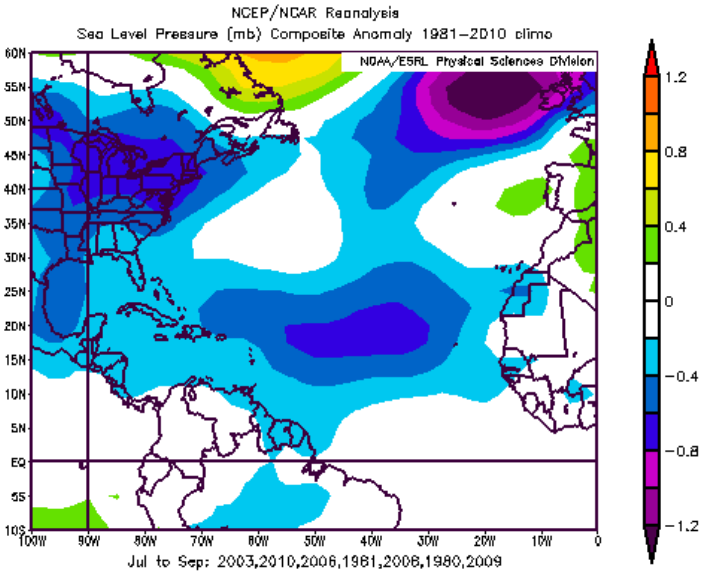

Composite map for sea level pressure (SLP) anomalies during the 7 lowest Fall NAO years between 1980-2010. Image provided by the NOAA/ESRL Physical Sciences Division, Boulder Colorado from their Web site at http://www.esrl.noaa.gov/psd/ (Kalnay et al., 1996).

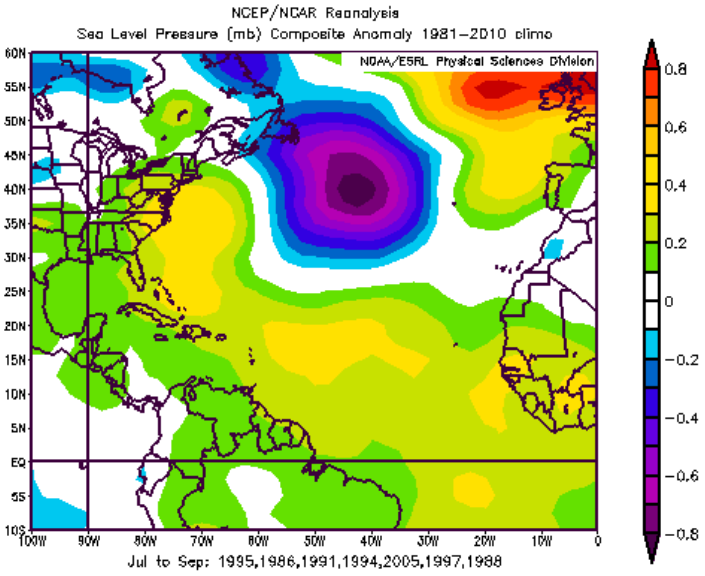

APPENDIX C – COMPOSITE ANALYSIS – FALL NAO

Composite map for sea surface temperature (SST) anomalies during the 7 highest Fall NAO years between 1980-2010. Image provided by the NOAA/ESRL Physical Sciences Division, Boulder Colorado from their Web site at http://www.esrl.noaa.gov/psd/ (Kalnay et al., 1996).

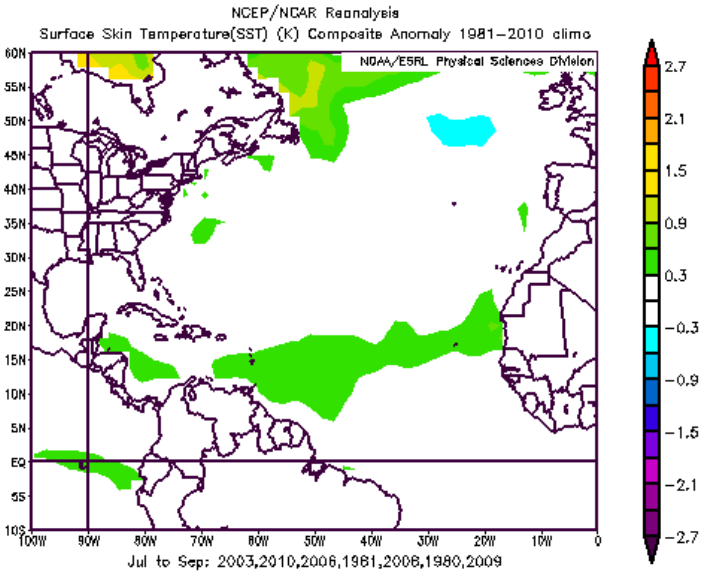

Composite map for sea surface temperature (SST) anomalies during the 7 lowest Fall NAO years between 1980-2010. Image provided by the NOAA/ESRL Physical Sciences Division, Boulder Colorado from their Web site at http://www.esrl.noaa.gov/psd/ (Kalnay et al., 1996).

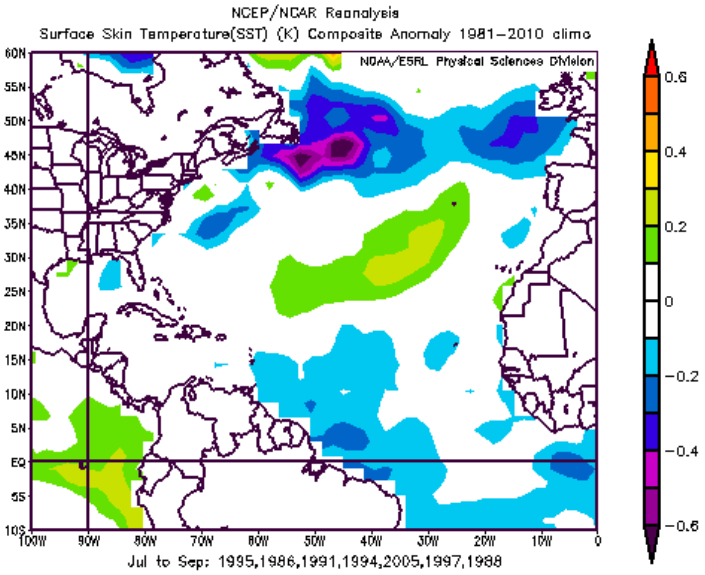

APPENDIX C – COMPOSITE ANALYSIS – FALL NAO

Composite map for 1000 mb vector wind anomalies during the 7 highest Fall NAO years between 1980-2010. Image provided by the NOAA/ESRL Physical Sciences Division, Boulder Colorado from their Web site at http://www.esrl.noaa.gov/psd/ (Kalnay et al., 1996).

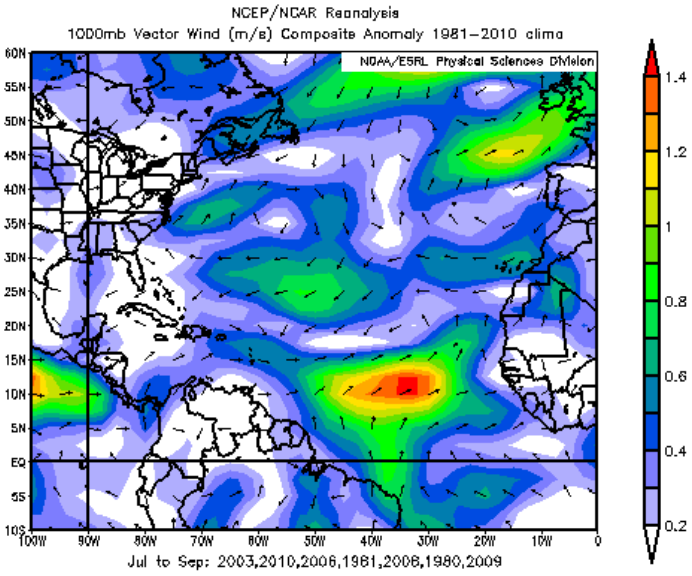

Composite map for 1000 mb vector wind anomalies during the 7 lowest Fall NAO years between 1980-2010. Image provided by the NOAA/ESRL Physical Sciences Division, Boulder Colorado from their Web site at http://www.esrl.noaa.gov/psd/ (Kalnay et al., 1996).

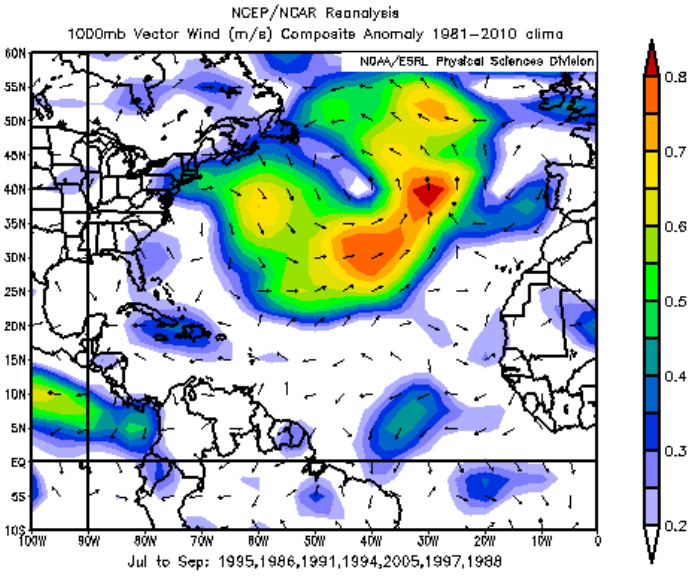

APPENDIX C – COMPOSITE ANALYSIS – SPRING NAO

Composite map for sea level pressure (SLP) anomalies during the 7 highest Spring NAO years between 1980-2010. Image provided by the NOAA/ESRL Physical Sciences Division, Boulder Colorado from their Web site at http://www.esrl.noaa.gov/psd/ (Kalnay et al., 1996).

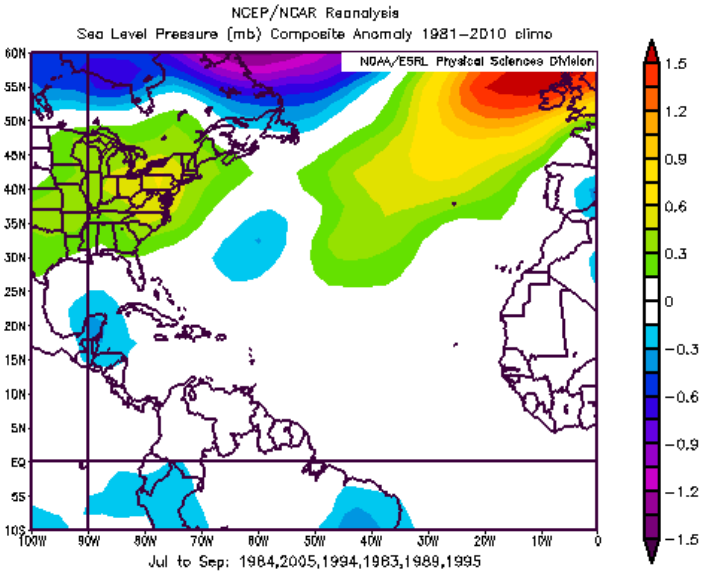

Composite map for sea level pressure (SLP) anomalies during the 7 lowest Spring NAO years between 1980-2010. Image provided by the NOAA/ESRL Physical Sciences Division, Boulder Colorado from their Web site at http://www.esrl.noaa.gov/psd/ (Kalnay et al., 1996).

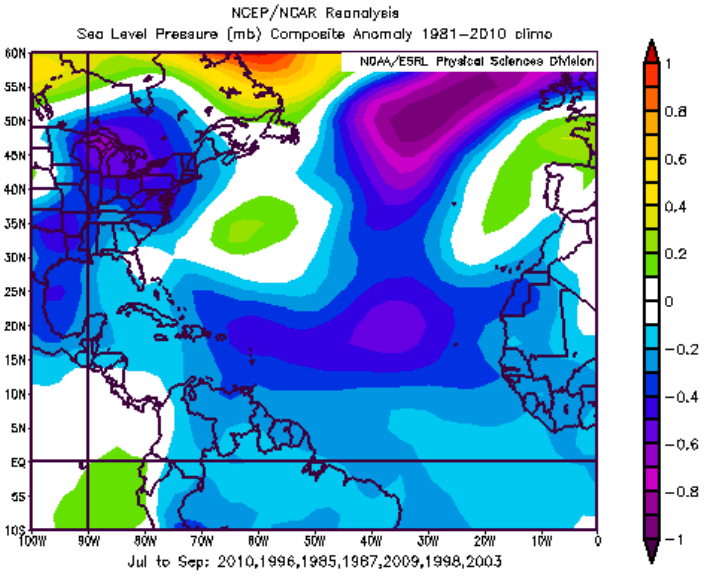

APPENDIX C – COMPOSITE ANALYSIS – SPRING NAO

Composite map for sea surface temperature (SST) anomalies during the 7 highest Spring NAO years between 1980-2010. Image provided by the NOAA/ESRL Physical Sciences Division, Boulder Colorado from their Web site at http://www.esrl.noaa.gov/psd/ (Kalnay et al., 1996).

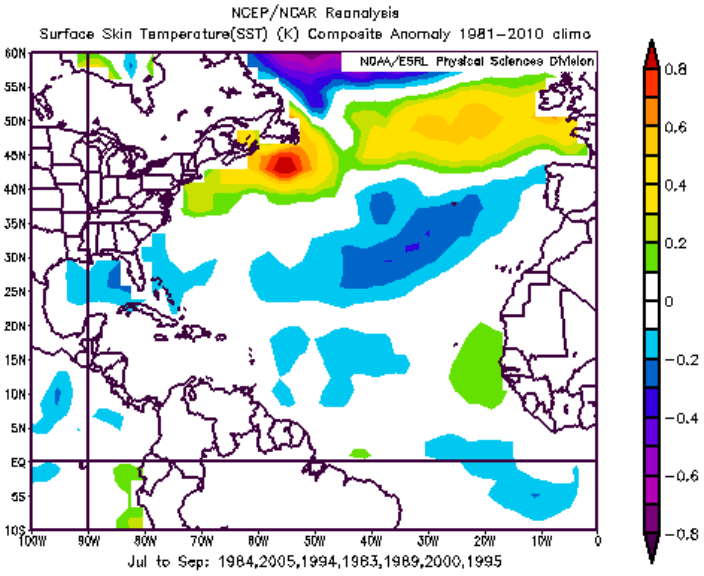

Composite map for sea surface temperature (SST) anomalies during the 7 lowest Spring NAO years between 1980-2010. Image provided by the NOAA/ESRL Physical Sciences Division, Boulder Colorado from their Web site at http://www.esrl.noaa.gov/psd/ (Kalnay et al., 1996).

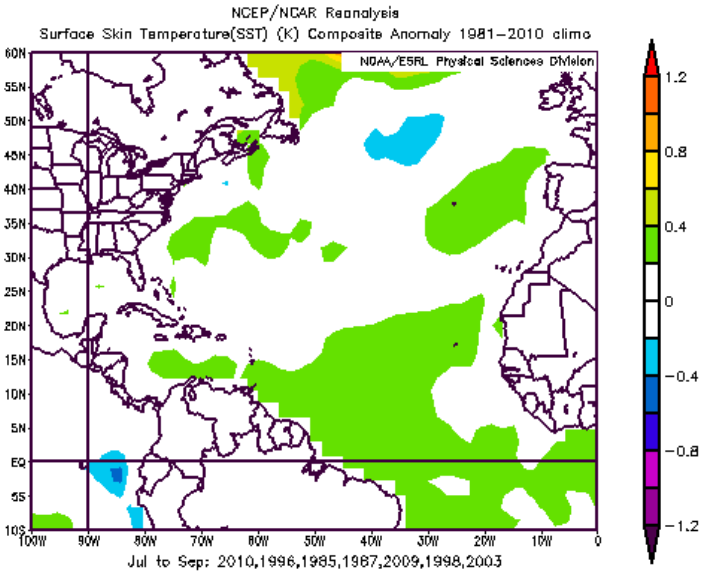

APPENDIX C – COMPOSITE ANALYSIS – SPRING NAO

Composite map for 1000 mb vector wind anomalies during the 7 highest Spring NAO years between 1980-2010. Image provided by the NOAA/ESRL Physical Sciences Division, Boulder Colorado from their Web site at http://www.esrl.noaa.gov/psd/ (Kalnay et al., 1996).

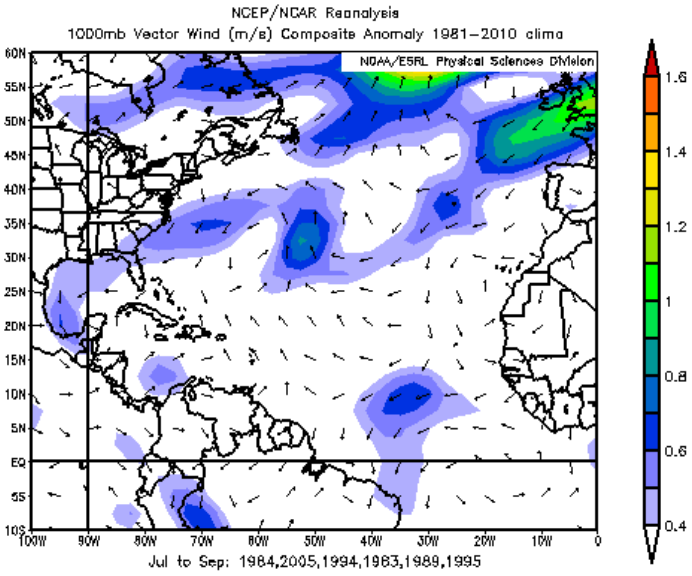

Composite map for 1000 mb vector wind anomalies during the 7 lowest Spring NAO years between 1980-2010. Image provided by the NOAA/ESRL Physical Sciences Division, Boulder Colorado from their Web site at http://www.esrl.noaa.gov/psd/ (Kalnay et al., 1996).

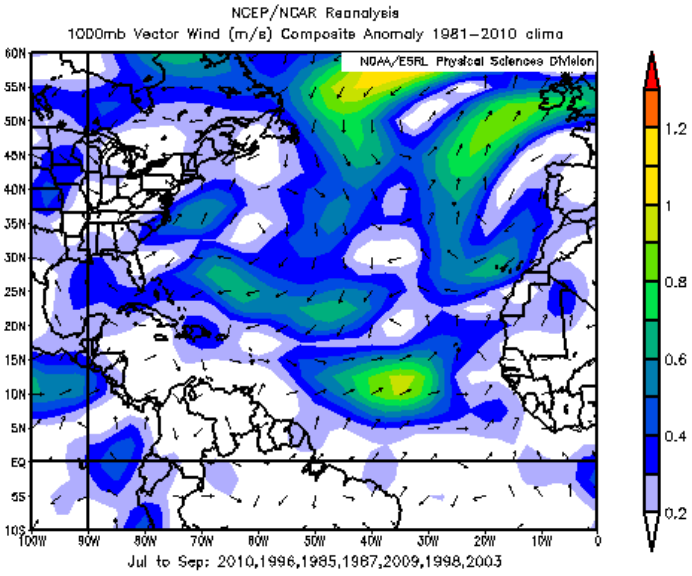

APPENDIX D – MATLAB CODE

```
%Load the input data.

%Cryosphere.
load 1980_2010_SCE.txt
load 1980_2010_SIA.txt
load 1980_2010_SIE.txt

%Teleconnections.
load tele_all_indices_by_season.txt

%Cyclone characteristics.
load TC_character_mindoy_maxdoy.txt
load TC_character_annual_landfall.txt
load TC_character_annual_ACE.txt
load TC_character_annual_peak_wind.txt
load TC_character_annual_lmd.txt
load TC_character_annual_cat0_count.txt
load TC_character_annual_MAJOR_count.txt
load TC_character_annual_minor_count.txt
load TC_totalseasonlength.txt
load TC_character_annual_PDI.txt
load TC_annual_counts.txt
load TC_character_annual_hurricane.txt

%Assign data to master arrays.
predictor(1:60,1:112)=NaN;
predictand(1:60,1:13)=NaN;

predictor(1:60,1:20)=tele_all_indices_by_season(:,2:21);
predictor(30:60,21:32)=X1980_2010_SCE(:,2:13);
predictor(30:60,33:72)=X1980_2010_SIA(:,2:41);
predictor(30:60,73:112)=X1980_2010_SIE(:,2:41);

predictand(1:60,1)=TC_annual_counts(:,2);
predictand(1:60,2)=TC_character_annual_cat0_count(:,2);
predictand(1:60,3)=TC_character_annual_hurricane(:,2);
predictand(1:60,4)=TC_character_annual_minor_count(:,2);
predictand(1:60,5)=TC_character_annual_MAJOR_count(:,2);
predictand(1:60,6)=TC_character_annual_ACE(:,2);
predictand(1:60,7)=TC_character_annual_PDI(:,2);
predictand(1:60,8)=TC_character_annual_landfall(:,2);
predictand(1:60,9)=TC_character_annual_peak_wind(:,2);
predictand(1:60,10)=TC_character_annual_lmd(:,2);
predictand(1:60,11:12)=TC_character_mindoy_maxdoy(:,2:3);
predictand(1:60,13)=TC_totalseasonlength(:,2);



%Specificy which predictors belong to which lead times. Climate modes only
dec_predictors_modes=1:5;
mar_predictors_modes=1:10;
jun_predictors_modes=1:15;
sep_predictors_modes=1:20;

%Define the predictor arrays for cryosphere and climate modes at different
%lead times.
dec_predictors_all=[1 2 3 4 5 21 25 29 33 37 41 45 49 53 57 61 65 69 73 77 81
85 89 93 97 101 105 109];
```

```
mar_predictors_all=[1 2 3 4 5 6 7 8 9 10 21 22 25 26 29 30 33 34 37 38 41 42
45 46 49 50 53 54 57 58 61 62 65 66 69 70 73 74 77 78 81 82 85 86 89 90 93 94
97 98 101 102 105 106 109 110];
jun_predictors_all=[1 2 3 4 5 6 7 8 9 10 11 12 13 14 15 21 22 23 25 26 27 29
30 31 33 34 35 37 38 39 41 42 43 45 46 47 49 50 51 53 54 55 57 58 59 61 62 63
65 66 67 69 70 71 73 74 75 77 78 79 81 82 83 85 86 87 89 90 91 93 94 95 97 98
99 101 102 103 105 106 107 109 110 111];
sep_predictors_all=1:112;

%Define predictor arrays for cryosphere predictors only at different lead
%times
dec_predictors_cryo=[21 25 29 33 37 41 45 49 53 57 61 65 69 73 77 81 85 89 93
97 101 105 109];
mar_predictors_cryo=[21 22 25 26 29 30 33 34 37 38 41 42 45 46 49 50 53 54 57
58 61 62 65 66 69 70 73 74 77 78 81 82 85 86 89 90 93 94 97 98 101 102 105 106
109 110];
jun_predictors_cryo=[21 22 23 25 26 27 29 30 31 33 34 35 37 38 39 41 42 43 45
46 47 49 50 51 53 54 55 57 58 59 61 62 63 65 66 67 69 70 71 73 74 75 77 78 79
81 82 83 85 86 87 89 90 91 93 94 95 97 98 99 101 102 103 105 106 107 109 110
111];
sep_predictors_cryo=21:112;
preddec_modes_31(1:31,1:13)=NaN;
predmar_modes_31(1:31,1:13)=NaN;
predjun_modes_31(1:31,1:13)=NaN;
predsep_modes_31(1:31,1:13)=NaN;
predictand_31=predictand(30:60,1:13);
predictor_31=predictor(30:60,1:112);
%models for climate modes only 31 Study period
for v=1:13

[b,se,pval,inmodel,stats,nextstep,history]=stepwisefit(predictor(30:60,dec_pre
dictors_modes),predictand(30:60,v));
    b=regress(predictand(30:60,v),[ones(length(predictand(30:60,v)),1)
predictor(30:60,dec_predictors_modes(find(inmodel==1)))]);
    preddec_modes_31(1:31,v)=b'*[ones(length(predictand(30:60,v)),1)
predictor(30:60,dec_predictors_modes(find(inmodel==1)))]';
    for w=1:31 %hindcast models
        include(1:31)=1;
        include(w)=0;
        g1=find(include==1);

hind_b=regress(predictand_31(g1,v),[ones(length(predictand_31(g1,v)),1)
predictor_31(g1,dec_predictors_modes(find(inmodel==1)))]); %finds coefficients
for g2
        hind_preddec_modes_31(w,v)=hind_b'*[ones(length(predictand_31(w,v)),1)
predictor_31(w,dec_predictors_modes(find(inmodel==1)))]';%hindcast result for
excluded row
        clear g1;
        clear include;
    end

[b,se,pval,inmodel,stats,nextstep,history]=stepwisefit(predictor(30:60,mar_pre
dictors_modes),predictand(30:60,v));
    b=regress(predictand(30:60,v),[ones(length(predictand(30:60,v)),1)
predictor(30:60,mar_predictors_modes(find(inmodel==1)))]);
    predmar_modes_31(1:31,v)=b'*[ones(length(predictand(30:60,v)),1)
predictor(30:60,mar_predictors_modes(find(inmodel==1)))]';
    for w=1:31 %hindcast models
        include(1:31)=1;
        include(w)=0;
        g1=find(include==1);
```

```
hind_b=regress(predictand_31(g1,v),[ones(length(predictand_31(g1,v)),1)
predictor_31(g1,mar_predictors_modes(find(inmodel==1)))]); %finds coefficients
for g2
        hind_predmar_modes_31(w,v)=hind_b'*[ones(length(predictand_31(w,v)),1)
predictor_31(w,mar_predictors_modes(find(inmodel==1)))]';%hindcast result for
excluded row
        clear g1;
        clear include;
    end

[b,se,pval,inmodel,stats,nextstep,history]=stepwisefit(predictor(30:60,jun_pre
dictors_modes),predictand(30:60,v));
    b=regress(predictand(30:60,v),[ones(length(predictand(30:60,v)),1)
predictor(30:60,jun_predictors_modes(find(inmodel==1)))]);
    predjun_modes_31(1:31,v)=b'*[ones(length(predictand(30:60,v)),1)
predictor(30:60,jun_predictors_modes(find(inmodel==1)))]';
    for w=1:31 %hindcast models
        include(1:31)=1;
        include(w)=0;
        g1=find(include==1);

hind_b=regress(predictand_31(g1,v),[ones(length(predictand_31(g1,v)),1)
predictor_31(g1,jun_predictors_modes(find(inmodel==1)))]); %finds coefficients
for g2
        hind_predjun_modes_31(w,v)=hind_b'*[ones(length(predictand_31(w,v)),1)
predictor_31(w,jun_predictors_modes(find(inmodel==1)))]';%hindcast result for
excluded row
        clear g1;
        clear include;
    end

[b,se,pval,inmodel,stats,nextstep,history]=stepwisefit(predictor(30:60,sep_pre
dictors_modes),predictand(30:60,v));
    b=regress(predictand(30:60,v),[ones(length(predictand(30:60,v)),1)
predictor(30:60,sep_predictors_modes(find(inmodel==1)))]);
    predsep_modes_31(1:31,v)=b'*[ones(length(predictand(30:60,v)),1)
predictor(30:60,sep_predictors_modes(find(inmodel==1)))]';
    for w=1:31 %hindcast models
        include(1:31)=1;
        include(w)=0;
        g1=find(include==1);

hind_b=regress(predictand_31(g1,v),[ones(length(predictand_31(g1,v)),1)
predictor_31(g1,sep_predictors_modes(find(inmodel==1)))]); %finds coefficients
for g2
        hind_predsep_modes_31(w,v)=hind_b'*[ones(length(predictand_31(w,v)),1)
predictor_31(w,sep_predictors_modes(find(inmodel==1)))]';%hindcast result for
excluded row
        clear g1;
        clear include;
    end
end

preddec_all(1:31,1:13)=NaN;
predmar_all(1:31,1:13)=NaN;
predjun_all(1:31,1:13)=NaN;
predsep_all(1:31,1:13)=NaN;
predictand_31=predictand(30:60,1:13);
predictor_31=predictor(30:60,1:112);
%models for climate modes and cryosphere 31 study period
```

```
for v=1:13

[b,se,pval,inmodel,stats,nextstep,history]=stepwisefit(predictor(30:60,dec_pre
dictors_all),predictand(30:60,v));
    b=regress(predictand(30:60,v),[ones(length(predictand(30:60,v)),1)
predictor(30:60,dec_predictors_all(find(inmodel==1)))]);
    preddec_all(1:31,v)=b'*[ones(length(predictand(30:60,v)),1)
predictor(30:60,dec_predictors_all(find(inmodel==1)))]';
    for w=1:31 %hindcast models
        include(1:31)=1;
        include(w)=0;
        g1=find(include==1);

hind_b=regress(predictand_31(g1,v),[ones(length(predictand_31(g1,v)),1)
predictor_31(g1,dec_predictors_all(find(inmodel==1)))]); %finds coefficients
for g2
        hind_preddec_all(w,v)=hind_b'*[ones(length(predictand_31(w,v)),1)
predictor_31(w,dec_predictors_all(find(inmodel==1)))]';%hindcast result for
excluded row
        clear g1;
        clear include;
    end

[b,se,pval,inmodel,stats,nextstep,history]=stepwisefit(predictor(30:60,mar_pre
dictors_all),predictand(30:60,v));
    b=regress(predictand(30:60,v),[ones(length(predictand(30:60,v)),1)
predictor(30:60,mar_predictors_all(find(inmodel==1)))]);
    predmar_all(1:31,v)=b'*[ones(length(predictand(30:60,v)),1)
predictor(30:60,mar_predictors_all(find(inmodel==1)))]';
    for w=1:31 %hindcast models
        include(1:31)=1;
        include(w)=0;
        g1=find(include==1);

hind_b=regress(predictand_31(g1,v),[ones(length(predictand_31(g1,v)),1)
predictor_31(g1,mar_predictors_all(find(inmodel==1)))]); %finds coefficients
for g2
        hind_predmar_all(w,v)=hind_b'*[ones(length(predictand_31(w,v)),1)
predictor_31(w,mar_predictors_all(find(inmodel==1)))]';%hindcast result for
excluded row
        clear g1;
        clear include;
    end

[b,se,pval,inmodel,stats,nextstep,history]=stepwisefit(predictor(30:60,jun_pre
dictors_all),predictand(30:60,v));
    b=regress(predictand(30:60,v),[ones(length(predictand(30:60,v)),1)
predictor(30:60,jun_predictors_all(find(inmodel==1)))]);
    predjun_all(1:31,v)=b'*[ones(length(predictand(30:60,v)),1)
predictor(30:60,jun_predictors_all(find(inmodel==1)))]';
    for w=1:31 %hindcast models
        include(1:31)=1;
        include(w)=0;
        g1=find(include==1);

hind_b=regress(predictand_31(g1,v),[ones(length(predictand_31(g1,v)),1)
predictor_31(g1,jun_predictors_all(find(inmodel==1)))]); %finds coefficients
for g2
        hind_predjun_all(w,v)=hind_b'*[ones(length(predictand_31(w,v)),1)
predictor_31(w,jun_predictors_all(find(inmodel==1)))]';%hindcast result for
excluded row
```

```
        clear g1;
        clear include;
    end

[b,se,pval,inmodel,stats,nextstep,history]=stepwisefit(predictor(30:60,sep_pre
dictors_all),predictand(30:60,v));
    b=regress(predictand(30:60,v),[ones(length(predictand(30:60,v)),1)
predictor(30:60,sep_predictors_all(find(inmodel==1)))]);
    predsep_all(1:31,v)=b'*[ones(length(predictand(30:60,v)),1)
predictor(30:60,sep_predictors_all(find(inmodel==1)))]';
    for w=1:31 %hindcast models
        include(1:31)=1;
        include(w)=0;
        g1=find(include==1);

hind_b=regress(predictand_31(g1,v),[ones(length(predictand_31(g1,v)),1)
predictor_31(g1,sep_predictors_all(find(inmodel==1)))]); %finds coefficients
for g2
        hind_predsep_all(w,v)=hind_b'*[ones(length(predictand_31(w,v)),1)
predictor_31(w,sep_predictors_all(find(inmodel==1)))]';%hindcast result for
excluded row
        clear g1;
        clear include;
    end
end

preddec_cryo(1:31,1:13)=NaN;
predmar_cryo(1:31,1:13)=NaN;
predjun_cryo(1:31,1:13)=NaN;
predsep_cryo(1:31,1:13)=NaN;

%models for cryosphere only 31 Study period
for v=1:13

[b,se,pval,inmodel,stats,nextstep,history]=stepwisefit(predictor(30:60,dec_pre
dictors_cryo),predictand(30:60,v));
    b=regress(predictand(30:60,v),[ones(length(predictand(30:60,v)),1)
predictor(30:60,dec_predictors_cryo(find(inmodel==1)))]);
    preddec_cryo(1:31,v)=b'*[ones(length(predictand(30:60,v)),1)
predictor(30:60,dec_predictors_cryo(find(inmodel==1)))]';
    for w=1:31 %hindcast models
        include(1:31)=1;
        include(w)=0;
        g1=find(include==1);

hind_b=regress(predictand_31(g1,v),[ones(length(predictand_31(g1,v)),1)
predictor_31(g1,dec_predictors_cryo(find(inmodel==1)))]); %finds coefficients
for g2
        hind_preddec_cryo(w,v)=hind_b'*[ones(length(predictand_31(w,v)),1)
predictor_31(w,dec_predictors_cryo(find(inmodel==1)))]';%hindcast result for
excluded row
        clear g1;
        clear include;
    end

[b,se,pval,inmodel,stats,nextstep,history]=stepwisefit(predictor(30:60,mar_pre
dictors_cryo),predictand(30:60,v));
    b=regress(predictand(30:60,v),[ones(length(predictand(30:60,v)),1)
predictor(30:60,mar_predictors_cryo(find(inmodel==1)))]);
    predmar_cryo(1:31,v)=b'*[ones(length(predictand(30:60,v)),1)
predictor(30:60,mar_predictors_cryo(find(inmodel==1)))]';
```

```
    for w=1:31 %hindcast models
        include(1:31)=1;
        include(w)=0;
        g1=find(include==1);

hind_b=regress(predictand_31(g1,v),[ones(length(predictand_31(g1,v)),1)
predictor_31(g1,mar_predictors_cryo(find(inmodel==1)))]); %finds coefficients
for g2
        hind_predmar_cryo(w,v)=hind_b'*[ones(length(predictand_31(w,v)),1)
predictor_31(w,mar_predictors_cryo(find(inmodel==1)))]';%hindcast result for
excluded row
        clear g1;
        clear include;
    end

[b,se,pval,inmodel,stats,nextstep,history]=stepwisefit(predictor(30:60,jun_pre
dictors_cryo),predictand(30:60,v));
    b=regress(predictand(30:60,v),[ones(length(predictand(30:60,v)),1)
predictor(30:60,jun_predictors_cryo(find(inmodel==1)))]);
    predjun_cryo(1:31,v)=b'*[ones(length(predictand(30:60,v)),1)
predictor(30:60,jun_predictors_cryo(find(inmodel==1)))]';
    for w=1:31 %hindcast models
        include(1:31)=1;
        include(w)=0;
        g1=find(include==1);

hind_b=regress(predictand_31(g1,v),[ones(length(predictand_31(g1,v)),1)
predictor_31(g1,jun_predictors_cryo(find(inmodel==1)))]); %finds coefficients
for g2
        hind_predjun_cryo(w,v)=hind_b'*[ones(length(predictand_31(w,v)),1)
predictor_31(w,jun_predictors_cryo(find(inmodel==1)))]';%hindcast result for
excluded row
        clear g1;
        clear include;
    end

[b,se,pval,inmodel,stats,nextstep,history]=stepwisefit(predictor(30:60,sep_pre
dictors_cryo),predictand(30:60,v));
    b=regress(predictand(30:60,v),[ones(length(predictand(30:60,v)),1)
predictor(30:60,sep_predictors_cryo(find(inmodel==1)))]);
    predsep_cryo(1:31,v)=b'*[ones(length(predictand(30:60,v)),1)
predictor(30:60,sep_predictors_cryo(find(inmodel==1)))]';
    for w=1:31 %hindcast models
        include(1:31)=1;
        include(w)=0;
        g1=find(include==1);

hind_b=regress(predictand_31(g1,v),[ones(length(predictand_31(g1,v)),1)
predictor_31(g1,sep_predictors_cryo(find(inmodel==1)))]); %finds coefficients
for g2
        hind_predsep_cryo(w,v)=hind_b'*[ones(length(predictand_31(w,v)),1)
predictor_31(w,sep_predictors_cryo(find(inmodel==1)))]';%hindcast result for
excluded row
        clear g1;
        clear include;
    end
end
```

VITA

Graduate School
Southern Illinois University

Johannes Mack

jmack13@siu.edu

Southern Illinois University Carbondale
Bachelor of Science, Geography & Environmental Resources, May 2011

Special Honors and Awards:

2011 – 2013, Graduate Assistantship, Southern Illinois University, Carbondale, Illinois
2010, Outstanding Senior in Geography Award, Southern Illinois University, Carbondale, Illinois

Thesis Title:

The Cryosphere and North Atlantic Tropical Cyclone Activity: Statistical Forecasting and Physical Mechanisms

Major Professor: Dr. Justin T. Schoof